2014

TRANSMURAL HETEROGENEITY OF CELLULAR LEVEL CARDIAC CONTRACTILE PROPERTIES IN AGING AND HEART FAILURE

Premi Haynes
University of Kentucky, premi.haynes@gmail.com

STUDENT AGREEMENT:

I represent that my thesis or dissertation and abstract are my original work. Proper attribution has been given to all outside sources. I understand that I am solely responsible for obtaining any needed copyright permissions. I have obtained needed written permission statement(s) from the owner(s) of each third-party copyrighted matter to be included in my work, allowing electronic distribution (if such use is not permitted by the fair use doctrine) which will be submitted to UKnowledge as Additional File.

I hereby grant to The University of Kentucky and its agents the irrevocable, non-exclusive, and royalty-free license to archive and make accessible my work in whole or in part in all forms of media, now or hereafter known. I agree that the document mentioned above may be made available immediately for worldwide access unless an embargo applies.

I retain all other ownership rights to the copyright of my work. I also retain the right to use in future works (such as articles or books) all or part of my work. I understand that I am free to register the copyright to my work.

REVIEW, APPROVAL AND ACCEPTANCE

The document mentioned above has been reviewed and accepted by the student's advisor, on behalf of the advisory committee, and by the Director of Graduate Studies (DGS), on behalf of the program; we verify that this is the final, approved version of the student's thesis including all changes required by the advisory committee. The undersigned agree to abide by the statements above.

Premi Haynes, Student

Dr. Kenneth S. Campbell, Major Professor

Dr. Bret N. Smith, Director of Graduate Studies

TRANSMURAL HETEROGENEITY OF CELLULAR LEVEL CARDIAC CONTRACTILE PROPERTIES IN AGING AND HEART FAILURE

DISSERTATION

A dissertation submitted in partial fulfillment of the requirements for the degree of

Doctor of Philosophy in the College of Medicine at the University of Kentucky

By

Premi Haynes

Lexington, Kentucky

Director: Dr. Kenneth S. Campbell

ABSTRACT

TRANSMURAL HETEROGENEITY OF CELLULAR LEVEL CARDIAC CONTRACTILE PROPERTIES IN AGING AND HEART FAILURE

The left ventricle of the heart relaxes when it fills with blood and contracts to eject blood into circulation to meet the body's metabolic demands. Dysfunction in either relaxation or contraction of the left ventricle can lead to heart failure. Transmural heterogeneity is thought to contribute to normal ventricular wall motion but it is not well understood how transmural modifications affect the failing left ventricle. The overall hypothesis of this dissertation is that normal left ventricles exhibit transmural heterogeneity in cellular level contractile properties and with aging and heart failure there are region-specific changes in cellular level contractile mechanisms.

Age is the biggest risk factor associated with heart failure and therefore we investigated transmural changes in Ca^{2+} handling and contractile proteins in aging F344 rats before the onset of heart failure. We found that in 22-month old F344 rats there is a region-specific decrease in cardiac troponin I phosphorylation in the sub-epicardium that may contribute to slowed myocyte relaxation in the sub-epicardial cells of the same age.

We then investigated the transmural patterns of contractile properties in myocardial tissue samples from patients with heart failure. Force and power output reduced most significantly in the samples from the mid-myocardial region when compared to sub-epicardium and sub-endocardium of the failing hearts. There was a region-specific increase in fibrosis is the mid-myocardium of the failing hearts. Myocardial power output was correlated with key sarcomeric proteins including cardiac troponin I, desmin and myosin light chain-1.

The results in this dissertation reveal novel region-specific modifications in contractile properties in aging and heart failure. These transmural effects can potentially contribute to disruption in normal wall motion and lead to ventricular dysfunction

KEYWORDS: transmural heterogeneity, left ventricle, human biospecimens, sarcomere, heart failure

Premi Haynes

TRANSMURAL HETEROGENEITY OF CELLULAR LEVEL CARDIAC CONTRACTILE PROPERTIES IN AGING AND HEART FAILURE

By

Premi Haynes

Kenneth S. Campbell

Director of Dissertation

Bret N. Smith

Director of Graduate Studies

19th March 2014

Date

This dissertation is dedicated to my mother, Soundhari Shekar

My strength comes from you

Acknowledgements

In Sanskrit, the word for mentor is “Guru” and the word for mentee is “shishya”. The Guru-shishya relation has been a part of the Indian tradition for more than a thousand years though not as prevalent in the modern age. On completion of the education the shishya gives the Guru a “Guru dakshina” a repayment for the knowledge and wisdom that was instilled in the shisya. This repayment was mostly a conglomeration of emotions-appreciation, gratitude, indebtedness and respect. Here we are in the 21st century and the emotions remain the same. I may not be able to give my mentor Dr. Kenneth Campbell a “Guru dakshina” for all that he has done for me but I hope I can pay it forward. I am truly thankful for his support, guidance and selflessness.

I would like to thank my committee members Dr. Karyn Esser, Dr. Brian Delisle and Dr. Susan Smyth for their expertise and advice throughout my graduate career. I would also like to thank Dr. Robert Hadley for taking time out and agreeing to be my outside examiner.

I would like to thank all the people who were in the Campbell lab since 2008 for all their help and support during my graduate career. I would especially like to thank Ben Lawson for his help with mechanical experiments and Halloween costumes, and Dr. Charles Chung for his tremendous and much needed help in the past year with proof reading manuscript/dissertation and listening to my crazy talk.

I would also like to thank Marisa Parmelee Campbell for being a wonderful and gracious person. One of the most valuable gifts that I have ever received was when she and Ken came to my wedding, which was all the way in India! I will always treasure those memories and our friendship.

I could not have made it this far without the love and support of my husband Michael Haynes. He has been my cheerleader. He has encouraged me everyday and made me lots of coffee and kept me going and brought me Major Leven (our pet bunny) to play with.

My sister, Priya Wattula is my friend and my inspiration. I value her advice more than anyone else's. I thank her for her encouragement and strength. I would also like to thank my brother-in-law Kyle Wattula who makes me laugh and he takes my mind off research with daft punk and board games!

Last but not least my parents. I would like to thank my dad for giving me the vision to come here and pursue my education and my mom whose sacrifices have been countless and whose resilience and strength makes me the person that I am today.

God has truly blessed me with a loving family and friends.

Table of Contents

Tables

Figures

Chapter 1. Introduction

1.1. Heart is a heterogeneous organ

William Harvey, a 17th century physician, was one of the first to describe the heart as a muscular organ. He proposed that the function of the heart was to expel blood from the ventricles through contraction and relaxation. He described these findings in his book titled "*On the motion of the heart and blood in animals*" in 1628 [1]. Physician Richard Lower built upon Harvey's work and described the anatomy of the heart in further detail in his book titled " *Tractatus de corde*" in 1669 [2]. He observed a complex arrangement of muscle fibers that formed "layers" and he speculated that the architectural complexity of the fibers were potentially important in the ejection of blood from the ventricles (Figure 1.1) [2]. In the 19th century, James Pettigrew did an exhaustive study of the heart anatomy in several vertebrates and found that the muscle "layers" could be peeled from the outside (sub-epicardium) of the left ventricle to the inside (sub-endocardium) of the left ventricular chamber. He observed that the fiber directions changed with every muscle "layer" he removed [3]. Intriguingly, the fibers in the middle "layers" were observed to be circumferentially arranged and were called "triebwerkzeug" which in the German language can be translated to "actuating fibers" because it was thought that these fibers were potentially important for ventricular ejection [4].

These historical observations about the muscle "layers" and fiber angles were further supported in a study done by Streeter *et al.* in 1969 [5]. In this study, they dissected a through-wall transmural piece of the left ventricular wall and then

histologically sliced them into 10 μm sections. This quantitative study showed that the muscle fiber arrangement shifted from -90° (relative to right-hand orientation) in the sub-epicardium, to ~0° in the mid-myocardium (circumferentially arranged fibers) to +90° in the sub-endocardium of the canine left ventricular wall (Figure 1.2 [5]). Similar muscle “layers” and fiber angles were reported in human left ventricles in a study done by Greenbaum *et al*. in 1981 [6].

All these observations from the past several centuries provide support for the distinct myocardial architecture across the ventricular wall. In the last 10 years sophisticated technologies like magnetic resonance diffusion tensor imaging are being used to visualize in detail the myocardial architecture and fiber angles in the ventricles [7]. Furthermore, several studies have linked structural heterogeneity in myocardial architecture across the left ventricular wall to the function of the heart. For example, cardiac imaging and computational modeling of the heart have shown that transmural myocardial heterogeneity can influence wall thickening, ejection fraction (volume fraction of blood pumped out of the ventricle with each heart beat) [8] and ventricular torsion (an index of the “wringing” motion of the heart) [9, 10]. Assessing myocardial heterogeneity in terms of cardiac function can be extremely useful when understanding human heart failure.

1.1.1. Heart failure and the left ventricular wall

Heart failure is a debilitating clinical syndrome in which the ventricles are unable to pump sufficient blood to meet the body’s metabolic demands. Currently, there are 5.1 million people in the United States who suffer from this syndrome. This

population is on the rise because advancing age is the number one risk factor for heart failure and 1 in 5 Americans will be >65 years of age by 2050 [11].

The progression of heart failure is classified into stages A through D by the American College of Cardiology Foundation (ACCF) and American Heart Association (AHA) and/or stages I through IV by New York Heart Association (NYHA). ACCF/AHA classification provides information about the progression of structural changes in the heart and NYHA classification yields information about the diminishing ability of patients to carry out physical activities. Some of the symptoms of heart failure are shortness of breath, fatigue and edema [11].

Heart failure can be divided into 2 groups-systolic heart failure and diastolic heart failure. In systolic heart failure the heart is not able to maintain cardiac output because of reduced ejection fraction (≤ 40%). In diastolic heart failure the ejection fraction is preserved (≥ 50%) but patients exhibit symptoms of heart failure such as, shortness of breath. Currently, it is much more difficult to diagnose diastolic heart failure but it is estimated that half of the patients with heart failure have diastolic dysfunction [11-13].

There are several causes of heart failure, which include hypertension, ischemia, genetic mutations (mutations in at least 10 sarcomeric genes have been identified) [14-16] or the cause maybe idiopathic (unknown) [11]. Even though the etiologies are varied there are common pathophysiological changes that occur in heart failure, called ventricular remodeling. Due to the complex nature of ventricular remodeling a consensus statement was released in the Journal of the

American College of Cardiology stating "*Cardiac remodeling may be defined as genome expression, molecular, cellular and interstitial changes that are manifested clinically as changes in size, shape and function of the heart after cardiac injury*" [17].

Ventricular remodeling can be adaptive at first but with progression of heart failure it can become maladaptive [17, 18]. Depending on the stressors there can either be concentric hypertrophy (thickening of the left ventricular wall by addition of myocytes in parallel) or cardiac dilation/eccentric hypertrophy (thinning of the left ventricular wall through alignment of myocytes in series and enlargement of the ventricular chamber) [19, 20] (Figure 1.3). Any of these modifications can potentially affect the ventricular wall transmurally [21].

1.1.1.1. End-stage heart failure

There are ~50,000 patients with end-stage heart failure (classified as stage D or IV) at any given time in the United States. These patients have structural heart disease (mostly severely dilated ventricles [13], Figure 1.3) and are unable to carryout any physical activity [11]. These patients generally have an ejection fraction of ≤ 20% [13]. At this stage the options for therapy are few and involve chronic inotropes, mechanical circulatory support and/or heart transplant surgery [11, 22]. Due to the limited number of available donors there are only ~ 2300 heart transplants each year [11].

1.1.2. Imaging studies evaluating transmural ventricular wall function

It is not fully understood how the left ventricle changes transmurally during heart failure. There are some imaging studies that have shown changes in fiber angle orientation [23, 24] with heart failure. For example, a study induced a myocardial infract in sheep and after 3 months excised the hearts and evaluated the hearts using diffusion tensor imaging. The authors showed that the mid-myocardial and the sub-epicardial fibers were disorganized and there were changes in fiber angles [25] that could ultimately lead to pump dysfunction.

In a quest to find better prognostic tools, several clinical studies in patients with cardiac dysfunction have shown that the shortening of the middle transmural region ($p=0.001$) of the ventricular wall is a better predictor of cardiovascular death, myocardial infarction and stroke than shortening of the endocardial region ($p=0.089$) and the gold standard ejection fraction ($p=0.085$) (Table 1.1 [26]). These results are surprising because ejection fraction (a measure of global ventricular function used in standard clinical practice) was not a good predictor of clinical end-points when compared to midwall shortening, which is an indicator of ventricular wall motion. These imaging studies have shown that transmural effects are clinically important and may potentially be of better prognostic value in predicting clinical endpoints [26-30]. However, the underlying mechanisms that give rise to these transmural effects are still unclear and may include tissue, cellular and molecular level heterogeneity in the ventricular wall.

1.1.2.1. Transmural tissue level changes in the ventricular wall

The myocardium is predominantly made up of myocytes and cardiac fibroblasts [31]. Cardiac fibroblasts are essential for extracellular matrix protein production and become hyperactive after injury or stress, which leads to fibrosis. Collagen protein makes up ~80% of the extra cellular matrix [31]. With heart failure there maybe an increase in fibrosis [31, 32], replacement of myocytes with fibrotic tissue and myocyte disarray [18, 33, 34]. These modifications can have detrimental effect on both the electrical and mechanical activity of the heart. For example studies have shown that discontinuities due to fibrosis can lead to conduction abnormalities and arrhythmias [34-36]. The replacement of myocytes with fibrotic tissue can also reduce the number of force generating sarcomeres, which can ultimately lead to reduction in contractile function [37].

Recent clinical studies have investigated the effect of the regional distribution of fibrosis through the ventricular wall and its effect on myocardial contractile properties using late gadolinium enhancement cardiovascular magnetic resonance. They found that midwall fibrosis may predict adverse cardiovascular outcomes in patients with cardiac dysfunction [38-40]. These studies allude to a region dependent increase in fibrosis. However, few studies have investigated the regional distribution of fibrosis across the left ventricular wall and its effect on cellular level contractile properties.

1.1.3. Cellular and molecular level transmural heterogeneity

Previous studies have demonstrated that there are distinct differences in action potential morphologies and action potential duration between the sub-epicardium, mid-myocardium and sub-endocardium of the left ventricles in various mammals including humans [41]. In heart failure there can be a reduction in the difference between the transmural action potential duration across the ventricular wall leading to arythmogenesis [42, 43]. Some of these changes are due to modifications in expression of several cardiac transporters and ion channels across the ventricular wall [44].

There are few reports in the animal-based literature which show that different regions of the left ventricular wall exhibit variable contractile properties [45 46 47]. van der Velden *et al.* [47] isolated sub-epicardial and sub-endocardial samples from the left ventricular wall of pig hearts 3 weeks after an induced myocardial infraction or a sham operation. They found that maximum force decreased by 35% in the sub-endocardial samples in the myocardial infract group when compared to sub-endocardial samples in the sham group.

In summary, the heart is a heterogeneous organ evidenced by transmural differences in myocardial architecture and fiber angles [2-5]. There are also cellular and molecular level differences which contribute to transmural differences in excitation of the left ventricular wall [36, 42-44]. However, transmural changes that may contribute to cellular level contraction have not been explored in aging and human heart failure.

1.2. Sarcomere function in the heart

1.2.1. Contraction and sarcomeric proteins

Sarcomeres are basic units of muscle, organized in series and in parallel in the cytosol of a myocyte. They are made up of thick and thin filaments, which slide past each other to undergo contraction [48, 49] (Figure 1.4). The z-disks of a sarcomere contains many different proteins including desmin, an intermediate filament protein which acts as a scaffold and connects sarcomeres at z-disks [50]. Six titin proteins (the biggest protein in the human body, ~33 MDa) span from the z-disk to the m-line of the sarcomere [51].

The cross bridge is a hexamer made up of two myosin heavy chains (MHC) whose tails polymerize with each other to form the thick filament. Attached to a MHC neck region are two proteins called the myosin light chain-1 (MLC-1) and myosin light chain-2 (MLC-2). On the head region of a MHC is an ATP binding site [52, 53] (Figure 1.4).

The thin filament is made up of a polymerized actin backbone. Tropomyosin a filamentous protein winds itself around every 7th actin on the thin filament and blocks the actin binding sites from myosin in the relaxed state [54]. Bound to tropomyosin is the troponin complex, which is made up of cardiac troponin T (cTnT) that binds to tropomyosin, cardiac troponin I (cTnI) which is the inhibitory unit that keeps actin and tropomyosin in place in the relaxed state, and cardiac troponin C (cTnC) which is the Ca^{2+} binding subunit [55] (Figure 1.4).

Before contraction can occur Ca^{2+} is released from the sarcoplasmic reticulum and binds to cTnC. This leads to a conformational change in cTnI which removes its inhibition and allows tropomyosin to move and expose the binding sites on actin for myosin to attach [56]. Myosin hydrolyzes ATP and binds to actin and undergoes a power stroke sliding the thin and thick filaments past each other causing contraction. After contraction has occurred Ca^{2+} in taken up by the sarcoplasmic reticulum through the sarcoplasmic reticulum Ca^{2+}-ATPase (SERCA) pump and thin filament proteins go back to their relaxed state. At the same time ATP binds to myosin allowing myosin to go back to its relaxed state [48, 49, 52, 56].

1.2.2. Mechanics of the heart

The heart must perform work against an afterload on a beat-to-beat basis to maintain cardiac output. This is not an easy task because ventricular filling and ejection is not uniform for every beat. The heart is able to correct for these changes due to the Frank-Starling mechanism (Figure 1.5). This mechanism is the intrinsic ability of the heart to change the force of contraction and therefore cardiac output in response to alteration (increase or decrease) in the end diastolic volume [57].

At the myocyte level, preload (the volume of blood during ventricular filling) stretches the myocytes, which in turn increase the sarcomere length. In this phase cytosolic Ca^{2+} concentration is ~100 nM and there are very few thick and thin filaments interactions. During contraction the Ca^{2+} concentration increase

upto ~1 μM which leads to thin filament activation [58]. At this phase cross bridges are able to attach to actin and undergo a power stroke leading to myocyte shortening and force production. This action allows the heart to generate power and perform work against an afterload (aortic pressure) [55, 59].

The process of contraction and relaxation are made of active and passive mechanical components. The active mechanical component is primarily due to the interaction of myosin motors on the thick filament with actin on the thin filament [60, 61]. The passive component is primarily due the sarcomeric protein titin and extracellular matrix protein collagen [62].

Furthermore, preload, afterload and contractility can all affect the Frank-Starling mechanism (Figure 1.5) of the heart and are highly regulated through alteration in content, isoform switch and posttranslational modifications of sarcomeric proteins [63]. Therefore, dysfunction in sarcomeric proteins can lead to mechanical pump dysfunction [63] and thus contribute to diastolic and/or systolic heart failure. The modification in sarcomeric proteins and its functional consequence will be discussed further in Chapter 3, 4 and 5.

1.3. Overall hypothesis and scope of this dissertation

The overall hypothesis of this dissertation is that normal left ventricles exhibit transmural heterogeneity in cellular level contractile properties and with aging and heart failure there are region-specific changes in cellular level contractile mechanisms.

In Chapter 3, we investigate the adaptive limits of myocytes before the onset of heart failure in a rodent model of aging. We evaluate the biochemical status of proteins that are involved in Ca^{2+} handling and contraction from the sub-epicardium, mid-myocardium and sub-endocardium of the left ventricular free wall of aging F344 rats.

In Chapter 4, we investigate the mechanical properties of ventricular samples from patients with end-stage heart failure where the hearts had already become maladaptive. Functional measurements were performed in chemically permeabilized multicellular preparations. These biospecimens were optimal for testing myofibrillar-level function and for investigating the effects of the extracellular matrix on passive mechanical properties. We also investigate biochemical status of sarcomeric proteins and the extent of fibrosis in through-wall left ventricular samples from the sub-epicardium, mid-myocardium and sub-endocardium of non-failing and failing human hearts.

In summary, we used both rodents and human biospecimens to investigate cellular and molecular modifications that affect properties involved in both relaxation and contraction across the ventricular wall to understand cellular level transmural effects in aging and end-stage heart failure.

Table 1.1. Predictors of cardiovascular endpoints.

Univariate baseline predictors of composite cardiovascular endpoints

	HR	95% CI	*P*
Systolic BP (10 mmHg)	1.00	0.861–1.156	0.976
Diastolic BP (10 mmHg)	0.90	0.723–1.130	0.375
Heart rate (10 bpm)	1.05	0.882–1.255	0.572
EFS (%)	0.96	0.915–1.006	0.089
Ejection fraction (%)	0.97	0.938–1.004	0.085
Stress-corrected fractional shortening (%)	0.99	0.978–1.005	0.217
MWS (%)	0.83	0.741–0.927	0.001
Stress-corrected MWS (%)	0.98	0.965–0.997	0.021
LVMI (g/m^2)	1.01	1.008–1.016	0.050
Relative wall thickness (per 0.05)	1.58	1.05–18.0	0.032

BP, blood pressure; CI, confidence interval; EFS, endocardial fractional shortening; HR, hazard ratio; LVMI, left ventricular mass index; MWS, midwall shortening.

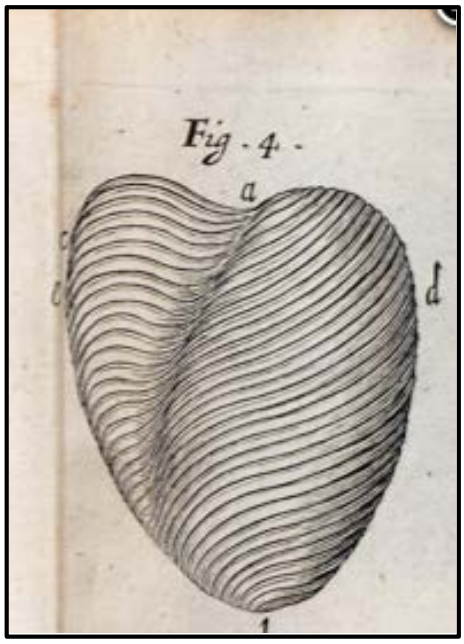

Figure 1.1. An illustration of the spiral myocardial fibers.

A sketch of the spiral myocardial fibers observed by Richard Lower from the anterior side of the heart (Figure 4, adapted from the book "*Tractatus de corde*", 1669 [2]).

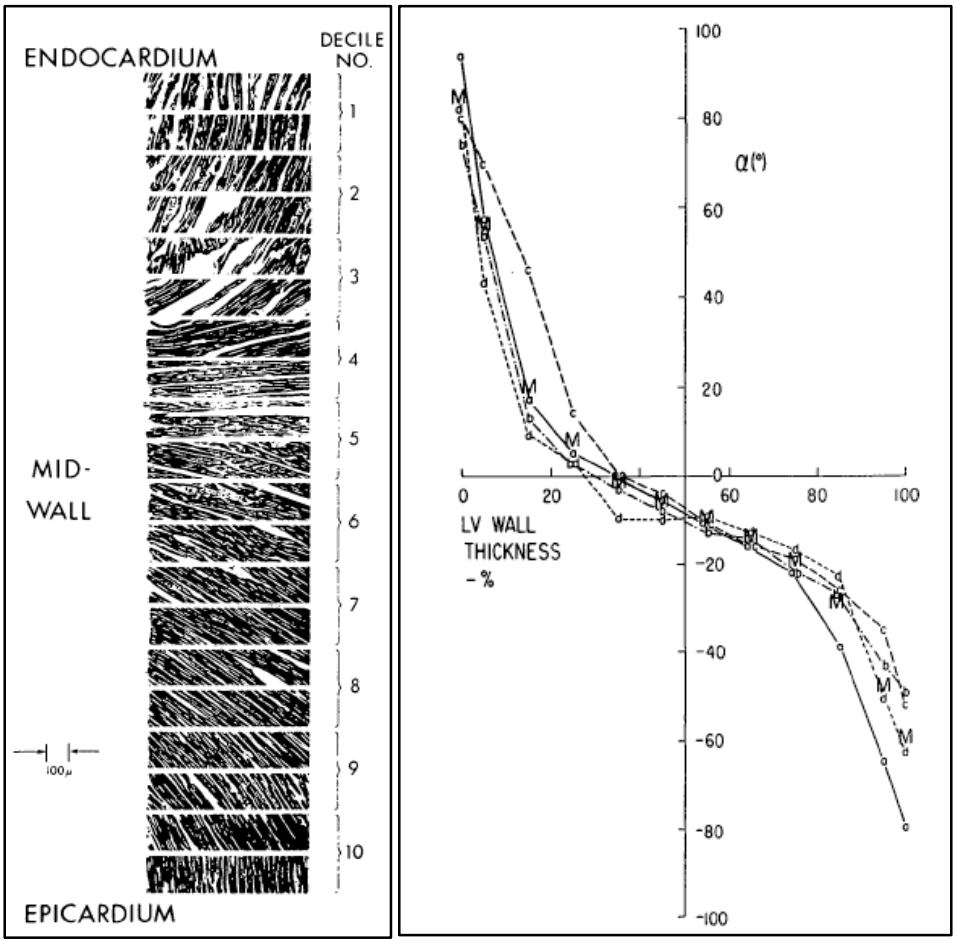

Figure 1.2. Photomicrographs of histological sections and fiber angles.

Typical sequence of photomicrographs showing fiber angles in successive sections taken from a heart in systole. The sections are parallel to the epicardial plane. Fiber angle is +90° at the endocardium, running through 0° at the midwall to -90° at the epicardium. The sequence of numbers refers to deciles of wall thickness (left panel). Fiber angles for four sampling sites, a through d, in section from a heart in diastole are plotted as a function of percent wall thickens. Zero percent of wall thickness implies the endocardial surface. M represents the mean of the data at these four sites. (Figure 3 and 4, adapted from Street *et al*.1969 [5])

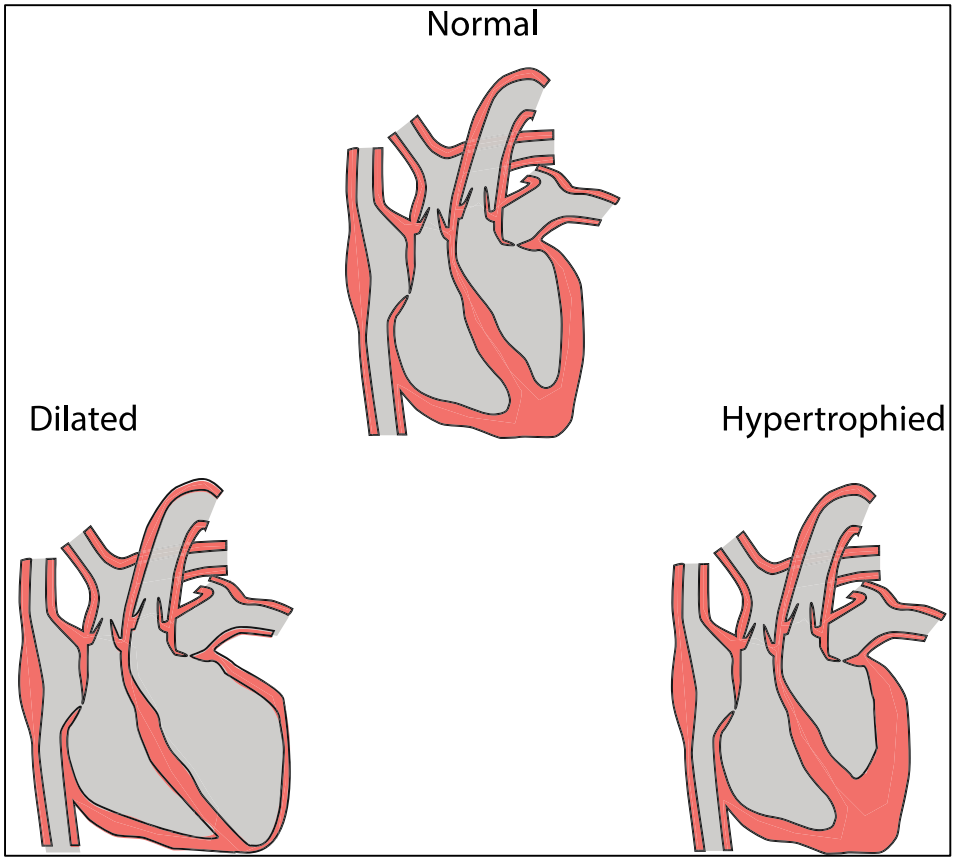

Figure 1.3. Pathological changes with progression of heart failure.

Dilated (left) and hypertrophied (right) heart showing left ventricular remodeling.

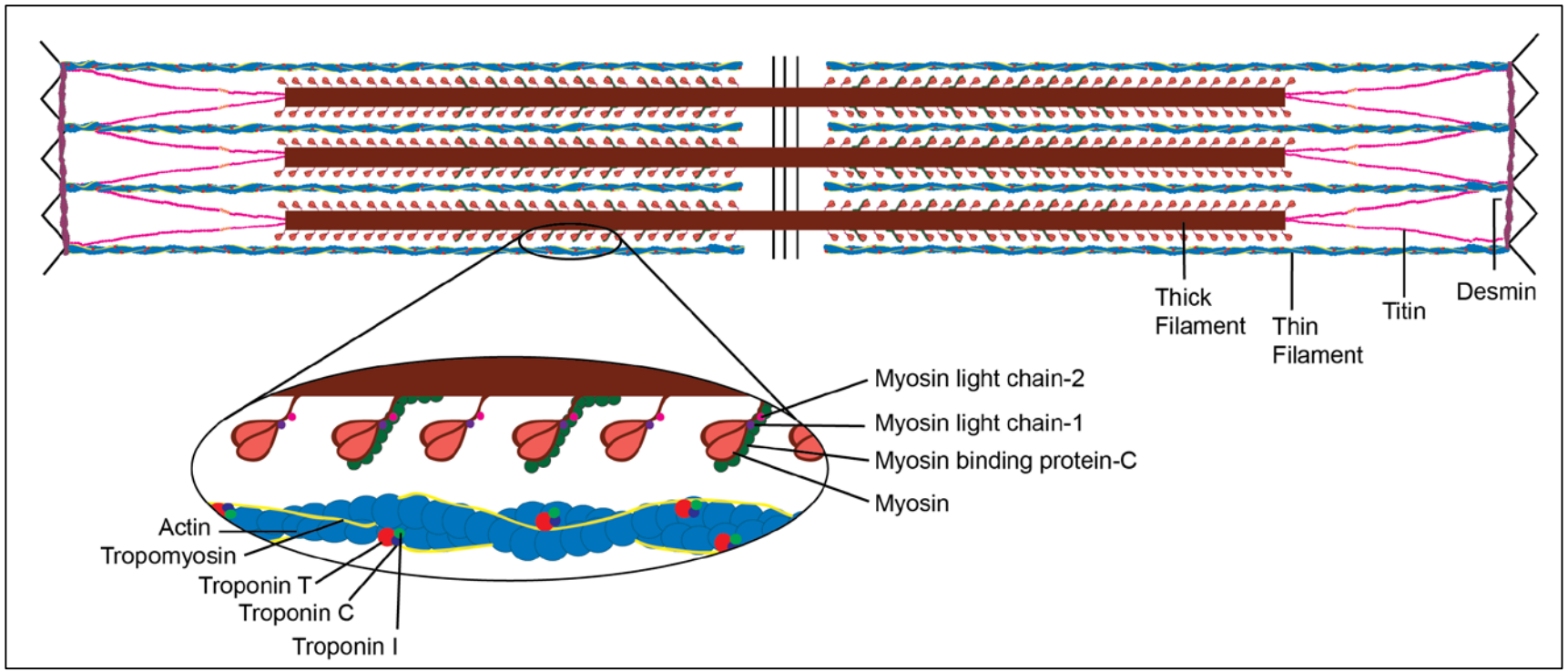
Thick Filament
Thin Filament
Titin
Desmin
Myosin light chain-2
Myosin light chain-1
Myosin binding protein-C
Myosin
Actin
Tropomyosin
Troponin T
Troponin C
Troponin I

Figure 1.4. Sarcomere.

Schematics of the major sarcomeric proteins.

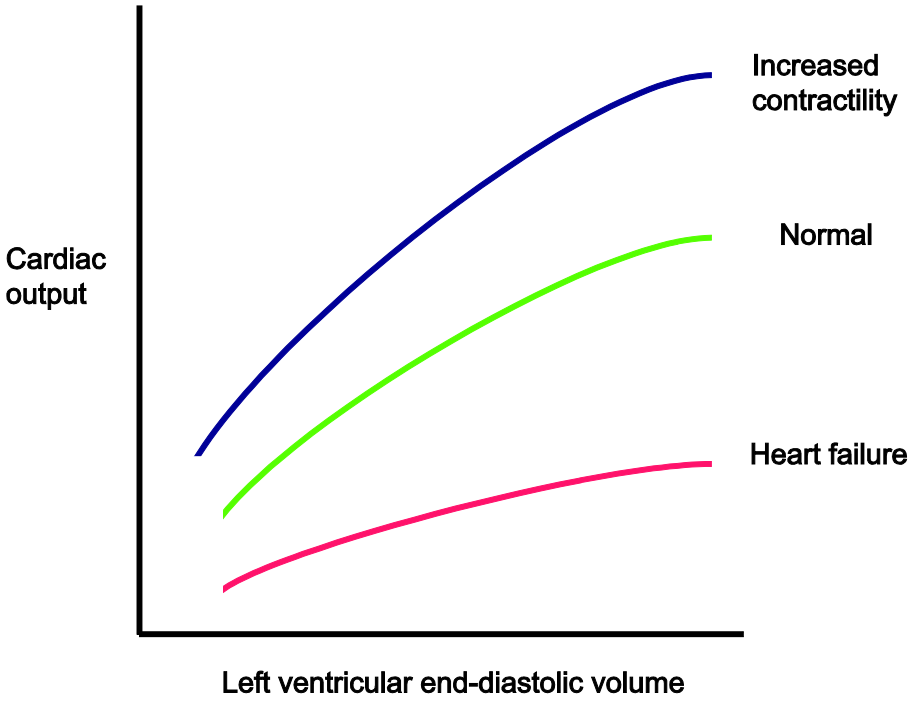

Figure 1.5. Frank-Starling mechanism of the heart.

The curves show the change in cardiac output for a given ventricular diastolic volume when there is increased contractility (dark blue curve), in a normal resting heart (green curve) and in a failing heart (red curve).

Chapter 2. Methods

2.1. Animal model and human cardiac tissue

2.1.1. Aging F344 rats

Female Fischer 344 rats were obtained from the National Institute on Aging colony maintained by Harlan (Indianapolis, IN). The rats purchased were of 6, 18, and 22 months of age (n=3 animals per age group). All animal procedures were approved by the University of Kentucky Institutional Animal Care and Use Committee and conformed to standards of the Guide for the Care and Use of Laboratory Animals.

We harvested the heart from each animal by first injecting heparin (800 U IP) and then anesthetizing each animal with an intraperitoneal injection of pentobarbital (50 mg/kg). We dissected the chest wall to expose the thoracic cavity and excised the heart rapidly. This heart was then cannulated at the aorta and the coronary arteries were perfused with ice-cold Krebs Henseleit solution (in mmol/L: 113 NaCl, 4.7 KCl, 0.6 KH2PO4, 1.2 MgSO4, 12 NaHCO3, 10 KHCO3, 10 4-(2-hydroxyethyl)-1-piperazineethanesulfonic acid [HEPES], 30 Taurine, 5.5 glucose, and 10 2,3-butanedione monoxime [BDM]) until the perfusate ran clear of blood from the coronaries.

The heart were then hung from a Langendorff perfusion apparatus and enzymatically digested for 10–12 min at 37°C with digestion solution (Krebs Henseleit containing 10 mM BDM, 20 μM $CaCl_2$, and 46 μg/ml Liberase TH, Roche Applied Science, Indianapolis, IN). After the initial digestion step, the left ventricular free wall was dissected and sectioned transmurally into three portions of equal thickness (sub- epicardium, mid-myocardium, and sub- endocardium), Figure 2.1 [64]. These tissues were then flash frozen in liquid nitrogen and then stored in -80°C for biochemical assays.

A separate set of F344 animals of ages 6, 18 and 22 months were used to assess left ventricular function using echocardiography. These animals were later sacrificed and the hearts were excised and perfused in the same fashion as mentioned above but were not flash frozen. Tissues from the three different regions were digested further and single myocytes were isolated. Ca^{2+} transients and unloaded shortening contractions were measured using electrically-excitable myocytes from the sub-epicardial, mid-myocardial and sub-enodcardial regions of the hearts. A computational model was also generated to predict how the sarcomere length of an unloaded myocyte would change in response to an intracellular Ca^{2+} transient [65]. These set of experiments were not a part of this dissertation but the results were used to make inferences about the biochemical results from the F344 aging rats.

2.1.2. Human cardiac biospecimens

2.1.2.1. Procurement and cryo-preservation of biospecimens

We obtained ventricular through-wall samples from patients undergoing heart transplants at the University of Kentucky and from organ donors who did not have prior history of heart failure through the Kentucky Organ Donors Affiliates (KODA). Figure 2.2 shows an external view of one donor and one failing human heart. We cut left ventricular tissue sections from the free wall just above the apex as soon as the heart was excised from the body by the surgeon and was passed to us. We then transported the tissue to the laboratory in specimen cups containing saline slush. We split the tissue sections transmurally into three parts of equal thickness to form the sub-epicardial, mid-myocardial and sub-endocardial samples. These specimens were then placed in 2 mL cryogenic vials, flash-frozen in liquid nitrogen, and subsequently stored at -150°C in the vapor phase of liquid nitrogen. All procedures were approved by the University of Kentucky Institutional Review Board and subjects gave informed consent.

2.1.2.2. Clinical characteristics of patients and donors

We studied left ventricular tissue from patients in end-stage heart failure receiving heart transplants and from organ donors. We had 5 patients with non-ischemic and 5 with ischemic heart failure in this study. The mean age of the patients with heart failure was 49 (range 20 to 65) while that of the organ donors

was 35 (range 18 to 59). Females donated 20% of the failing hearts and 50% of the non-failing organs. Data describing the patients and donors are shown in Table 2.2.

2.2. Muscle mechanics

We performed mechanical assays on chemically permeabilized multicellular preparations obtained from human hearts. We analyzed a total of 141 multicellular preparations from 48 samples (3 transmural regions from each of 6 non-failing and 10 failing human hearts). Jweied *et al.* showed that previously frozen and fresh tissue samples yield comparable data with these techniques [66]. We saved the permeabilized samples that were not used for functional tests for subsequent biochemical assays. Following sub-sections describe the overview of the procedures to prepare and perform these biophysical assays.

2.2.1. Solutions

We used relaxing solution to isolate multicellular preparations that contained (in mmol L^{-1}): 100 KCl, 10 imidazole, 4 ATP, 2 EGTA and 5 $MgCl_2$ and two protease inhibitors (phenylmethylsulfonide 500 µmol L^{-1} and leupeption 40 µmol L^{-1}). We used pCa (= $-\log_{10}[Ca^{2+}]$) solutions for the mechanical experiments which contained (in mmol L^{-1}): 20 imidazole, 14.5 creatine phosphate, 7 EGTA, 4 MgATP, 1 free Mg^{2+}, free Ca^{2+} ranging from 1 nmol L^{-1} (pCa 9.0) to 32 µmol L^{-1} (pCa 4.5) and sufficient KCl to adjust the ionic strength to 180 mmol L^{-1}. The

precise composition of each pCa solution was determined using Maxchelator software (version 2.50) and NIST stability constants [67].

2.2.2. Chemically permeabilized multicellular preparations

We obtained multicellular cardiac preparations as previously described for rat samples [68]. We took frozen tissue specimens (~5 x 5 x 5 mm) acquired using the methods mentioned in section 2.1.2.1 and placed it in 10 ml of relaxing solution (see section 2.2.1 for solutions). We then mechanically disrupted the tissue using a tissue homogenizer (Polytron, Brinkman Instruments, Westbury, NY), and chemically permeabilized the tissue using Triton X-100 (30 min, 1% v/v). We then stored the permeabilized samples in relaxing solution at 4°C for upto 12 hours before use (Figure 2.3).

2.2.3. Mechanical assays with varying Ca^{2+} concentrations

We attached individual preparations (Figure 2.4) between a force transducer (resonant frequency 600 Hz, model 403, Aurora Scientific, Aurora, Ontario, Canada) and a servo motor (step time 0.6 ms, model 312B, Aurora) by crimping their ends into metal troughs (shaped from 27 gauge tubing) with overlays of 4-0 nylon monofilament as previously illustrated in Figure 1B of Campbell & Moss [69] (Figure 2.3). The experimental temperature was 15°C. We stretched the sample in pCa 9.0 solution (see section 2.2.1 for solutions) by manually adjusting the manipulator holding the motor until the mean sarcomere length of the preparation

(measured by video microscopy) was within 1% of 2.20 µm. We estimated the cross-sectional area ($2.17 \pm 0.07 \times 10^{-8}$ m^2) from the video images by assuming that each preparation had a circular profile. Once the sarcomere length was set the average length of the preparations was calculated to be 688 ± 11 µm. If it is assumed that single human myocytes [70] have average dimensions of 100 x 25 x 25 µm, and that the relative collagen content of the preparations ranged from 5 to 58%, each myocardial preparation probably contained between 13 and 30 single myocytes.

Initially each preparation was immersed in pCa 4.5 solution to maximally activate the sample. Once tension had attained steady-state, we subjected the muscle to 3 'saw-tooth' lengthening/shortening perturbations (magnitude 0.04 l_0, velocity of 0.12 l_0 s^{-1}, inter-perturbation interval 100 ms, where l_0 is the muscle length) and a rapid shortening/re-stretch maneuver (0.2 l_0, 20 ms duration) before it was returned to pCa 9.0 solution (Figure 2.5). This protocol has been described previously [68, 71]. We subsequently performed similar trials for each preparation using solutions with pCa values ranging from 9.0 to 5.0.

2.2.3.1. Tension-pCa curves

Tension-pCa curves were generated with isometric force values measured in these trials and by fitting the raw data to an equation of the form

$$y = A + B\frac{\left[Ca^{2+}\right]^n}{\left[Ca^{2+}\right]^n + \left[Ca_{50}^{2+}\right]^n} \quad (1)$$

where A corresponds to passive force, B represents Ca^{2+} activated force, n is the Hill coefficient, and $\left[Ca_{50}^{2+}\right]$ is the free Ca^{2+} concentration required to develop half the maximum Ca^{2+}-dependent force.

2.2.3.2. Rate of tension recovery

After the rapid shortening/re-stretch maneuver, the rate of tension recovery (k_{tr}) was calculated by fitting a single exponential function to the recovery time-course as -ln(1/2)/($t_{1/2}$), where $t_{1/2}$ is the time required for tension to rise from the Presid to 1/2(Pmax + Presid) and where Pmax is the maximum tension attained after restretch. Presid was defined as the minimum tension occurring after restretch (Figure 2 of Campbell, 2006 [72]).

2.2.3.3. Short-range force and short-range stiffness

Short-range force and short-range stiffness values were calculated for each stretch response at each level of Ca^{2+} activation. The short-range force is the non-linear force response due to strained cross bridges when the preparation is stretched by 4% of the original length at a speed of 0.12 l_0 s^{-1}after the preparation reached steady state. Short-range force was determined using the algorithm

illustrated in Figure 2A of Mitov et. al., 2009 [68]. Short-range stiffness values are expressed as Young's Moduli and were calculated by fitting regression lines to the force responses measured during imposed 4% length changes [68].

2.2.4. Force-velocity assays

Once we completed the measurements at intermediate Ca^{2+} levels (section 2.2.3), the preparation was re-activated in the pCa 4.5 solution. After force had reached the steady-state for this condition, we initiated a sequence of trials in which the preparation was allowed to shorten for 75 ms against a variety of pre-set loads (Figure 2.6A). This technique was used to establish the preparation's force-velocity curve. We determined the shortening velocity for each trial from the slope of a regression line fitted to the final 50 ms of the force clamp [73]. The average r^2 value for these lines was 0.991 which indicates that the velocity of interfilamentary movement was not markedly dependent on the total distance shortened [74, 75].

A hyperbolic curve was fitted to the force-velocity data using Hill's equation

$$(F + a)\cdot(V + b) = (F_0 + a)\cdot b \qquad (2)$$

where F is the force at shortening velocity V, and F_0 is the maximum isometric force [76]. The constants a and b have dimensions of force and velocity respectively. Power values were calculated as the product of force and velocity (Figure 2.6B).

We performed all mechanical tests using SLControl software [77]. We performed curve-fitting and data analysis using custom software written in MATLAB (Mathworks, Natick, MA).

2.3. Histology

We evaluated the relative collagen content of human myocardial tissue studied in this work by picrosirius red staining and bright field imaging [78].

The tissue samples were first transferred from long-term storage in the vapor phase of liquid nitrogen to a cryostat maintained at -26°C. The samples were then placed in 10 x 10 x 5 mm cryomolds and were covered with optimal cutting temperature (OCT) medium (Schaumburg, IL). We then cut the samples into 10 µm sections and air dried them on glass slides for 1 hour at room temperature. The staining method used was similar to the one described by Hanley *et al.* [79]. The slides were initially covered in Bouin's fixative solution and incubated at 56ºC for an hour. Next, we rinsed the slides in deionized water and placed them for 2 hours in a 0.1% Sirius red solution (w/v) dissolved in 1.3% saturated picric acid. We then washed the slides with 0.5% acetic acid, dehydrated in 95% and 100% ethanol, and finally equilibrated them in xylene [79]. We then imaged the sections, which had an average cross-sectional area of ~16 mm^2 in bright field [78] with a 10x objective (Olympus BX61VS microscope) and analyzed the images using custom software written in MATLAB (The Mathworks, Natick, MA). For this work

we analyzed a total of 150 images (1-6 images from each region of each heart) in duplicate by observers who were blinded to the experimental groups.

2.4. Biochemical assays

2.4.1. Assessment of Ca^{2+} handling and sarcomeric proteins modified by aging in the myocardium of F344 rats

2.4.1.1. Phosphorylation of sarcomeric proteins

We examined the relative phosphorylation of selected sarcomeric proteins MLC-2, cTnI, cTnT, and tropomyosin using gel electrophoresis (n = 3 animals/age group). We prepared the samples by homogenizing small pieces of ventricular tissue (described in section 2.1.1) in a urea-thiourea sample buffer (in mol L^{-1}, 8 Urea, 2 Thiourea, 0.075 M DTT, and 0.05 Tris-HCl, with 3% SDS w/v, pH 6.8) [80]. We measured the protein concentration in each sample using a Lowry protein assay (RC-DC kit, Bio-Rad, Hercules, CA). We then modified each sample by adding 0.03% Bromophenol blue and 30% glycerol before boiling it at 95°C for 3 min and subsequently cooling it on ice. We then loaded precast polyacrylamide gels (Mini-Protean TGX 10%, 15-well combs, Bio-Rad) with 3 µl of each sample (protein concentration 1 µg/µl) and ran the gel at 200 V for 30 min. We stained each gel with Pro-Q Diamond phosphoprotein gel stain (Invitrogen, Carlsbad, CA), scanned the gel using a Typhoon Trio+ imager (GE Healthcare, Piscataway,

NJ), restained the gel with SYPRO Ruby (Invitrogen), and finally scanned the gel again. We quantified the phosphorylation levels by integrating the densitometry profile (ImageQuant TL software, GE Healthcare) of each band in the Pro-Q Diamond image and dividing that result by the corresponding integral calculated for the SYPRO Ruby stained image. We calculated relative phosphorylation levels for the different samples by normalizing to data obtained using an external control [81] myocardial sample that was run on each gel and which was subsequently expressed relative to the data for a single 6-month-old epicardial sample.

2.4.1.2. Content of α- and β-MHC isoforms

We determined the relative content of the α- and β-MHC isoforms in the tissue homogenates using gel electrophoresis. As described by Tikunov [82], we extracted myosin from the tissue homogenates using a buffer containing 100 mM KCl, 100 mM KH_2PO_4, 50 mM K_2HPO_4, 10 mM EDTA, 10 mM $Na_4P_2O_7 \cdot 10H_2O$, 4 mM β-Mercaptoethanol and 5% (vol/vol) Triton X-100 (pH 6.5, 4–8°C, 100-µl volume, 24 h). We then added Laemmli buffer (80 µl) to each sample, after which it was heated to 95°C for 4 min. We then resolved the treated samples using gels that were 60 × 80 × 0.75 mm and contained 7% acrylamide (50:1 with bis-Acrylamide) and 35% glycerol. We ran these gels at a constant current of 3.0 mA for ~18 h at 4°C and subsequently silver stained the gels with a commercial kit (SilverStain Plus, Bio-Rad). We then obtained scanned images

using a conventional office scanner (V500 Photo, Epson, Long Beach, CA). We determined the relative content of each isoform by fitting the densitometry profiles with asymmetrical Gaussian functions using GelBandFitter software previously developed by our laboratory [83].

2.4.1.3. Expression of SERCA2a

In order to assess the expression of sarco-/endoplasmic reticulum Ca^{2+} ATPase (SERCA2a), we first took 4 µl of each sample (Urea-Thiourea sample buffer; 1 µg/µl protein concentration) and loaded them onto precast polyacrylamide gels (Mini-Protean TGX 4–15%, 15-well combs, Bio-Rad). We ran each gel at 200 V for 30 min and subsequently transferred them onto a polyvinylidene difluoride membrane using a semi-dry transfer cell. We then probed the membrane with an antibody (sc-8094, Santa Cruz Biotechnology) to SERCA2a at a 1:1,000 dilution [84]. We then incubated the membrane with a fluorescent secondary antibody (Alexa Fluor 680 donkey anti-goat IgG, Life Technologies) at a 1:7,500 dilution. Immunoblotted bands were visualized using a LI-COR Odyssey imaging system (LI-COR Biosciences, Lincoln, NE) and analyzed using Odyssey version 3.0 software. As described above for the analysis of myofibrillar proteins, we calculated relative SERCA2a contents by normalizing to data from an external control sample that was run on each gel and subsequently expressed relative to the data for a single 6-month epicardial sample. This facilitated statistical analysis of data from multiple western blots.

2.4.2. Assessment of sarcomeric proteins modified by heart failure in humans

We spun down and froze in eppendorf tubes, chemically permeabilized specimens that had been prepared for functional testing but were not used for that purpose for future biochemical assays. A total of 48 samples were biochemically analyzed in this study (3 regions from 6 non-failing and 10 failing hearts).

Some posttranslational modifications are thought to be regulated on a beat to beat basis in living myocardium and may thus be sensitive to the precise experimental conditions [85]. However, the biochemical data we reported here should be representative of the preparations that were analyzed in the functional measurements.

2.4.2.1. Phosphorylation and content of sarcomeric proteins

The relative content (titin, myosin, cMyBP-C, α-actinin, desmin, actin, cTnI, MLC-1, and MLC-2 and phosphorylation status (titin, cMyBP-C, desmin, cTnI, MLC-1) of key sarcomeric proteins were evaluated using SDS-PAGE.

We homogenized the samples in a urea-thiourea sample buffer and determined the protein concentration in the sample using a Lowry protein assay. We loaded precast polyacrylamide gels (Tris-HCl, 26 well, Bio-Rad, Hercules, CA) with samples containing 1 µg of protein. We ran each gel at 200 V for 55 minutes and

then stained them to assess phosphoproteins using Pro-Q Diamond stain and then re-stained with SYPRO Ruby to assess total protein content (as described in section 2.4.1.1). We calculated relative phosphorylation levels and relative protein contents by normalizing to data obtained for a non-failing sub-epicardial sample that was loaded onto every gel as a control [65].

2.4.2.2. Assessment of titin isoform content and phosphorylation

The relative contents and phosphorylation levels of the N2B and N2BA isoforms of titin was assessed using a vertical agarose gel system [86]. The gel was cast using 1.2% w/v Sea Kem Gold Agarose, 30% v/v Glycerol, 0.05 M Tris-base, 0.384 M Glycine, and 0.1% w/v SDS. We loaded the samples (3 µL at a protein concentration of 1 µg μL^{-1}) on the gels and ran the gels at 4°C at a constant voltage of 40 V for the first 3hours, and then at 70 V for ~4 hours. We stained the gels with Pro-Q Diamond and SYPRO Ruby and analyzed them as described in section 2.4.1.1. We calculated relative phosphorylation levels and relative protein contents by normalizing to data obtained for a non-failing sub-endocardial sample that was loaded onto every gel as a control.

2.4.2.3. Assessment of myosin heavy chain isoform content

We assessed the relative expression of α- and β-MHC using specialized gels cast as described in section 2.4.1.2. We loaded the samples (3 µL at a protein concentration of 1 µg μL^{-1}) made with urea-thiourea sample buffer onto the gels.

We used atrial samples as positive controls. We stained the gels with SYPRO Ruby stain for total protein and imaged and analyzed the gels as described in section 2.4.1.2.

2.4.3. Site-specific phosphorylation of proteins

We performed immunoblotting to assess the site-specific phosphorylation of cTnI and cMyBP-C. We performed experiments investigating the phosphorylation of cTnI at Ser23/24 using commercially available antibodies [87] (PSer23/24, antibody # 4004, Cell Signaling Technologies, Danvers, MA; cTnI, sc-52266, Santa Cruz, Dallas, TX). The antibodies we used to assess site-specific phosphorylation of cMyBP-C at Ser-273, Ser-282, and Ser-302 have been described by Govindan *et al.* [88].

We ran samples (3 µL volume, at a protein concentration of 1 µg μL^{-1}) on 10% precast polyacrylamide gels (Mini-Protean TGX, 15 well, Bio-Rad) for 30 minutes at 200 V and then transferred them onto polyvinylidene difluoride membranes. We first incubated each membrane with the primary antibody (1:1000 dilution) and then with the fluorescent secondary antibody (anti-mouse DyLight 680 for cTnI, PSer23/24 cTnI, and cMyBP-C; anti-rabbit 800 for phosphorylated cMyBP-C, both antibodies from Cell Signaling Technologies) at a 1:7500 dilution. We subsequently visualized all bands using a LI-COR Odyssey imaging system (LI-COR Biosciences, Lincoln, NE) and analyzed the bands using Odyssey V3.0 image analysis software.

We calculated the relative phosphorylation of the site by integrating the densitometry profiles for the phosphorylated protein and total protein bands, and normalizing to data for a single rabbit muscle sample (for phosphorylated and total cTnI) or a non-failing sub-epicardial human sample (for phosphorylated and total cMyBP-C) that was loaded on to every gel as a control.

2.5. Statistics

We analyzed the experimental data in SAS 9.1.3 (SAS Institute, Cary, NC) using linear mixed effects models for A) the aging F344 rat study: incorporating 2 main effects (age and transmural region) and their interaction and B) the human heart failure study: incorporating 2 main effects (condition and transmural region) and their interaction. Post-hoc analyses were performed using the Tukey-Kramer method.

We used the mixed effect model because there was a fixed and a random effect in the experimental designs. The animal ID/subject was a random effect while the transmural region was a fixed effect (the 3 discrete regions-sub-epicardium, mid-myocardium and sub-endocardium).

We assumed compound symmetry for the covariance structure because it is assumed that every observation collected from an animal/subject (random effect) was equally correlated with every other observation from the same subject.

Advantages of using the mixed effect model; for example in analyzing the mechanical experiments for the human heart failure study was that it accounted for an unbalanced design (6 non-failing and 10 failing hearts), allowed for repeated measures (the 3 regions for each subject came from the same heart, therefore the samples were spatially repeated) and the experiments were hierarchically nested (2-3 preparations from the same region). Furthermore, the linear mixed effects model method provided more statistical power than ANOVA when multiple samples are analyzed from each heart.

Similar to a two –way ANOVA the interaction term in the linear mixed effect model tells us if one main effect depends on the other. For example, if the transmural regional pattern changes in the heart failure group when compared to the transmural regional pattern in the non-failing group for a given response then there is an interaction between the heart failure status and the transmural region.

We also analyzed the biochemical data for the aging F344 rat study and the histology and biochemical data for the human heart failure study using the linear mixed model data.

For the correlation plots, linear regression tests were performed in MATLAB (Mathworks, Natick, MA). For all statistical analysis p values less than 0.05 were considered significant. Data were reported as mean $\pm$ SEM.

Table 2.2. Clinical characteristics.

A. Patients with heart failure

Sex	Age (y)	Cardiomyopathy	Medications
F	49	Non ischemic, idiopathic	Diuretic, Inotropes, Digoxin
M	65	Ischemic	Diuretic, ACE inhibitor/ARB, β-blockers, Inotropes, Digoxin, Statin, Insulin
M	63	Ischemic	Diuretic, ACE inhibitor/ARB, β-blockers, Statin
M	49	Non ischemic, idiopathic	Diuretics, Inotropes
M	39	Non ischemic**,** idiopathic	Inotropes, Statin
M	64	Ischemic	Diuretics, β-blockers, Inotropes, digoxin
M	61	Ischemic	Diuretic, ACE inhibitor/ARB, Inotropes, Statin -
F	23	Non ischemic, postpartum	Diuretic, ACE inhibitor/ARB, β-blockers, Inotropes
M	20	Non ischemic, idiopathic	Diuretic, ACE inhibitor/ARB, Digoxin
M	53	Ischemic	Diuretic, β-blockers, Inotropes, Digoxin

B. Donors with Non-failing hearts

Sex	Age (y)	Cause of death
F	31	Stroke
M	59	Stroke
F	18	Head Trauma
F	38	Stroke
M	28	Head Trauma
M	33	Head Trauma

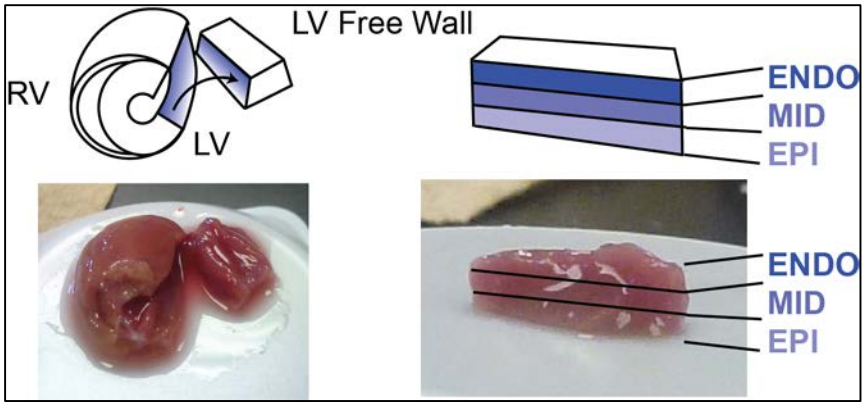

Figure 2.1. Transmural dissection of the left ventricle of a rodent myocardium.

(A) Schematic (top) and images (bottom) of separation of transmural regions from the LV free wall. After hearts were removed from the cannulae, the LV free wall was dissected (left) and separated into three transmural regions: sub-epicardium (Epi), mid-myocardium (Mid), and sub-endocardium (Endo) of even thickness (Figure 1A, adapted from Chung *et al.,* 2013 [64]).

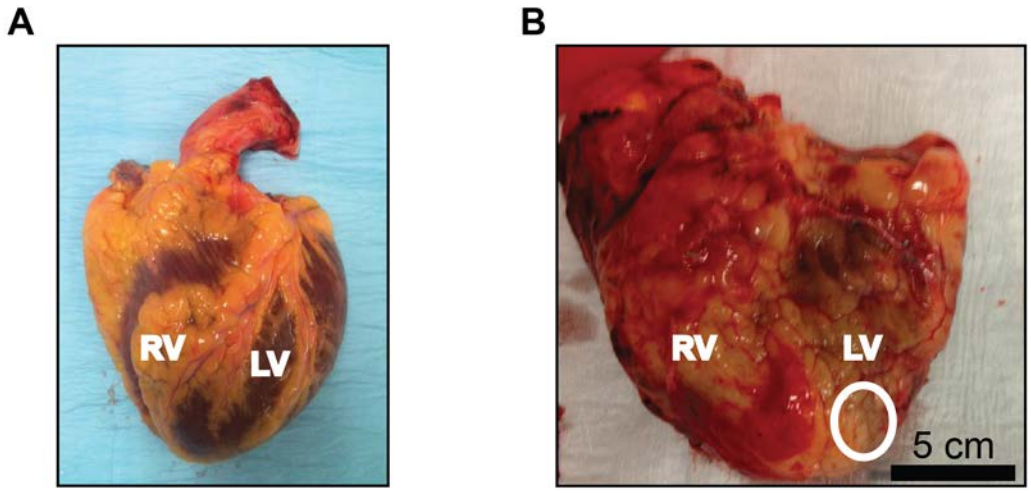

Figure 2.2 External view of human hearts.

A) Non-failing and B) failing heart.

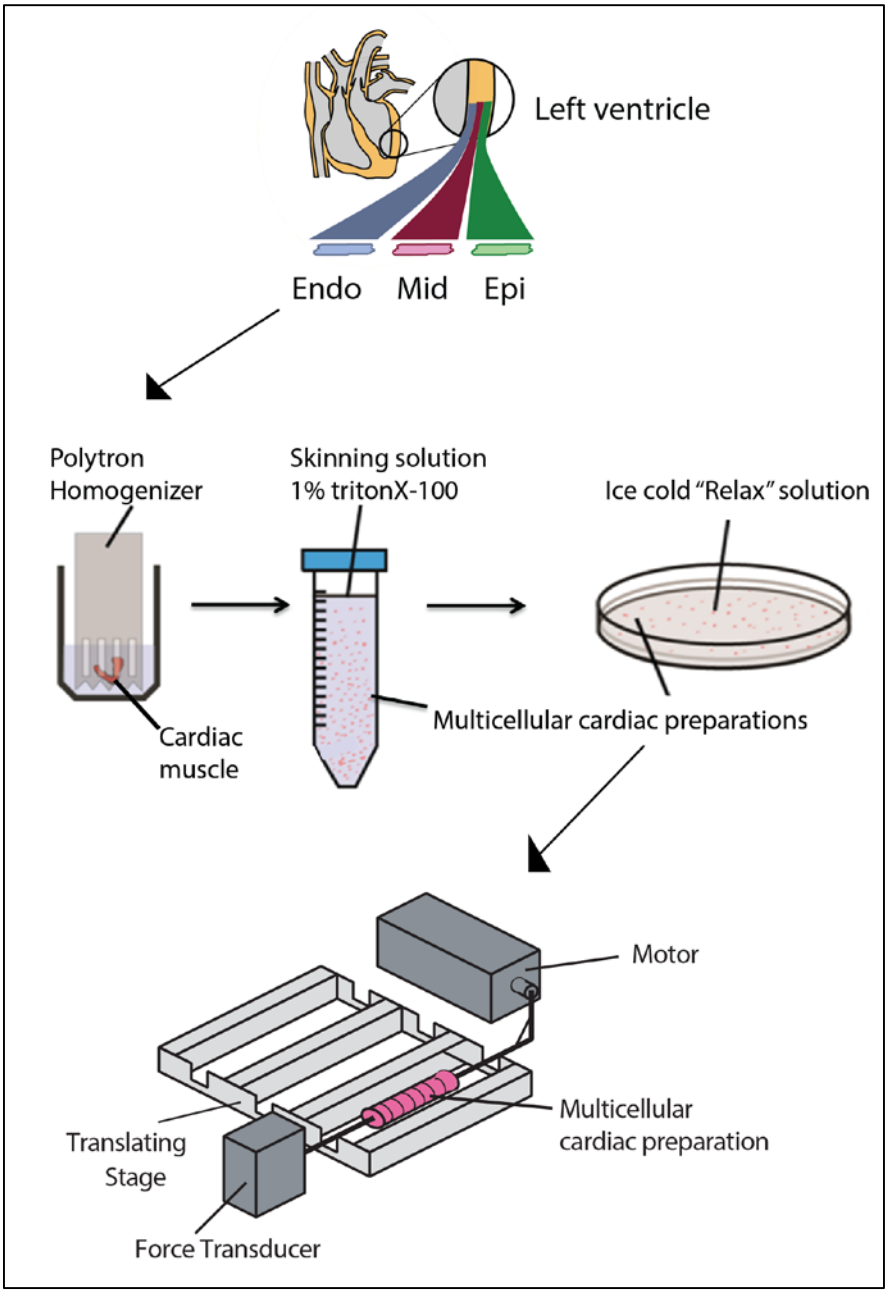

Figure 2.3. Chemically permeabilized multicellular preparation.

A frozen tissue sample from one region of the left ventricular heart was mechanically disrupted and chemically permeabilized and one multicellular preparation was tied between a force transducer and a motor.

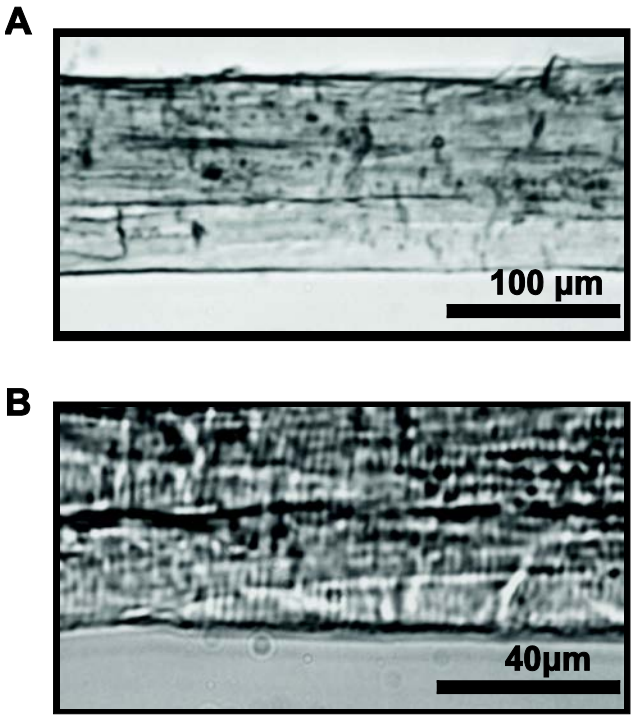

Figure 2.4. Experimental preparations.

A) Low and B) high magnification views of the central section of a representative myocardial preparation immersed in a solution with a pCa value of 9.0.

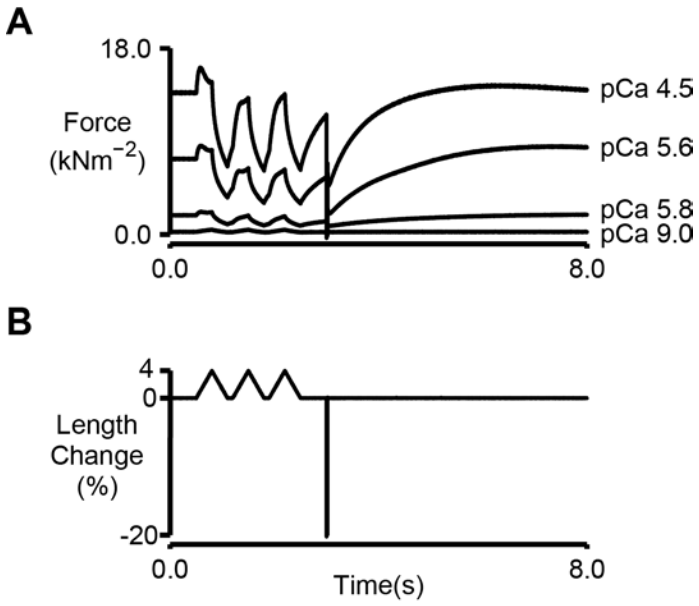

Figure 2. 5. Raw traces of the 3-stretch mechanical protocol with varying Ca^{2+}concentrations.

Representative A) force and B) length records for a multicellular preparation immersed in solutions with different free Ca^{2+} concentrations. The short-range force can be prominently observed as a non-linear force response to the first stretch (4% of l_0). The rate of tension recovery (k_{tr}) is the rate at which tension recovers after the shortening perturbation (20% of l_0).

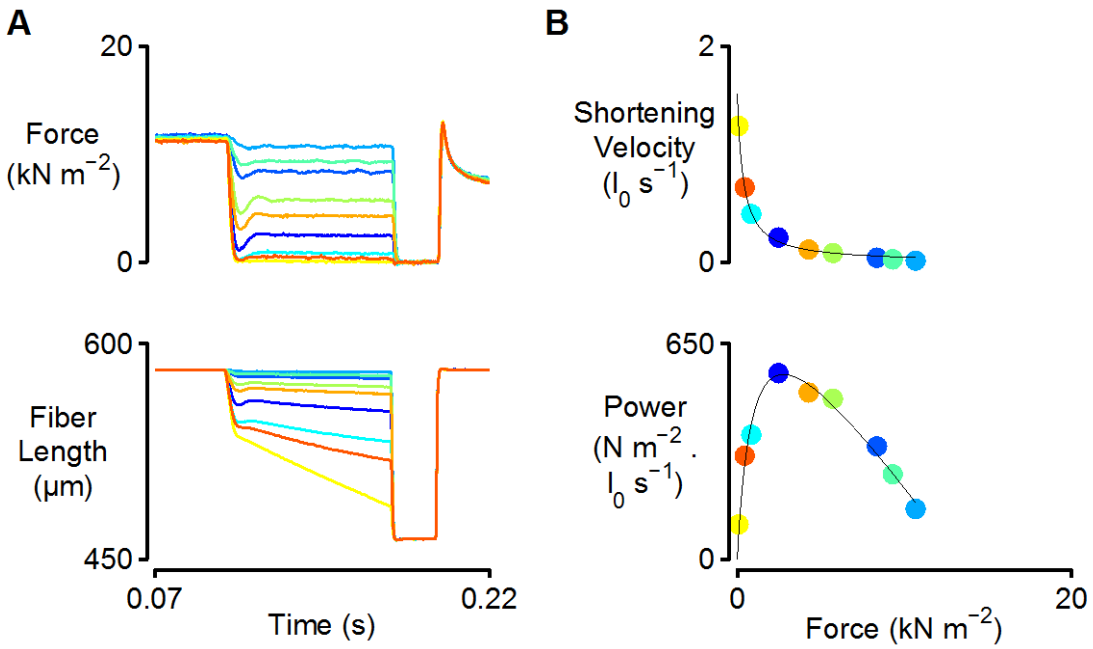

Figure 2.6. Force-velocity raw traces and curves.

A) Superposed force and length records obtained during force-velocity experiments performed with a representative preparation isolated from a multicellular preparation B) Force-velocity (top) and Force-power (bottom) curves for the same preparation. Colors show the corresponding data.

Chapter 3. Decrease in cardiac troponin I phosphorylation contributes to transmural pattern of myocyte relaxation that precede heart failure in aging F344 rats

Aspects of this chapter were reported in the manuscript titled, “Altered ventricular torsion and transmural patterns of myocyte relaxation precede heart failure in aging F344 rats”. American Journal of Physiology: Heart and Circulatory Physiology, September 2013, 305:H676-H686. PMID: 23792678

In this dissertation only the biochemical analysis and interpretation of the biochemical results pertaining to the functional and computational analysis will be discussed.

3.1. Introduction

The lifetime risk of developing heart failure is 20% for Americans ≥ 40 years of age [11, 12, 89, 90]. Epidemiological studies show that ~ 50% of patients with heart failure have diastolic dysfunction and the prevalence of diastolic heart failure increases with age [91]. Patients with diastolic dysfunction have preserved ejection fraction but their ventricles are unable to relax completely when filling with blood. Due to which the heart cannot maintain cardiac output and this can lead to heart failure (Figure 1.5).

Age associated structural modifications like increased myocardial fibrosis [92] and left ventricular remodeling [93] are thought to contribute to ventricular stiffness, a hallmark of diastolic dysfunction [91, 94]. However, growing evidence suggests mechanisms more intrinsic to the myocyte. For example, our laboratory had previously reported that increased myocardial stiffness in aging F344 rats (an animal model of aging-associated heart failure [95, 96]) are potentially due to attached cross bridges during diastole (defined as short-range stiffness) [68]. Furthermore, the increase in ventricular stiffness correlated with the increased proportion of β-MHC in aging [68]. Other studies have reported modifications in Ca^{2+} handling proteins and/or increase in expression of β-MHC to be involved in prolonged myocyte contraction and relaxation in older F344 animals [97, 98].

Age-associated cardiovascular changes can be adaptive at first and potentially beneficial but with progression of age they can become maladaptive and lead to disease [7]. Investigating the age-dependent modifications in myocyte function can therefore reveal aberrant mechanisms that precede heart failure. Furthermore, transmural cellular-level changes in the left ventricular wall with age could help us identify region-specific changes that are beneficial in understanding ventricular filling.

In this study, we examined F344 rodents at three ages: 6-, 18-, and 22-months. To study the effects of normal aging we investigated the myocardial properties between the 6- and 18-month old animals because F344 rats at these ages are largely free of systemic disease [95, 96]. To detect the adaptive limit of myocardial

aging we studied the differences in myocardial properties between the 18- and 22-month old animals. We did not study animals beyond the 22-month time point because by ~ 24-months of age F344 animals exhibit both systolic and diastolic dysfunction [95, 96] and high rates of mortality [99]. We investigated the transmural changes that may occur in the sub-epicardium, mid-myocardium and sub-endocardium of the left ventricle because transmural heterogeneity in the ventricular wall is thought to affect ventricular torsion [100, 101], a potential prognostic tool to detect diastolic dysfunction.

We measured diastolic function and ventricular torsion using echocardiography. Ca^{2+} transients and unloaded cell shortening properties (time constant of Ca^{2+} decay (τ_{Ca}), time to peak (TP) of unloaded sarcomere shortening, time from peak to 50% sarcomere re-lengthening (RT50)) were investigated using single myocytes isolated from the 3 transmural regions (sub-epicardium, mid-myocardium and sub-endocardium) of the left ventricles of the 6, 18- and 22-month old F344 animals (Figure 3.1). Molecular mechanisms that would predict slowed relaxation were simulated using computational modeling (Figure 3.3). As mentioned previously in section 2.1.1, these results can be reviewed in further detail in the published study [65]. Here we will discuss the biochemical results that pertain to the functional properties measured.

3.2. Results

We investigated the relative content and phosphorylation status of key sarcomeric proteins that may contribute to the slowed relaxation with aging. SERCA2a protein expression, assessed by Western blot and densitometry analysis (methods-section 2.1.1) revealed that the sub-endocardial samples from the 6-month old animals had significantly lower SERCA2a content than the sub-epicardial ($p=0.039$) and the mid-myocardial ($p=0.032$) samples (Figure 3.4).

Relative α- and β-MHC isoform expression was also measured in tissue homogenates (methods-section 2.1.1). The relative content of α-MHC trended downward with age, but the effect was not statistically significant (Figure 3.5).

We used Pro-Q Diamond staining to measure the relative total phosphorylation of cTnI in our experimental samples (Figure 3.6). Post-hoc tests revealed that the 22-month old sub-epicardial samples were significantly less phosphorylated than the mid-myocardial ($p=0.037$) and the sub-endocardial ($p=0.016$) samples of the same age (Figure 3. 7). Similar tests were performed for other myofilament proteins but we did not see any significant differences among the groups (Table 3.1, 3.2, and 3.3).

3.3. Discussion

In the spectrum of heart failure progression, many studies focus on the extremes where the heart becomes maladaptive and heart failure is irreversible. If we can

identify mechanisms that precede overt heart failure then we can potentially treat it at an early stage. This study sought to identify transmural molecular level modifications that underlie myocardial and cellular level functional changes that occur in aging F344 rats.

Our data not only confirmed an age-dependent change in cardiac function seen in prior studies [102] but also revealed a novel statistical age-region interaction with slowed relaxation in the F344 myocytes (Figure 3.1 and 3.2 [65]). Specifically, Figure 3.1 [65] showed that the transmural regional pattern of relaxation properties (τ_{Ca}-p=0.02, TP-p<0.05, RT50-p<0.001) were similar between the 6- and the 18-month old animals. However, this transmural pattern was disrupted in the 22-month old animals and the sub-epicardial myocytes from the 22-month old animals were affected the most (Figure 3.1 and 3.2 [65]).

We studied the relative content of SERCa2a, a major Ca^{2+} handling protein as it could contribute to the alteration in τ_{Ca} values (Figure 3.1 [65]). We found that there was a heterogeneous expression of SERCa2a in the 6-month old animals where both the sub-epicardial and mid-myocardial samples had significantly higher SERCa2a content than the sub-endocardial samples (Figure 3.4). This result qualitatively agreed with the increased τ_{Ca} values (measure of Ca^{2+} decay) in both the 6-month sub-epicardial and mid-myocardial myocytes (Figure 3.1 [65]). This finding suggested that the increased expression of SERCa2a could potentially lead to an increase in Ca^{2+} uptake and therefore slower Ca^{2+} transient decay [103, 104]. However, SERCa2a content did not seem to contribute to the

reduced τ_{Ca} values in the 18- and 22-month old animals. This suggested the contribution of other mechanisms for example, phosphorylation of phospholamban (regulates SERCA) has been previously shown to reduce with age [105].

When τ_{Ca}-RT50 relationship was assessed in the sub-epicardial, mid-myocardial and sub-endocardial samples of all three age groups it was evident that the RT50 of the 22-month old sub-epicardial cells was highly sensitive to τ_{Ca} (Figure 3.2.) This meant that the slowed relaxation in the 22-month old sub-epicardial cells could be due to modifications in contractile proteins. In order to identify the molecular mechanisms simulations of unloaded sarcomere shortenings were performed to predict τ_{Ca}-RT50 relationship. It was evident that alteration in the proportion of β-MHC isoform (which is known to modulate cross bridge kinetics [68, 106]) did not change the relationship. However, the dissociation of Ca^{2+} from the troponin complex increased the slope of the τ_{Ca}-RT50 relationship (Figure 3.3).

We confirmed these predictions (Figure 3.3) by first investigating the relative expression of MHC isoform. We saw a qualitative decrease in the proportion of α -MHC isoform with age, similar to previous studies [68, 97] but we did not find any significant differences within groups (Figure 3.5).

The effect of dissociation of Ca^{2+} from the troponin complex could not be tested directly but a previous study suggested that the decrease in phosphorylation of cTnI slows cardiac relaxation by reducing the rate at which Ca^{2+} unbinds from the

troponin complex [107]. Therefore, we analyzed relative cTnI phosphorylation in the F344 animals. A significant decrease in phosphorylation of cTnI was found in the sub-epicardial samples when compared to the mid-myocardial and sub-endocardial samples of the 22-month old animals (Figure 3.6 and 3.7). This biochemical result confirmed the computational prediction (Figure 3.3). Previous studies also support our results because cTnI phosphorylation has been shown to decrease with heart failure [108, 109] and can affect myocyte kinetics [107, 110] and Ca^{2+} sensitivity [108, 109].

3.3.1. Conclusion

In this study, the decrease in phosphorylation of cTnI seems to be an important modulator of myocyte relaxation in a region-specific manner of the aging F344 rat myocardium. Specifically, the reduced cTnI phosphorylation in the sub-epicardial cells contributes to the slowed relaxation observed in 22-month old sub-epicardial cells. Both of these molecular and cellular level alterations in the sub-epicardial cells may contribute to the reduction in ventricular torsion observed in these animals at 22-months [65]. Together these results suggest that region-specific changes in the left ventricular wall may precede heart failure and lead to diastolic dysfunction in aging F344 rats.

Table 3.1. Content of selected sarcomeric proteins.

		Myosin	Actin	cTnT	cTnI
6-month old	Epi	0.71±0.16	0.66±0.18	0.24±0.24	0.93±0.08
	Mid	0.70±0.09	0.82±0.25	0.47±0.09	0.68±0.08
	Endo	0.68±0.07	0.50±0.07‡	0.48±0.27	0.58±0.05
18-month old	Epi	0.70±0.12	0.58±0.13	0.29±0.04	0.49±0.08
	Mid	0.60±0.05	0.58±0.08	0.25±0.08	0.62±0.09
	Endo	0.47±0.07	0.68±0.12	0.60±0.35	0.78±0.25
22-month old	Epi	0.54±0.09	0.81±0.24	0.43±0.14	0.70±0.18
	Mid	0.89±0.23	0.66±0.15	0.52±0.15	0.93±0.35
	Endo	0.57±0.05	0.41±0.03§	0.28±0.03	0.81±0.09
Main statistical effects and interaction (p values)	Age	0.676	0.967	0.965	0.617
	Region	0.174	0.147	0.928	0.942
	Age *Region	0.223	0.132	0.165	0.259

Protein contents are expressed in arbitrary units and were calculated by normalizing to data obtained for each protein from a 6-month old sub-epicardial sample that was loaded onto every gel as a control. Different from the sub-epicardial region of the same condition: § $p<0.05$. Different from the mid-myocardial region of the same condition: ‡ $p<0.05$.

Table 3.2. Content of selected sarcomeric proteins.

		Tropomyosin	MLC-2	MLC-1
6-month old	Epi	0.51±0.25	0.49±0.27	0.76±0.22
	Mid	0.53±0.18	0.49±0.15	0.74±0.12
	Endo	0.41±0.08	0.17±0.02	0.68±0.08
18-month old	Epi	0.29±0.04	0.15±0.01	0.48±0.03
	Mid	0.46±0.10	0.31±0.12	0.56±0.21
	Endo	0.46±0.10	0.36±0.04	0.61±0.12
22-month old	Epi	0.35±0.13	0.34±0.15	0.43±0.18
	Mid	0.43±0.10	0.57±0.28	0.72±0.33
	Endo	0.32±0.04	0.19±0.05	0.70±0.11
Main statistical effects and interaction (p values)	Age	0.770	0.763	0.658
	Region	0.363	0.160	0.565
	Age *Region	0.567	0.285	0.764

Protein contents are expressed in arbitrary units and were calculated by normalizing to data obtained for each protein from a 6-month old sub-epicardial sample that was loaded onto every gel as a control.

Table 3.3. Phosphorylation of selected sarcomeric proteins.

		Phospho cTnT	Phospho Tropomyosin	Phospho MLC-2
6-month old	Epi	1.11±0.26	1.87±0.56	1.46±0.30
	Mid	0.95±0.31	1.32±0.132	2.09±0.35
	Endo	1.90±0.62	1.69±0.21	2.11±0.38
18-month old	Epi	0.85±0.41	2.05±0.27	2.79±0.73
	Mid	1.50±0.81	1.57±0.27	2.07±0.12
	Endo	1.25±0.72	1.34±0.32	1.55±0.17
22-month old	Epi	0.87±0.40	2.98±1.66	1.79±0.75
	Mid	1.22 ±0.26	2.20±0.38	1.27±0.18
	Endo	1.80±0.24	2.24±0.17	2.17±0.64
Main statistical effects and interaction (p values)	Age	0.965	0.364	0.433
	Region	0.165	0.368	0.885
	Age *Region	0.689	0.971	0.313

Phosphorylation levels are expressed in arbitrary units and were calculated by normalizing to data obtained for each protein from a 6-month old sub-epicardial sample that was loaded onto every gel as a control.

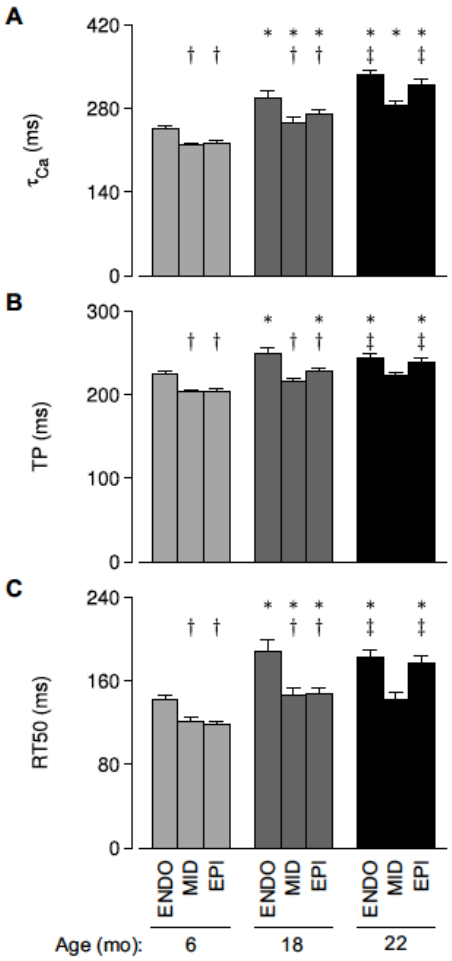

Figure 3.1. Transmural patterns of Ca^{2+} handling and contraction dynamics are altered with age.

A) Mean values (±SEM) of the time constant of $F_{340/380}$ decay after peak (τ_{Ca}) for each age-region group. (B, C) Same as panel A but showing time-to-peak (TP) unloaded sarcomere shortening and time from peak to 50% sarcomere re-lengthening (RT50). * $p < 0.05$ vs. cells from the same region at 6 months of age. † $p < 0.05$ vs. endocardial cells at the same age. ‡ $p < 0.05$ vs. midmyocardial cells at the same age.

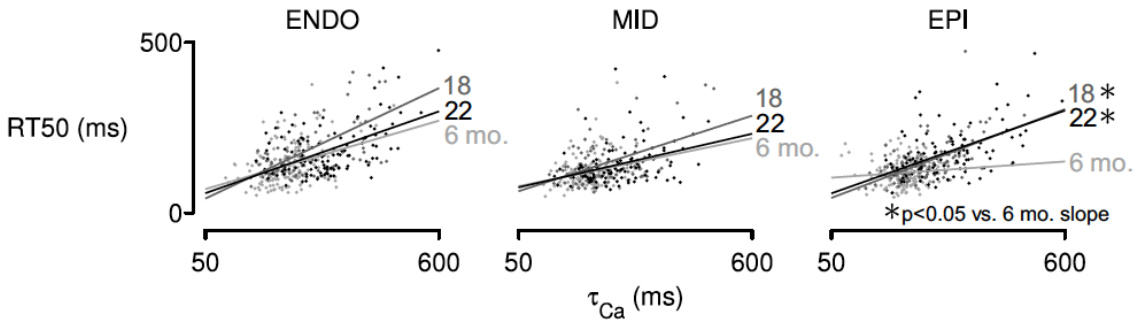

Figure 3.2. Aging alters Ca^{2+}-relaxation coupling in epicardial myocytes.

Plotted points show RT50 vs. τ_{Ca} for each cell in the study, grouped according to region and animal age. Analysis of covariance on τCa-RT50 relations indicates that the slope depends significantly on the age-region group ($p < 0.001$). RT50 in epicardial myocytes from 6-month-old rats was significantly less sensitive to τ_{Ca} than in 18- and 22-month-old cells from the same region.

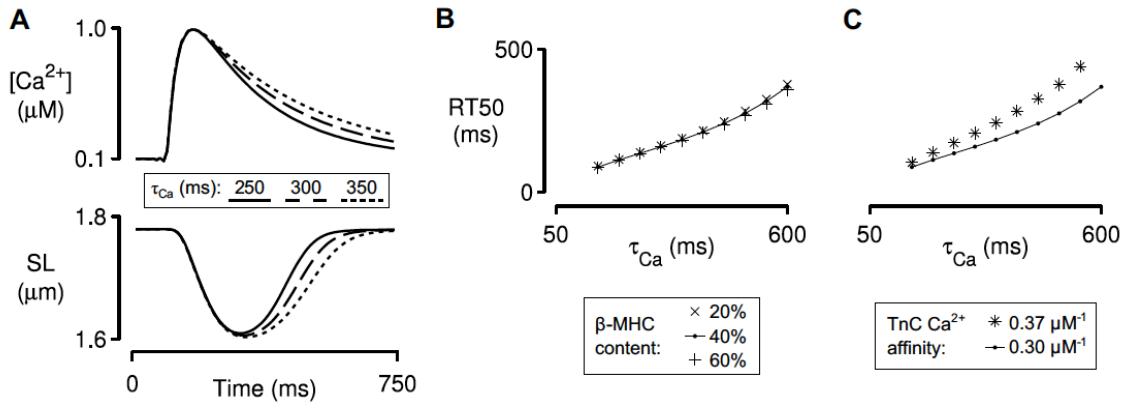

Figure 3.3. Computer simulations of unloaded sarcomere shortening.

Ca^{2+} transients with various rates of decay (τ_{Ca}) were used as inputs to predict relationships between τ_{Ca} and RT50 (time from peak shortening to 50% re-lengthening) under different conditions. A) Example input Ca^{2+} transients of increasing τ_{Ca} and corresponding SL outputs for the baseline model (40% β-MHC, TnC Ca^{2+} affinity 0.3 μmol L^{-1}). B) Sensitivity of the τ_{Ca}-RT50 relation to doubling and halving relative β-MHC content. C) Sensitivity of the τ_{Ca}-RT50 relation to a 20% increase in TnC Ca^{2+} affinity.

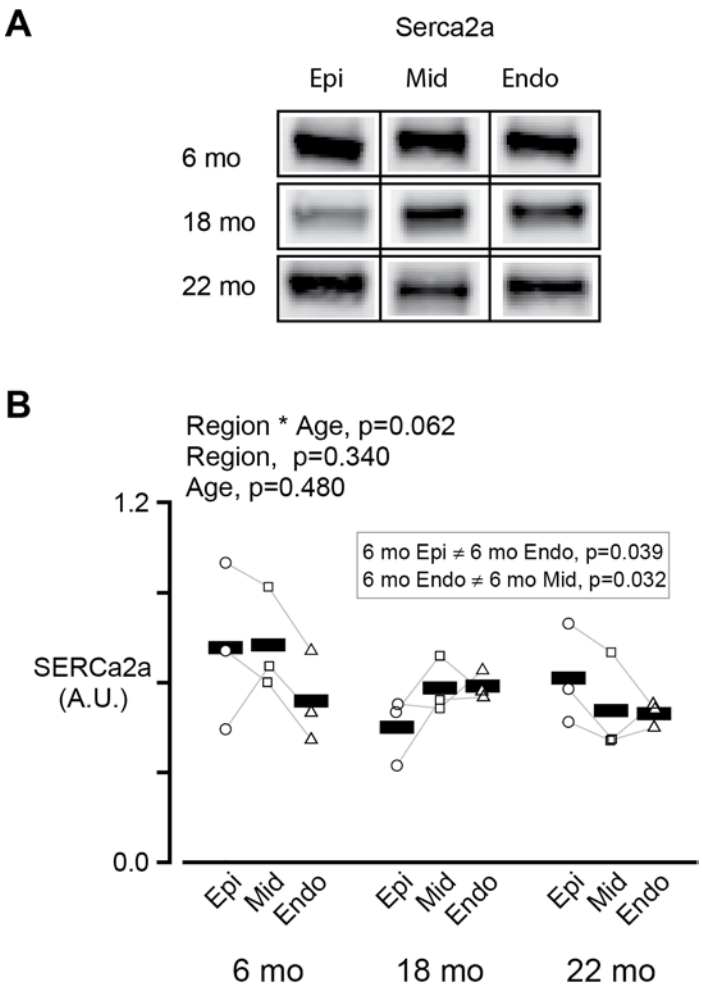

Figure 3.4. Expression of SERCa2a.

A) Representative immunoblots showing SERCa2a expression in F344 rats. B) Symbols show the mean SERCa2a measured for each region for each heart. A.U. stands for arbitrary units. In this figure, and in all similar panels, thin lines join data points from the same heart. Thick bars show the mean data for the region. The text above the plot shows p values for the main statistical effects. Significant differences between regions, tested separately for the three ages, are listed in the inset box. Significant differences due to aging, tested separately for

each region, are indicated by asterisks (* indicates $p<0.05$, ** indicates $p<0.01$, *** indicates $p<0.001$).

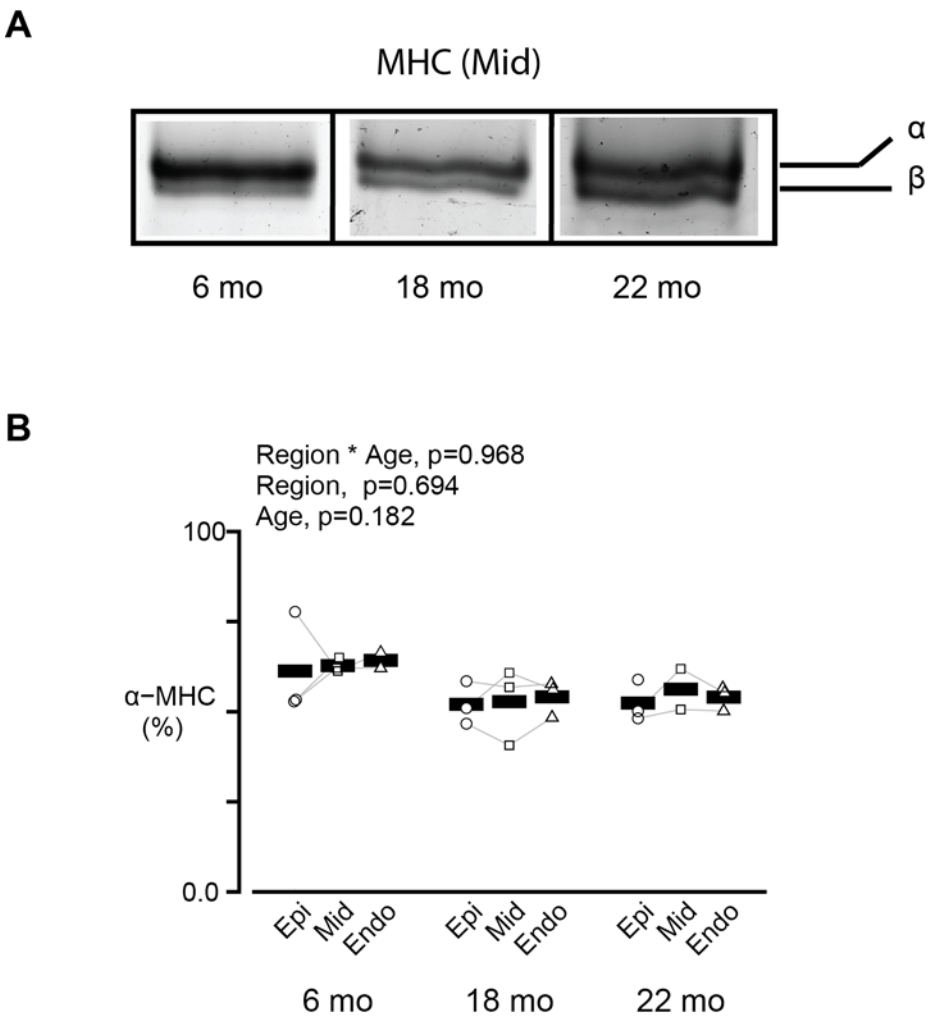

Figure 3.5. Shift in MHC isoform.

A) Representative bands from mid-myocardial samples of various ages showing separated α- and β-MHC isoforms and B) the mean α-MHC isoform percentages across groups.

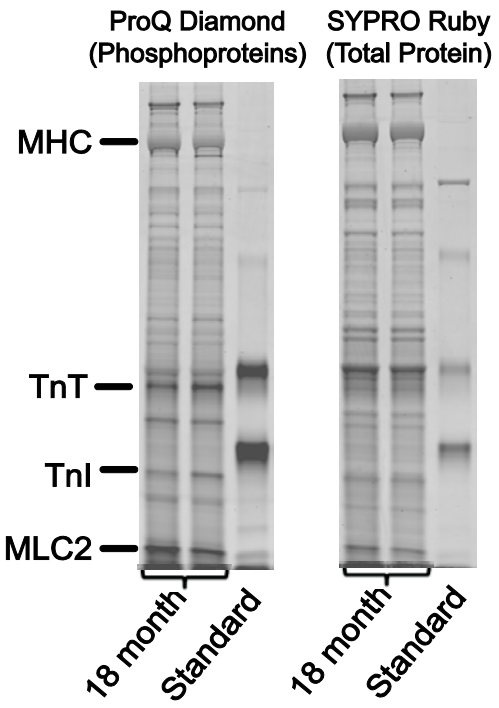

Figure 3.6. Broadrange gel stained for phosphorylated and total sarcomeric proteins.

Two images of a single representative gel stained with Pro-Q Diamond (left) and SYPRO Ruby (right). The Pro-Q Diamond stain is more sensitive to phosphoproteins while SYPRO Ruby indicates total protein content.

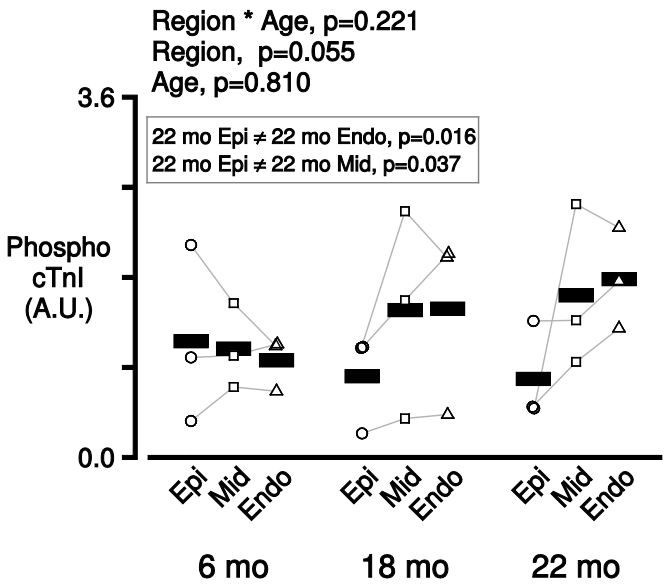

Figure 3.7. Decreased cTnI phosphorylation in 22 month old sub-epicardial samples.

A) Symbols show the mean Phospho cTnI measured for each region for each heart using Pro-Q Diamond (phospho-sensitive stain). A.U. stands for arbitrary units.

Chapter 4. Transmural heterogeneity of cellular level contractile function in human heart failure

Aspects of this chapter will be reported in the manuscript titled, “Transmural heterogeneity of cellular level power output is reduced in human heart failure”. Journal of Molecular and Cellular Cardiology, accepted.
DOI:10.1016/j.yjmcc.2014.02.008

4.1. Introduction

Clinical studies have shown that transmural variation in the contractile function of human myocardium may influence clinical end-points [26, 28]. For example, a study by Wachtell *et al.* [26] followed 840 patients for 3,914 patient-years and showed that shortening of the middle transmural region of the left ventricular free wall is a better predictor of cardiovascular death, myocardial infarction, and stroke, than the shortening of other regions, or ejection fraction. However, the mechanisms that underlie these results, which may include transmural variation in cellular and molecular properties, are not well understood.

Previous studies using human hearts have demonstrated that action potentials and Ca^{2+} transients vary systematically across the left ventricular free well, and that these effects probably reflect transmural-region specific expression of ion channels and ionic transporters [43, 44]. There are a few reports in the animal-based literature showing that tissue samples from different parts of the ventricular wall

(specifically the sub-epicardial, mid-myocardial, and sub-endocardial regions) express different sarcomeric proteins and exhibit variable contractile properties [97, 100, 101, 111]. Less is currently known about potential transmural variation in contractile function. Therefore, the goals of our study was to test the hypotheses that human hearts exhibit transmural heterogeneity of cellular level contractile properties, and that heart failure produces region-specific changes in contractile function. In order to evaluate both the active and passive mechanical properties of the tissue samples, we performed experiments using multicellular chemically permeabilized preparations.

The results showed that cellular level indices of systolic function (power output and isometric force) exhibit transmural heterogeneity in non-failing human hearts. Specifically, samples from the mid-myocardium developed more power and more force than samples from the sub-epicardial and sub-endocardial regions. Heart failure reduced power and force by ~20% but affected mid-myocardial samples more than tissue from the other regions. As a result, failing hearts exhibited less transmural heterogeneity. Additional data from histological and biochemical assays suggested that these contractile changes reflect a region-specific increase in fibrosis and modifications to the content and phosphorylation status of sarcomeric proteins including cTnI, desmin and MLC-1.

4.2. Results

4.2.1. Power output

We measured maximum power output, an *in vitro* index of systolic function, using multicellular permeabilized preparations (Figure 2.4 and 4.1). Figure 4.2A shows force-velocity and force-power curves that we measured using preparations obtained from the sub-epicardial, mid-myocardial and sub-endocardial regions of one non-failing and one failing heart. In the non-failing samples, peak power output was higher for the mid-myocardial sample than it was for the sub-epicardial and sub-endocardial samples (lower left panel). The failing samples exhibited less transmural variation (lower right panel).

Figure 4.2B shows collated data for the 6 non-failing and 10 failing hearts. We found a significant interaction (p=0.030) between region and heart failure condition, which implies that the heart failure status affects the sub-epicardial, mid-myocardial, and sub-endocardial regions in different ways. Maximum power output was significantly lower (p=0.009) for the heart failure samples (0.37 ± 0.02 $\mu W\ mg^{-1}$) than for the non-failing samples (0.50 ± 0.03 $\mu W\ mg^{-1}$). The post-hoc tests revealed that in the non-failing samples, the maximum power output of the mid-myocardial preparations (0.59 ± 0.06 $\mu W\ mg^{-1}$) was greater than that of the sub-epicardial (0.46 ± 0.03 $\mu W\ mg^{-1}$, p value=0.021) and the sub-endocardial preparations (0.46 ± 0.04 $\mu W\ mg^{-1}$, p value=0.015). We observed no significant transmural differences in the heart failure samples. Heart

failure thus lowered the power output of mid-myocardial samples more than it lowered the power output of sub-epicardial and sub-endocardial preparations.

4.2.2. Isometric force

Figure 4.3A shows that the isometric force also exhibited transmural variation in non-failing hearts and that the transmural pattern of variation was altered by heart failure ($p<0.001$). Since power is the product of force and velocity, these data suggest that the transmural variation in power output primarily reflects changes in force-generating capacity rather than changes in shortening velocity (which did not exhibit significant differences, Figure 4.3B). Heart failure lowered isometric force values normalized to cross-sectional area from 12.27 ± 0.61 kN m^{-2} to 9.78 ± 0.37 kN m^2 ($p=0.042$). Post-hoc analysis showed that the non-failing samples exhibited transmural heterogeneity. Specifically, the maximum force generated by samples from the mid-myocardium (14.3 ± 1.33 kN m^2) was higher than the force generated by the sub-epicardial (10.96 ± 0.74 kN m^{-2}, $p=0.008$) and the sub-endocardial (11.47 ± 0.86 kN m^{-2}, $p=0.026$) preparations. In these experiments, the samples from the failing hearts also exhibited heterogeneity, with the mid-myocardial preparations generating the least amount of force (8.80 ± 0.09 kN m^{-2}). Heart failure thus lowered the force generating capacity of the mid-myocardial preparations more than that of the sub-epicardial and sub-endocardial samples.

4.2.3. Calcium sensitivity

Figure 4.4A shows normalized isometric tension plotted as a function of the activating Ca^{2+} concentration (where $pCa = -\log_{10}[Ca^{2+}]$) for preparations from the three transmural regions of non-failing (left panel) and failing (right panel) hearts. In the non-failing samples, Ca^{2+} sensitivity (assessed as the Ca^{2+} concentration required to produce half the maximum force) was 0.075 pCa units greater in the sub-endocardial samples than in the sub-epicardial samples ($p=0.010$, Figure 4.4B). No transmural differences were observed in the failing samples. The progressive transmural change in calcium sensitivity that occurs in non-failing hearts is thus disrupted by heart failure (interaction term, $p=0.047$).

4.2.4. Short-range components

Figure 4.5A shows that the short-range stiffness exhibited transmural variation in non-failing hearts and that the transmural pattern of variation was altered by heart failure ($p<0.001$). Post-hoc analysis showed that the non-failing samples exhibited transmural heterogeneity. Specifically, short-range stiffness of samples from the mid-myocardium was higher than short-range stiffness of samples from the sub-epicardium ($p=0.026$). Samples from the failing hearts also exhibited transmural heterogeneity. The mid-myocardial samples were the least stiff and significantly different than the sub-epicardial samples ($p=0.016$). We did not find significant interaction between region and heart failure status for relative short-range force ($p=0.475$, Figure 4.5B). These results suggest that heart failure

lowered the short-range stiffness in the mid-myocardial preparations more than the sub-epicardial and sub-endocardial samples suggesting a decrease in myocardial stiffness due attached cross bridges.

4.2.5. Rate of tension redevelopment

The rate of tension redevelopment was plotted as a function of relative tension for both the non-failing and failing samples from different transmural regions (Figure 4.6). We did not find any significant difference in the rate of tension redevelopment (k_{tr}) at high Ca^{2+} concentration (pCa 4.5) with heart failure status or region (Figure 4. 7A). However, we found that there was a region dependence ($p=0.008$) in k_{tr} at submaximal level of Ca^{2+} (pCa 5.7). Furthermore, the sub-endocardial samples of failing hearts had significantly slower k_{tr} than the sub-epicardial ($p=0.009$) and the mid-myocardial ($p=0.001$) samples of the failing hearts (Figure 4. 7 B).

4.2.6. Collagen content

Figure 4.8 shows representative images of myocardial sections that had been stained with picrosirius red. Quantification showed that there was a significant interaction ($p=0.020$), which implied that heart failure affected the regions differentially. Heart failure also increased the proportion of tissue that was collagen from 0.103 ± 0.007 to 0.219 ± 0.012 ($p=0.021$, Figure 4.9A). Unlike the non-failing samples (which were not transmurally heterogeneous), the sections

cut from the three transmural regions of failing tissue all had collagen contents that were significantly different from each other (p values for all post-hoc tests < 0.05). In the failing samples, the collagen to tissue ratio in the mid-myocardial sections was greater than that in the sub-epicardial and sub-endocardial sections by ~0.117 and ~0.041 respectively.

The collagen to tissue ratio in the stained sections was negatively correlated with the relative contents of actin (Figure 4.9B) and myosin (Figure 4.9C) in wet tissue samples from the same biospecimens. This is consistent with a mechanism in which myocytes are replaced by extracellular matrix proteins when fibrosis develops.

4.2.7. Modifications in sarcomeric proteins

We investigated the potential changes in the isoform content and posttranslational status of sarcomeric proteins using gel electrophoresis and western blotting (see methods-section 2.4). The key findings were that heart failure status decreased the relative content of cTnI ($p=0.021$, Figure 4.10 and 4.11A), reduced relative phosphorylation of cTnI at Ser23/24 ($p=0.012$) in the failing samples (Figure 4.12), increased the content of desmin protein ($p<0.001$, Figure 4.10 and 4.13A), reduced desmin's relative level of phosphorylation ($p=0.006$, Figure 4.10 and 4.13B), and increased the relative content of N2BA isoform of titin ($p=0.047$, Figures 4.14).

No other statistically significant effects of heart failure status and/or transmural region were revealed by the linear mixed model analyses (Tables 4.1, 4.2, 4.3, 4.4 and 4.5).

4.2.7.1. Cardiac troponin I

Cardiac troponin I (cTnI) content was reduced by 23% in samples from heart failure patients ($p=0.021$, Figure 4.10 and 4.11A). There was a region dependent difference in phosphorylation of cTnI ($p=0.041$). Post-hoc analysis showed that the sub-epicardial region was more phosphorylated than the sub-endocardial region of the heart failure group ($p=0.004$). The relative phosphorylation of cTnI at Ser23/24 was also reduced ($p=0.012$) in the failing samples (Figure 4.12).

4.2.7.2. Desmin

Heart failure increased the content of desmin protein ($p<0.001$, Figure 4.10 and 4.13A) but reduced its relative level of phosphorylation ($p=0.006$, Figure 4.10 and 4.13B).

4.2.7.3. Cardiac myosin binding protein-C

There was no significant difference in total phosphorylation of cMybp-c and its content (Tables 4.1 and 4.4). However, western blotting with a site-specific antibody showed that the phosphorylation of cMyBP-C at Ser302 depended on

transmural region (p=0.014, Figure 4.15). In non-failing hearts, this residue was also more phosphorylated in samples from the sub-epicardial region than in tissue from the mid-myocardium (p=0.047, Figure 4.15B).

4.2.7.4. Titin

Titin isoform content was also altered by heart failure. The relative amount of this protein expressed as the larger N2BA isoform increased from 0.541 ± 0.028 in the non-failing samples to 0.653 ± 0.022 in the samples from failing hearts (p=0.047, Figure 4.14A and B). Sub-endocardial preparations from failing hearts also exhibited higher levels of N2BA phosphorylation than sub-epicardial (p=0.006) and mid-myocardial (p=0.037) preparations (Figure 4.14C).

4.2.8. Molecular mechanisms influencing contractile function

Most of the functional parameters we measured in this work exhibited large within-group variability. For example, the power output of mid-myocardial preparations from non-failing hearts ranged from 0.443 to 0.747 μW mg^{-1}, a span of 51%. We therefore used linear regression tests to test whether changes in the content and posttranslational status of sarcomeric proteins could explain the variance of the functional measures. This analysis revealed 24 relationships with p values less than 0.05. These relationships are shown in Tables 4.6 and 4.7 and Figures 4.16 and 4.17.

4.2.8.1. Power output

Figure 4.16A shows that power increased with the relative content of cTnI ($p=0.042$). Figure 4.16B and C show that power decreased with the relative content of desmin ($p=0.041$) but increased with its relative phosphorylation ($p=0.046$). Finally, Figure 4.16D and E show that power increased with the relative content of MLC-1 ($p=0.034$) but decreased with the molecule's relative phosphorylation ($p=0.006$).

4.2.8.2. Rate of tension redevelopment

At maximal Ca^{2+} activation k_{tr} was significantly correlated with thick filament associated proteins. Figure 4.17A and B show that k_{tr} increased with cMyBP-C ($p=0.002$) and decreased with its phosphorylation ($p=0.031$). Figure 4. 17C and D show that k_{tr} increased with MLC-1 content ($p<0.001$) and its phosphorylation ($p=0.013$) and Figure 4.17E shows that k_{tr} increased with MLC-2 ($p=0.001$). Other significant correlations between k_{tr} and other sarcomeric protein are listed in Table 4.6.

4.2.8.3. Other functional-biochemical relationships

Table 4.7 shows that force ($p=0.045$) increased with the relative content of cTnI. Resting tension was positively correlated with the relative phosphorylation of cTnI at Ser23/24 ($p=0.006$) which suggests that this residue may influence the

mechanical properties of titin and/or the regulation of binding sites for myosin on the actin filament. The relative phosphorylation of cMyBP-C at Ser282 (p=0.001) and at Ser273 (p=0.023) predicted the maximum shortening velocity of the preparations. These posttranslational modifications are mediated primarily by PKA [112] and this kinase is known to increase the maximum shortening velocity of rat myocardium [113]. However, the specific relationships between the phosphorylations of Ser282 and Ser273 and shortening velocity are new findings.

4.3. Discussion

Clinicians already recognize the significance of transmural variation in contractile function. For example, imaging studies have shown that shortening of the middle transmural region is a better predictor of cardiovascular death than traditional measures of global ventricular function such as ejection fraction [26, 28]. The American Society of Echocardiography also notes in its guidelines that "Contraction of muscle fibers in the LV midwall may better reflect intrinsic contractility than contraction of fibers at the endocardium" [114]. Our current work reveals four new cellular and molecular level results that may help to explain these clinically-relevant observations [26, 28].

First, non-failing human hearts exhibit transmural heterogeneity of contractile properties (Figures 4.2- 4.4). Second, heart failure depresses power and force and has its biggest negative impact on mid-myocardial tissue. Failing hearts thus exhibit less transmural heterogeneity in cellular level contraction than non-failing

hearts (Figures 4.2 and 4.3). Third, human heart failure produces more fibrosis in mid-myocardial tissue than it does in sub-epicardial and sub-endocardial samples (Figure 4.9). This may explain why heart failure produces the greatest contractile deficits in the mid-myocardium as the additional connective tissue is likely to displace functioning myocytes. Fourth, power and rate of tension redevelopment correlate with the relative content and relative phosphorylation of key sarcomeric proteins (Figure 4.16 and 4.17 and Table 4.7). Therefore, therapies targeting these proteins may be particularly effective treatments for human heart failure.

4.3.1. Region-specific modifications in systolic function

During systole, the heart contracts against its afterload to eject blood from the ventricle. This can be mimicked *in vitro* by allowing permeabilized myocardial preparations to shorten against a controlled force [115] (Figure 4.1). The power output for each load is calculated by multiplying the force that the muscle generates by its shortening velocity. Figure 4.2 shows that the maximum power output exhibited significant transmural variation in non-failing hearts and was reduced by ~25% in failing organs ($p=0.009$). Further analysis suggests that these effects primarily reflect altered force generation (Figure 4.3A) since maximum shortening velocity was not influenced by heart failure status or transmural region (Figure 4.3B).

No previous studies have used human samples to assess transmural variation in power output. However, a few studies have measured the effect of heart failure on isometric force generation, with potentially conflicting results. For example, separate studies using epicardial biopsies [116] and samples from unspecified regions of the heart [117] have shown that isometric force is reduced by ~80% in patients with heart failure. Other works, using samples from unspecified regions of the left ventricle, suggests that there is no significant effect of heart failure on maximum isometric force [118-120]. In the present experiments, heart failure reduced the average force generated by the experimental preparations (Figure 4.3A, $p=0.042$). However, post-hoc analysis of the different transmural regions showed that the effect was only significant for the mid-myocardial samples ($p<0.001$) and that heart failure did not significantly reduce the force generated by the sub-epicardial ($p=0.935$) or the sub-endocardial ($p=0.120$) preparations. These results imply that heart failure influences force generation in a transmural specific manner in humans. Researchers developing future studies in this area may therefore wish to consider including transmural region as an independent grouping factor when they design their experiments.

4.3.2. Failing hearts have increased mid-myocardial fibrosis

Increased fibrosis was an important factor in these experiments. Figure 4.9A show that heart failure increased the relative content of collagen in the myocardial sections, and that the mid-myocardial samples of the failing hearts

contained more collagen than the matching sub-epicardial ($p<0.001$) and sub-endocardial ($p=0.043$) sections. Increased collagen was also associated with lower relative contents of actin and myosin (Figure 4.9B-C). Additional analyses showed that force ($p=0.325$, Figure 4.18A) and maximum power $p=0.012$, Figure 4.18B) were correlated with actin content. Together these data support the hypothesis that in human heart failure, increased fibrosis depresses contractile function by replacing myocytes with extracellular matrix proteins.

The increased fibrosis might have been expected to raise passive force in the samples from the failing hearts. However, linear mixed model analyses showed that neither passive force (Figure 4.19A) nor passive stiffness (Figure 4.19B) at a sarcomere length of 2.2 μm were influenced by heart failure status or transmural region (all main statistical effects > 0.05). This probably reflects a compensatory effect of titin isoform expression. Consistent with previous studies [121, 122], samples from failing hearts had a greater relative content of the large N2BA isoform of titin ($p=0.047$, Figure 4.14B). This isoform shift tends to decrease passive stiffness and seems to counteract the mechanical effect of increased fibrosis in the samples from the failing hearts.

Titin phosphorylation has also been shown to change passive stiffness [123]. Although phosphorylation of N2BA isoform of titin did not change with heart failure (condition $p=0.825$, Figure 4.14C), the experimental data revealed a novel transmural heterogeneity. Sub-endocardial samples from failing hearts had

greater levels of phosphorylation than samples from the other regions (p=0.037 versus mid-myocardium, p=0.006 versus sub-epicardium, Figure 4.14C).

Another aspect of myocardial stiffness comes from the cross bridges that remain attached to the actin filaments during diastole. In this study short-range stiffness was significantly lower in heart failure (Figure 4.5A). The combined functional data of passive stiffness and short-range stiffness suggests that the failing myocardial samples may not be stiff. This is possible because most of the failing hearts in this study were dilated and dilated ventricles are thought to be compliant [124].

4.3.3. Region-specific Modification in Ca^{2+} sensitivity

In vivo function may be particularly sensitive to changes in Ca^{2+} sensitivity (defined as the free Ca^{2+} concentration required to generate half-maximum force) since myocytes are not maximally activated during a normal heartbeat. According to a Chapter 3, transmural variation in Ca^{2+} sensitivity may also modulate ventricular torsion [65]. In the present experiments (Figure 4.4) non-failing samples exhibited a statistically significant increase in Ca^{2+} sensitivity (p=0.010, ΔpCa_{50}=0.075) going from the sub-epicardial to the sub-endocardial preparations. However, samples from failing hearts did not show a significant transmural trend.

Two previous studies using human myocytes isolated from unspecified ventricular locations have shown that Ca^{2+} sensitivity increases with heart failure

[108, 125]. Another study [117] documents no change. Again, similar to the previous discussion relating to isometric force generation, it is difficult to interpret these data without more information about the transmural source of the sample [108, 117, 125].

Two additional projects have used animal tissues to assess potential transmural changes in Ca^{2+} sensitivity in pigs [47] and rats [46]. Both studies showed that Ca^{2+} sensitivity increased from the epicardium to the endocardium in healthy hearts, similar to the present work. The rodent study also showed that transmural variation in Ca^{2+} sensitivity was eliminated [46] 14 weeks after a myocardial infarction which is, again, broadly consistent with the current data from failing hearts (Figure 4.4).

Modulation of Ca^{2+} sensitivity is complex. The current data suggest that one molecular mechanism that may modulate the transmural variation in pCa_{50} in non-failing hearts (Figure 4.4) is phosphorylation of cMyBP-C. Post-hoc tests showed that Ser302 phosphorylation in non-failing epicardial samples was greater than in non-failing mid-myocardial tissue ($p=0.047$, Figure 4.15A-B) Regression analysis showed that pCa_{50} values for the non-failing preparations were negatively correlated with both total cMyBP-C phosphorylation ($p=0.002$, Figure 4.20A) and Ser302 phosphorylation ($p=0.045$, Figure 4.20B). The former finding reinforces data from a previous study using myocardial samples from unspecified regions of human hearts [120] but the new link between phosphorylation of cMyBP-C at Ser302 and pCa_{50} is a novel finding.

Other groups have shown that cTnI phosphorylation can also influence Ca^{2+} sensitivity [118, 126]. In this study, site-specific cTnI phosphorylation was reduced in heart failure samples at Ser23/24 (Figure 4.12B, p=0.012) but there was not a significant relationship between this parameter and pCa_{50} (r=0.034, p=0.850, data not shown). Total cTnI phosphorylation was not correlated with pCa_{50} either (r=-0.011, p=0.942, data not shown). However, site-specific phosphorylation of cTnI at Ser 23/24 correlated with cMyBP-C (Figure 4.21). cTnI undergoes many complex posttranslational modifications – the human cardiac isoform has 14 phosphorylation sites [127]. It is therefore possible that more detailed analysis might have revealed significant relationships. For example, phosphorylation of cTnI at Ser149 has been shown to increase Ca^{2+} sensitivity [128] but this modification was not investigated in this study.

Another posttranslational modification that has been linked to changes in myocardial Ca^{2+} sensitivity is phosphorylation of MLC-2. Davis *et al*. [100] have reported that MLC-2 phosphorylation is greater in sub-epicardial than in sub-endocardial tissue. Data from rat trabeculae [129] suggest that this phosphorylation gradient would increase Ca^{2+} sensitivity in epicardial tissue. However, the situation is complex, because van der Velden *et al*. [109] have shown that increased phosphorylation of MLC-2 decreases pCa_{50} values. Unfortunately, MLC-2 phosphorylation was not studied in this work.

4.3.4. Proteins that influence power output

The transmural heterogeneity of myocardial power output and its modification by heart failure are the key findings of this study. However, it was not possible to identify a specific sarcomeric protein that explains the functional changes.

The content of intact cTnI (Figure 4.11A) was reduced in biospecimens from failing hearts (p=0.021) but did not exhibit transmural variation (interaction term, p=0.853). Further analysis of these data showed that cTnI content was lower in patients with ischemic heart failure than in patients with non ischemic disease (p=0.029, Figure 4.22). This is consistent with a study by McDonough *et al*. which showed that cTnI is degraded in human hearts after ischemic injury [130]. Degradation of cTnI inhibits contractility in mice [131] and the current data show that this mechanism probably impacts human myocardial function too. Power output (Figure 4.16A) and force (Table 4.7) both correlated with the relative cTnI content, indicating that proteolyis of cTnI may be another impact factor in human disease [131].

Desmin, a structural protein that links myofibrils at Z-disks and maybe involved in force transmission [132], has been proposed as a potential biomarker for heart failure [133, 134]. Pawlak *et al.* [134] had previously shown that desmin content is increased in endocardial biopsies from patients with heart failure and this result was confirmed in the present work (Figure 4.13A). There was also a decrease in the total phosphorylation of desmin in samples from failing hearts (Figure 4.13B) [135]. Although desmin content did not vary with transmural region (p=0.514), the

regression tests summarized in Figure 4.16B-C show that changes to the content and phosphorylation of this protein may modulate power output.

Similarly, power increased linearly with MLC-1 content (p=0.034, Figure 4.16D) and decreased with MLC-1's relative phosphorylation (p=0.006, Figure 4.16E). Since MLC-1 binds to the lever arm of the myosin head near the convertor domain, it is ideally positioned to influence force generation and/or kinetics. For example, previous work by Morano *et al*. [136] and new data in Table S7 show that MLC-1 phosphorylation decreases V_{max}. There are only a few studies describing MLC-1 phosphorylation but phosphorylation sites corresponding to the human isoform are known as Thr64 and Ser194/195 [137]. Intriguingly, phosphorylation of MLC-1 has recently been shown to increase the molecule's degradation by matrix metalloproteinase-2 [138-140]. When combined with these previous findings, the new data presented in this manuscript show that MLC-1 modulates power output in human myocardium, and that loss of MLC-1 (perhaps following its phosphorylation) decreases contractility. To our knowledge, this is the first study to identify significant correlations between the power output of human myocardium and modifications to the content and phosphorylation status of cTnI, desmin and MLC-1.

4.3.5. Proteins that influence rate of tension redevelopment

The rate at which the myosin cross bridges generate force is an *in vitro* measure of the rate at which the ventricles generate pressure during systole. This property did not change significantly with heart failure status in our study (Figure 4.7).

In animal models of cardiac disease and aging k_{tr} has been shown to modulate with a shift in the isoform content of MHC. For example, F344 rats express more β-MHC with age [15] and this shift in the relative content of MHC isoform has been shown to significantly correlate with slowed k_{tr} [68, 106, 141]. In humans a shift in MHC isoform content in less likely to modulate k_{tr} because ~95% of MHC expressed in the left ventricles is β-MHC and does not change much with heart failure [142]. In our study the relative expression of α and β-MHC content was unaffected by heart failure. None of the ventricular samples contained detectable amounts of the α isoform although paired α and β myosin heavy chain bands were clearly resolved in atrial samples used as positive controls (Figure 4.23). These results suggested that there are other proteins that modulate k_{tr} in human myocardium. In our study we found cMyBP-C, MLC-2 and MLC-1, three proteins that were structurally bound to MHC to be significantly correlated with k_{tr} (4.17).

Previous studies have shown that k_{tr} increases significantly in cMyBP-C knockout mice [143, 144] and by phosphorylation of cMyBP-C through PKA incubation at submaximal concentration of calcium [145]. Both of these findings suggest that the relative content and phosphorylation of cMyBP-C can modulate k_{tr}, similar to our study (Figure 4.17A and B).

Similarly MLC-1 and MLC-2 both are located on the lever arm of the myosin head and are known to affect cross bridge kinetics [146-148]. In our study k_{tr} increased significantly with the contents of both these proteins (Figure 4.17C and E).

Another important result was that cMyBP-C was highly correlated with MLC-1 and MLC-2 content ($p<0.001$, Figure 4.24), which suggested that the effect of each of these thick filament protein may be masked by the other (called multicolinearity in statistical terms). Therefore an animal model maybe useful to investigate the effect of each of these proteins on k_{tr}.

4.3.6. Conclusion

This is the first study to show that (1) the contractile properties of non-failing human hearts exhibit transmural variation, and that (2) heart failure alters the transmural pattern as well as depressing overall function.

Table 4.1. Content of selected sarcomeric proteins in non-failing and failing tissue

		cMyBP-C	cTnT	Actinin
Non-failing	Epi	1.17±0.18	1.63±0.47	1.07±0.17
	Mid	1.03±0.10	1.21±0.31	0.94±0.09
	Endo	1.11±0.10	1.25±0.37	0.92±0.07
Heart failure	Epi	1.03±0.07	1.10±0.29	1.06±0.07
	Mid	1.09±0.07	1.20±0.31	1.14±0.10
	Endo	0.88±0.10	1.01±0.34	0.99±0.30
Main statistical effects and interaction (p values)	Condition	0.388	0.616	0.439
	Region	0.448	0.655	0.452
	Condition *Region	0.231	0.455	0.537

Protein contents are expressed in arbitrary units and were calculated by normalizing to data obtained for each protein from a non-failing sub-epicardial sample that was loaded onto every gel as a control.

Table 4.2. Content of myosin light chain proteins in non-failing and failing tissue.

		MLC-1	MLC-2
Non-failing	Epi	1.24±0.14	1.22±0.22
	Mid	1.09±0.08	1.11±0.10
	Endo	1.16±0.11	1.22±0.22
Heart failure	Epi	1.12±0.10	1.15±0.11
	Mid	1.18±0.09	1.15±0.10
	Endo	0.95±0.14	1.01±0.15
Main statistical effects and interaction (p values)	Condition	0.589	0.702
	Region	0.395	0.725
	Condition *Region	0.243	0.639

Protein contents are expressed in arbitrary units and were calculated by normalizing to data obtained for each protein from a non-failing sub-epicardial sample that was loaded onto every gel as a control.

Table 4.3. Content of Myosin Heavy Chain (MHC) and Actin in non-failing and failing tissue.

		MHC	Actin
Non-failing	Epi	0.79±0.08	0.71±0.10
	Mid	0.71±0.05	0.71±0.04
	Endo	0.78±0.06	0.71±0.04
Heart failure	Epi	0.74±0.03	0.66±0.02
	Mid	0.69±0.04	0.58±0.03
	Endo	0.71±0.07	0.62±0.07
Main statistical effects and interaction (p values)	Condition	0.345	0.092
	Region	0.534	0.764
	Condition*Region	0.920	0.772

Protein contents are expressed in arbitrary units and were calculated by normalizing to data obtained for each protein from a non-failing sub-epicardial sample that was loaded onto every gel as a control, and corrected for the initial weight of the original tissue sample.

Table 4.4. Phosphorylation of selected sarcomeric proteins in non-failing and failing tissue.

		Phospho cMyBP-C	Phospho cTnT	Phospho MLC-1
Non-failing	Epi	1.03±0.09	1.24±0.33	1.02±0.14
	Mid	1.05±0.1	1.59±0.30	1.26±0.18
	Endo	0.95±0.1	1.77±0.47	1.17±.0.11
Heart failure	Epi	0.79±0.05	1.91±0.46	1.34±0.19
	Mid	0.77±0.06	1.68±0.39	1.34±0.26
	Endo	0.86±0.16	2.16±0.49	1.52±0.24
Main statistical effects and interaction (p values)	Condition	0.094	0.53	0.367
	Region	0.999	0.237	0.345
	Condition *Region	0.554	0.484	0.457

Phosphorylation levels are expressed in arbitrary units and were calculated by normalizing to data obtained for each protein from a non-failing sub-epicardial sample that was loaded onto every gel as a control.

Table 4.5. Site-specific phosphorylation of cMyBP-C at Ser273 and Ser282 in non-failing and failing tissue.

		PSer273 cMyBP-C	PSer282 cMyBP-C
Non-failing	Epi	1.38±0.28	1.01±0.17
	Mid	1.39±0.35	1.01±0.14
	Endo	1.38±0.35	1.01±0.21
Heart failure	Epi	1.31±0.27	0.97±0.08
	Mid	1.35±0.27	0.94±0.07
	Endo	1.03±0.16	0.97±0.08
Main statistical effects and interaction (p values)	Condition	0.685	0.76
	Region	0.406	0.96
	Condition *Region	0.428	0.900

Phosphorylation levels are expressed in arbitrary units and were calculated by normalizing to data obtained for each protein from a non-failing sub-epicardial sample that was loaded onto every gel as a control.

Table 4.6. Statistically significant linear relationships between ktr and biochemical data.

Biochemical variable	r	p value
Myosin	0.402	0.006
Actin	0.367	0.012
Actinin	0.290	0.045
MLC-2	0.535	<0.001
Phospho Desmin	0.425	0.031
Phospho cTnI	0.298	0.039

Table 4.7. Statistically significant linear relationships between functional and biochemical data.

Biochemical variable	Functional parameter	r	p value
cTnI	Maximum force	0.291	0.045
Actin	Maximum force	0.027	0.034
Phospho cMyBP-C	pCa_{50}	-0.450	0.001
Phospho MLC-1	V_{max}	-0.287	0.048
PSer273 cMyBP-C	V_{max}	0.396	0.023
PSer282 cMyBP-C	V_{max}	0.396	0.023
PSer23/24-cTnI	Passive stiffness	0.390	0.025
PSer23/24-cTnI	Passive force	0.390	0.006

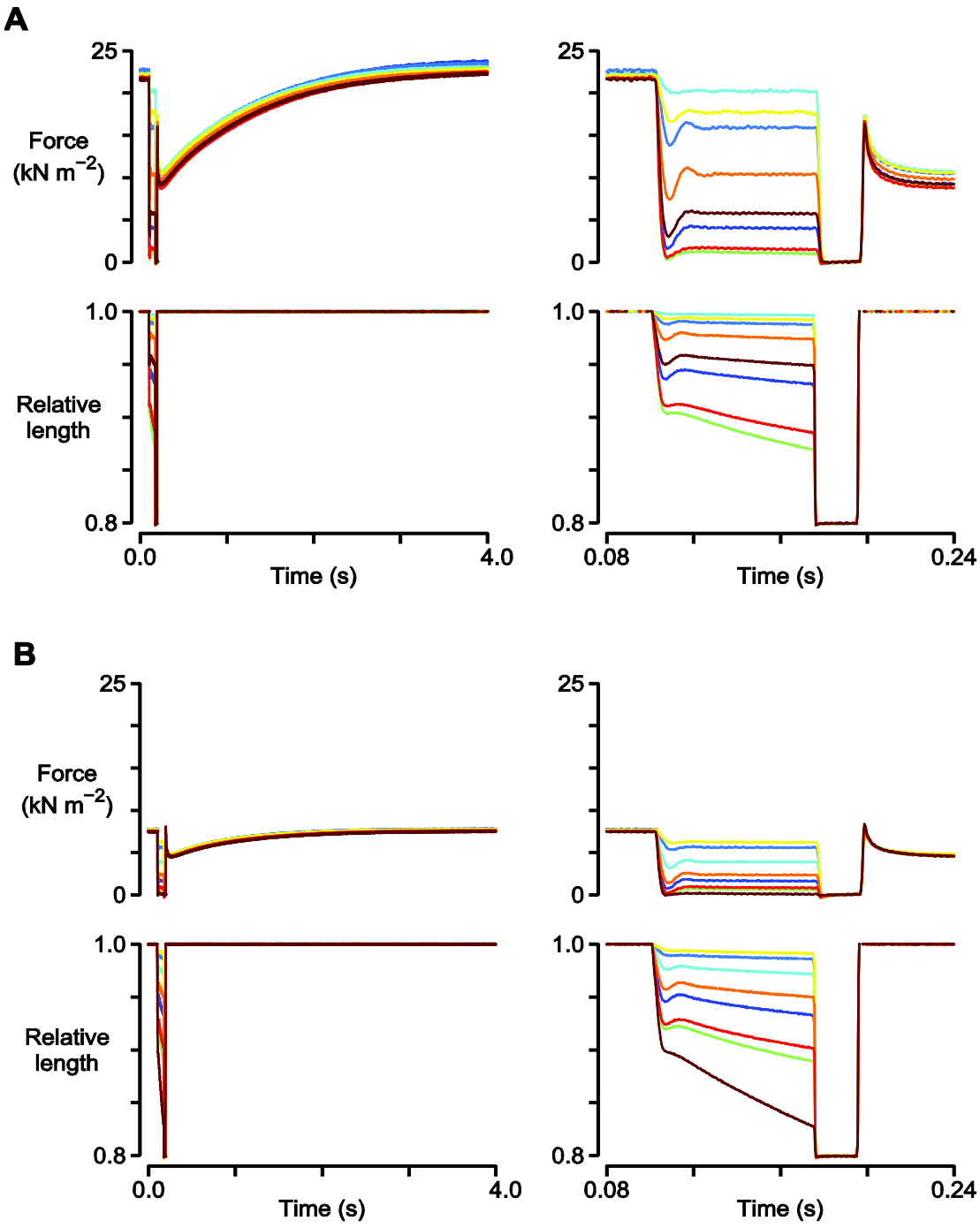

Figure 4.1. Mechanical records.

Superposed force and length records obtained during force-velocity experiments performed with a representative preparation isolated from the mid-myocardium of A) a non-failing heart and B) a failing heart (Force-velocity and force-power

curves from these records are shown in Figure (4.2). The left hand shows the x-axis time-scale for the complete experiments. The right hand side shows the expanded x-axis time-scale for the same experiments.

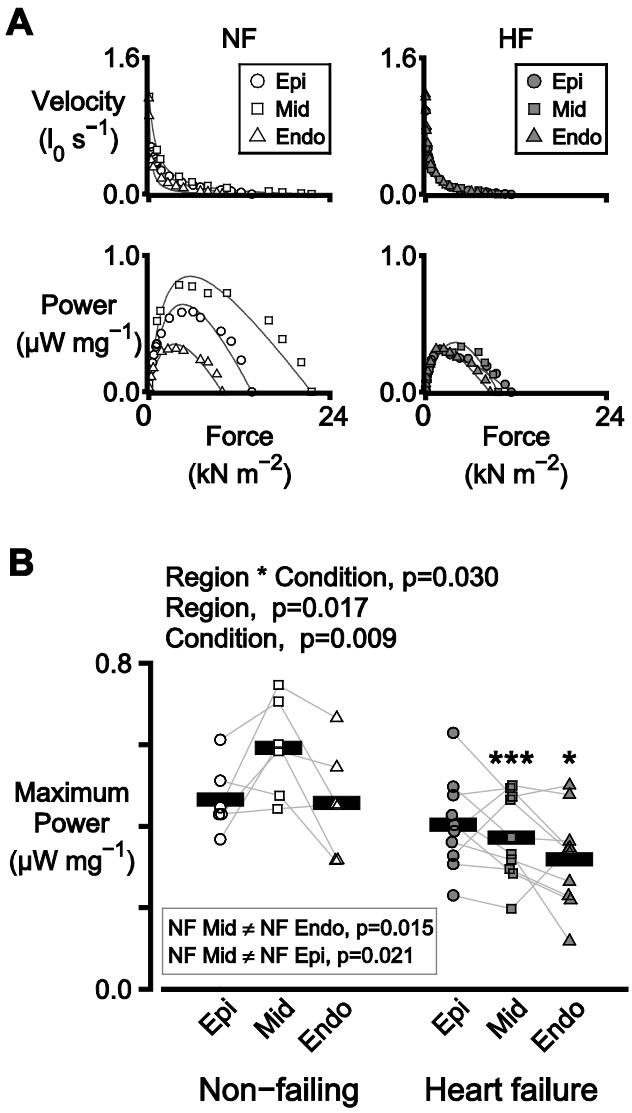

Figure 4.2. Transmural heterogeneity of power output is reduced in heart failure.

A) Representative force-velocity and force-power curves measured using individual preparations from the sub-epicardial, mid-myocardial, and sub-endocardial regions of the left ventricle of one non-failing (NF, left) and one failing (HF, right) heart. B) Symbols show the mean of the power outputs

measured from 2 or 3 preparations from each region for each heart. In this figure, and in all similar panels, thin lines join data points from the same heart. Thick bars show the mean data for the region. The text above the plot shows p values for the main statistical effects. Significant differences between regions, tested separately for non-failing and failing hearts, are listed in the inset box. Significant differences due to heart failure, tested separately for each region, are indicated by asterisks (* indicates $p<0.05$, ** indicates $p<0.01$, *** indicates $p<0.001$).

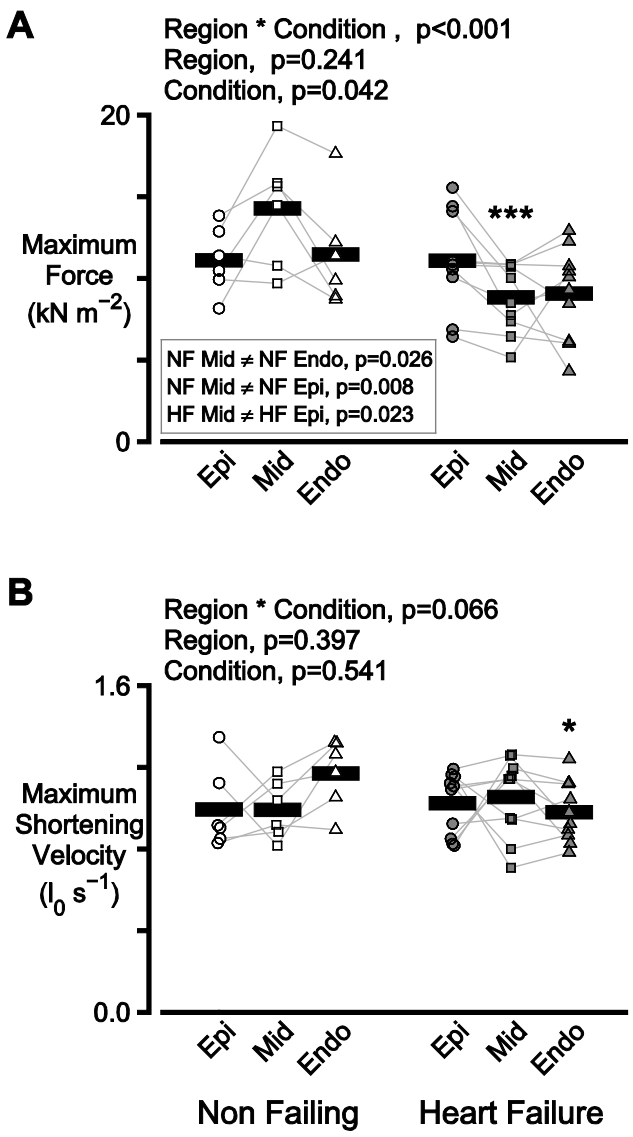

Figure 4.3. Transmural heterogeneity is reduced in heart failure with isometric force but not with maximum shortening velocity.

A) Symbols show the mean of the maximum isometric forces measured from 2 or 3 preparations from each region for each heart. B) Symbols show the mean of the maximum shortening velocities measured from 2 or 3 preparations from each region for each heart.

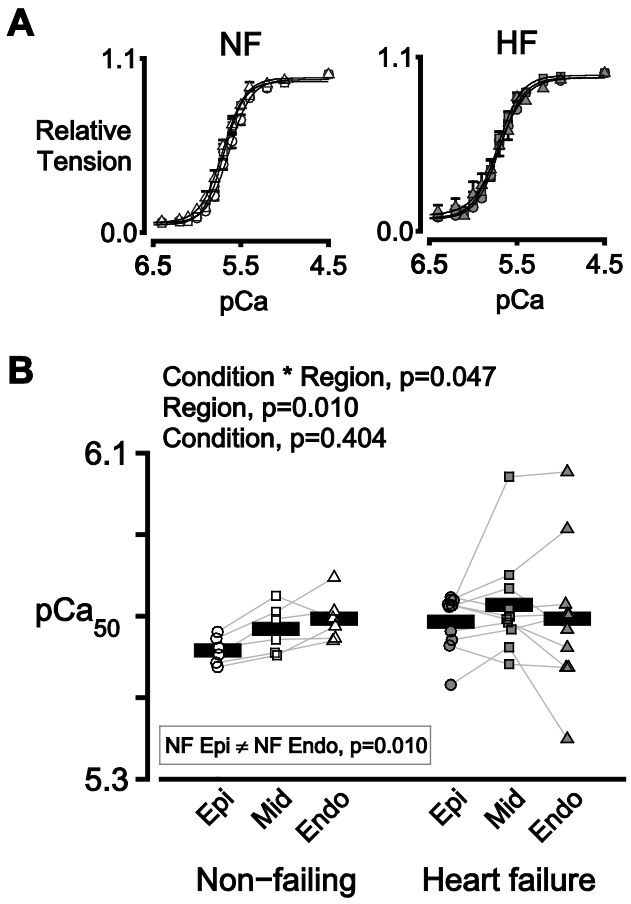

Figure 4.4. Transmural variation in Ca^{2+} sensitivity is disrupted in heart failure.

A) Mean values of normalized isometric tension plotted against pCa (= $-\log_{10}[Ca^{2+}]$) for preparations from the three transmural regions of non-failing (left) and failing (right) hearts. Circles, squares, and triangles show data for sub-epicardial, mid-myocardial, and sub-endocardial preparations respectively. B) Symbols show the mean of the pCa_{50} values measured using 2 or 3 preparations from each region for each heart.

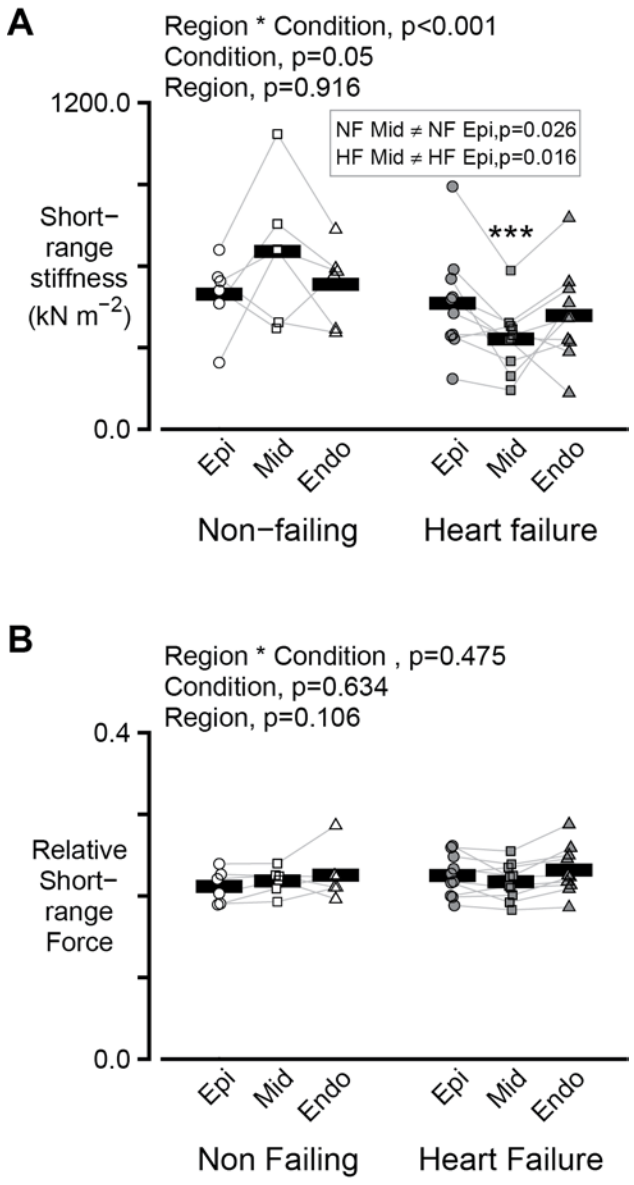

Figure 4.5 Relative short-range stiffness depends on heart failure status.

A) Short-range stiffness and B) relative short-range force measured in pCa 4.5 solution. Stiffness values are expressed as Young's Moduli and were calculated by fitting regression lines to the force responses measured during 4% length

changes imposed at a speed of 0.12 l_0 s^{-1}. In both plots, symbols show the mean data value measured from 2 or 3 preparations from each region for each heart.

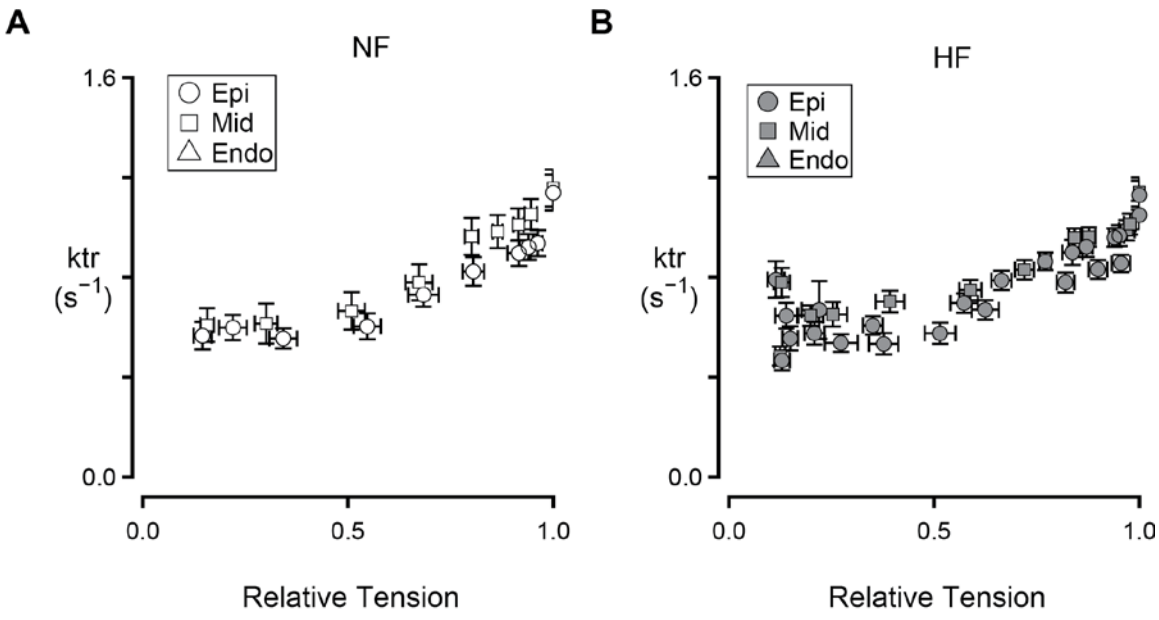

Figure 4.6. Rate of tension redevelopment dependence on the concentration of calcium.

k_{tr} plotted as a function of relative isometric tension for A) non-failing samples and B) failing samples. Symbols show the mean of the k_{tr} values measured using 2 or 3 preparations from each region for each heart in different pCa solutions plotted against relative isometric tension. The relative tension in pCa 4.5 solution was defined as 1.

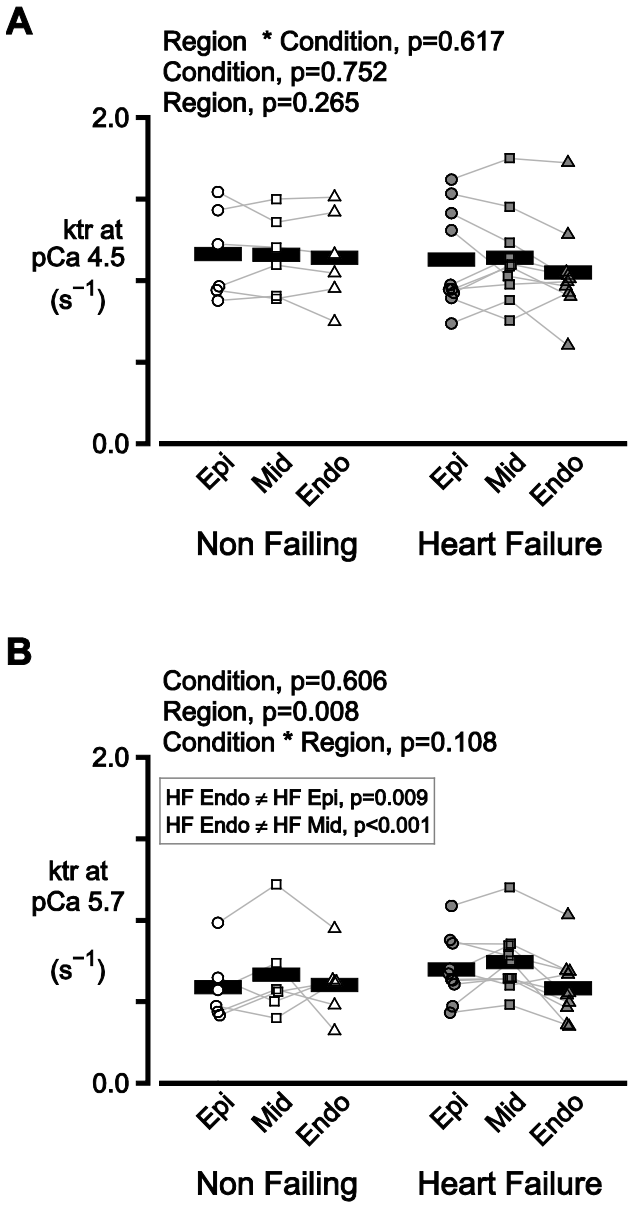

Figure 4.7 Rate of tension redevelopment (k_{tr}) does not depend on heart failure status.

Symbols show the mean of the k_{tr} measured from 2 or 3 preparations from each region for each heart in A) pCa 4.5 and B) pCa 5.7.

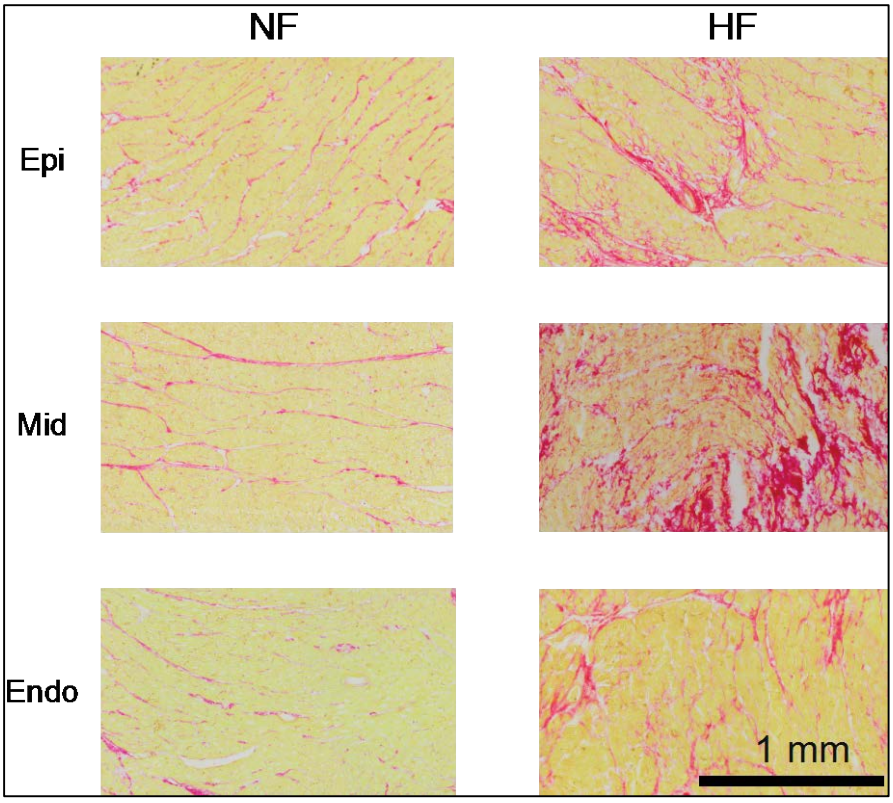

Figure 4.8. Representative images of myocardial sections from one non-failing and one failing heart stained with picrosirius red.

Red staining indicates collagen. Yellow staining shows non-fibrotic tissue.

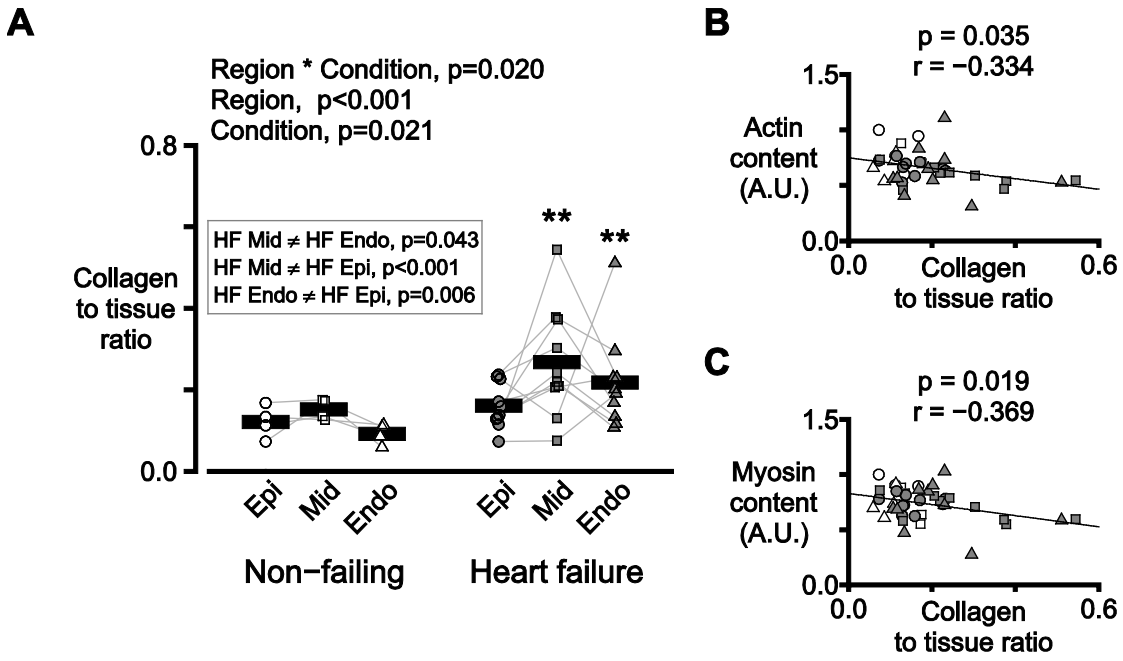

Figure 4.9. Collagen content is elevated in heart failure and is greatest in mid-myocardial tissue.

A) Symbols show the mean collagen to tissue ratio measured from 1-6 sections from each region for each heart. B) Actin and C) myosin contents (determined by Lowry protein assays and gel electrophoresis) plotted against the collagen to tissue ratios from panel B. A.U. stands for arbitrary units. Symbols follow the same shape and color conventions as in panel B. The plots also show the best-fit straight lines determined by linear regression and the corresponding p and r values.

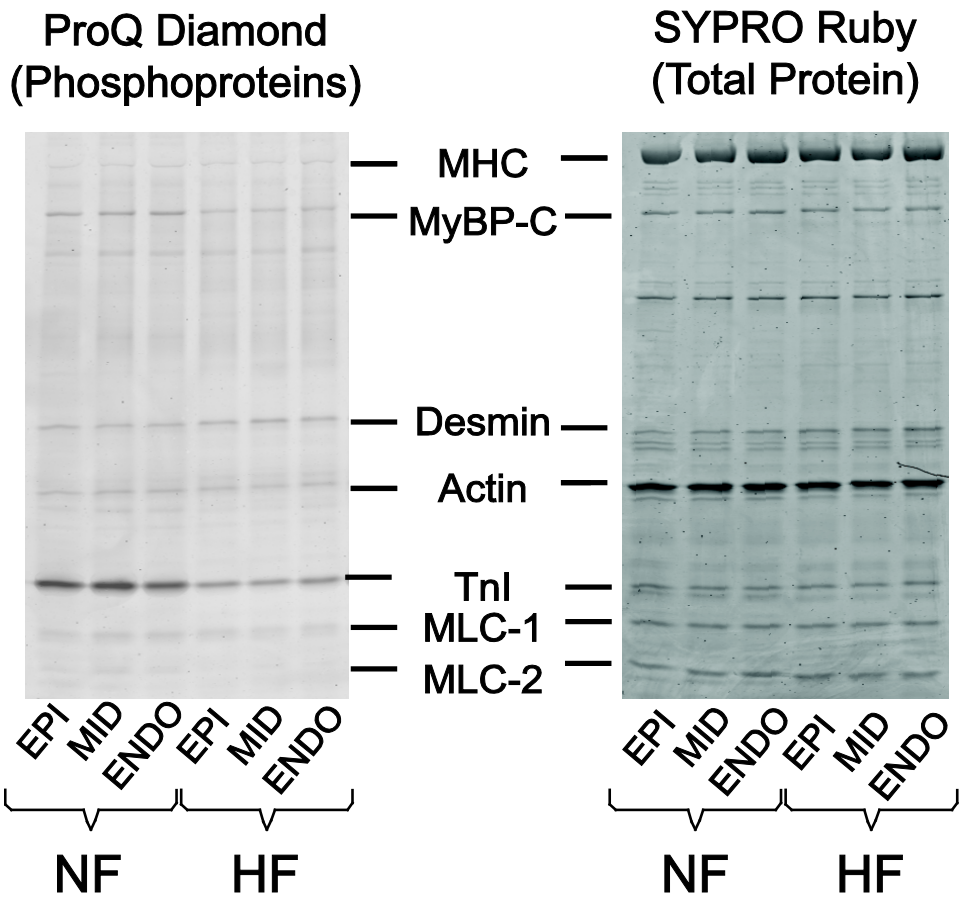

Figure 4.10. Broadrange gel stained for phosphorylated and total sarcomeric proteins.

Two images of a single representative gel stained with Pro-Q Diamond (left) and SYPRO Ruby (right). The Pro-Q Diamond stain is more sensitive to phosphoproteins while SYPRO Ruby indicates total protein content.

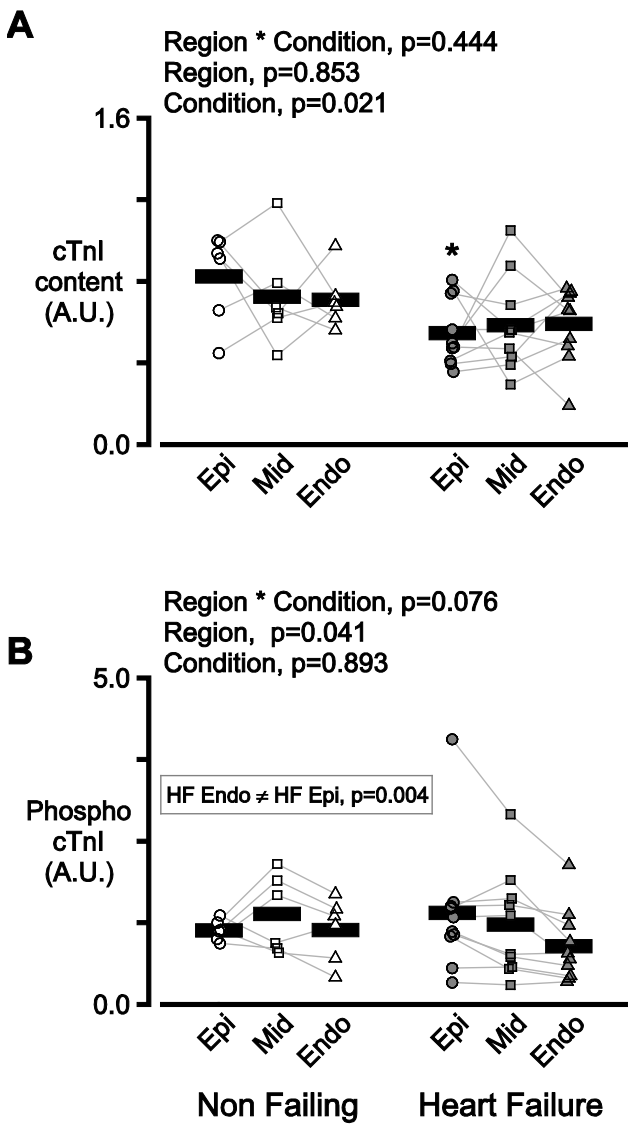

Figure 4.11. cTnI content decreases with heart failure and phospho cTnI depends on transmural region.

A) Symbols show the relative content of cTnI for each region for each heart using SYPRO Ruby stain for total protein. B) Symbols show the mean Phospho cTnI measured for each region for each heart using Pro-Q Diamond (phospho-sensitive stain). A.U. stands for arbitrary units.

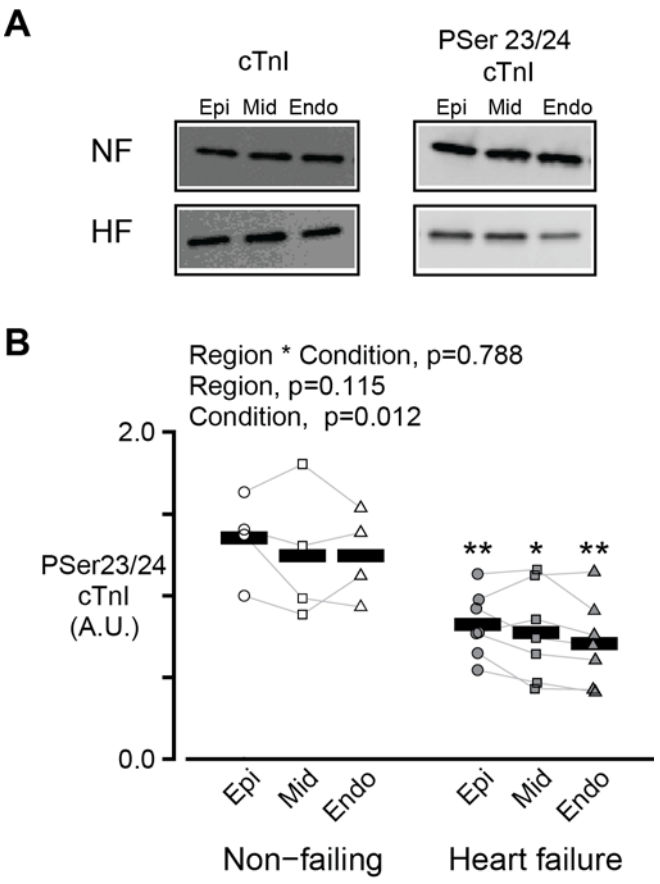

Figure 4.12. PSer23/24 cTnI is reduced in heart failure.

A) Representative immunoblots showing total cTnI and PSer23/24 cTnI for non-failing and failing hearts. B) Symbols show the mean PSer23/24 cTnI measured for each region for each heart. A.U. stands for arbitrary units

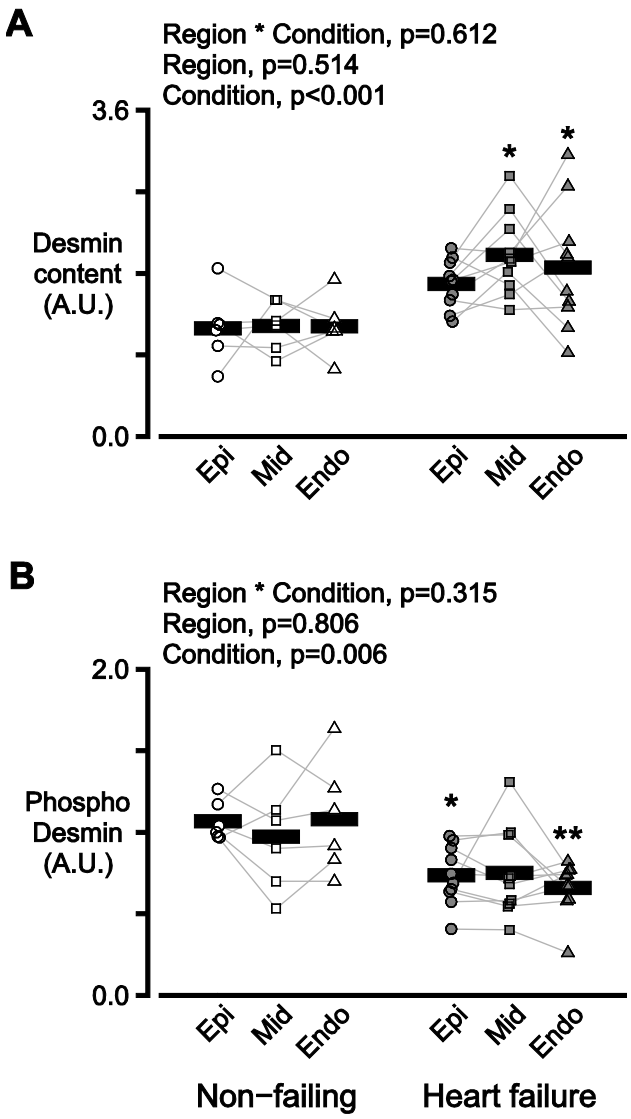

Figure 4.13. Desmin content increases and its phosphorylation decreases with heart failure

A) Symbols show the relative content of desmin for each region for each heart using SYPRO Ruby stain for total protein. B) Symbols show the mean phospho desmin measured for each region for each heart using Pro-Q Diamond (phosphor-sensitive stain). A.U. stands for arbitrary units.

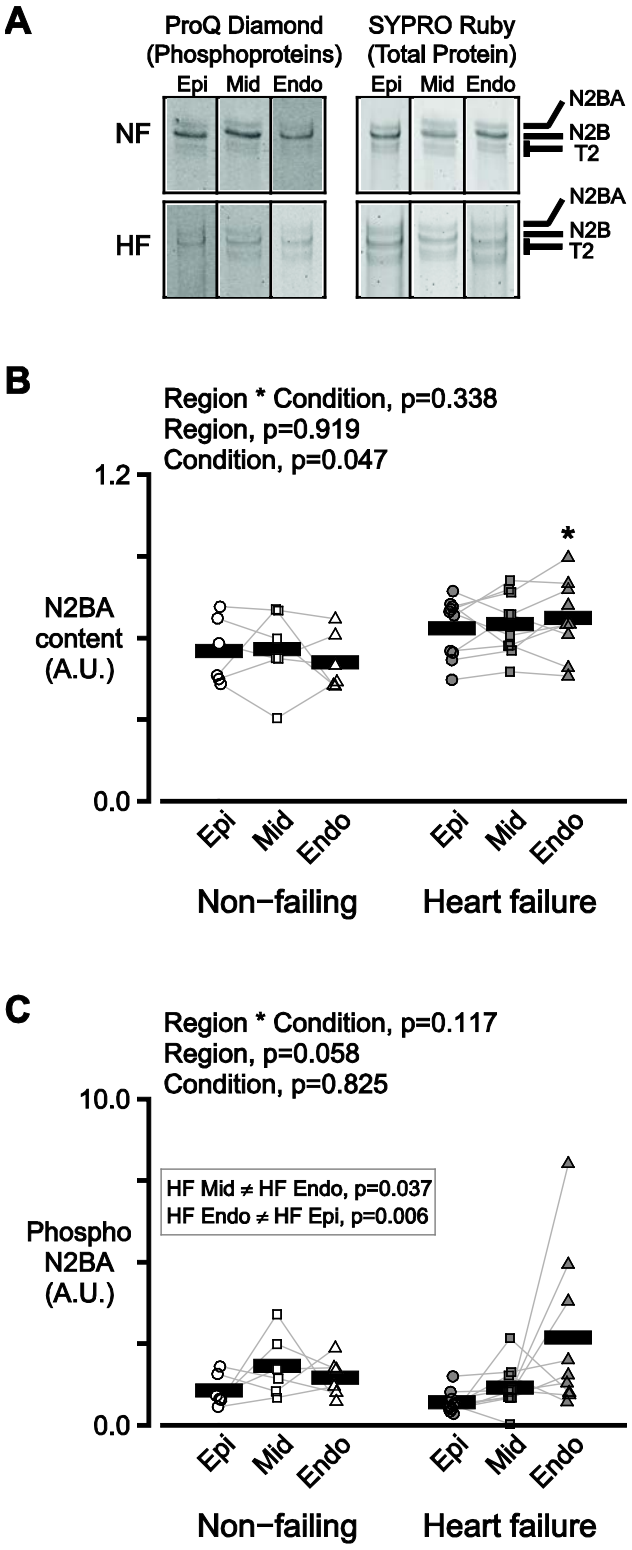
A
ProQ Diamond
(Phosphoproteins)
SYPRO Ruby
(Total Protein)
Epi Mid Endo
Epi Mid Endo
NF
HF
N2BA
N2B
T2
N2BA
N2B
T2
B
Region * Condition, p=0.338
Region, p=0.919
Condition, p=0.047
1.2
0.0
N2BA
content
(A.U.)
*
Epi Mid Endo Epi Mid Endo
Non−failing
Heart failure
C
Region * Condition, p=0.117
Region, p=0.058
Condition, p=0.825
10.0
0.0
Phospho
N2BA
(A.U.)
HF Mid ≠ HF Endo, p=0.037
HF Endo ≠ HF Epi, p=0.006
Epi Mid Endo Epi Mid Endo
Non−failing
Heart failure

Figure 4.14. The relative content of the N2BA isoform of titin is increased in heart failure.

A) Titin gels stained with Pro-Q Diamond (left) and SYPRO Ruby (right). The figure shows lanes collated from several gels. The Pro-Q Diamond stain is sensitive to phosphoproteins while SYPRO Ruby indicates total protein content. B) Symbols show the relative content of the N2BA isoform for each region for each heart. A.U. stands for arbitrary units. C) As for panel B but showing the relative content of phosphorylated N2BA protein.

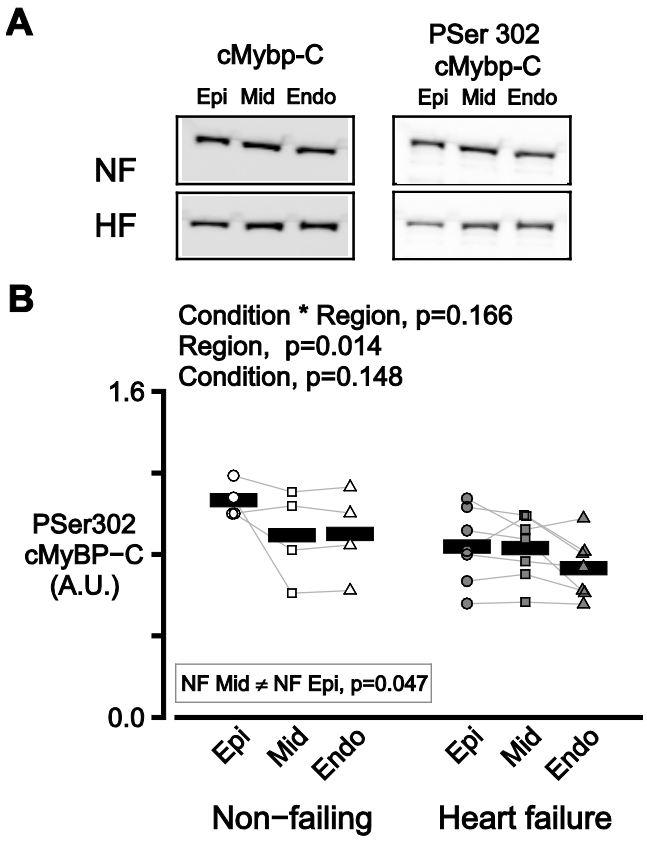

Figure 4.15. PSer302 cMyBP-C depends on transmural region.

A) Representative immunoblots showing total cMyBP-C and PSer302 cMyBP-C for non-failing and failing hearts. B) Symbols show the mean PSer302 cMyBP-C measured for each region for each heart. A.U. stands for arbitrary units.

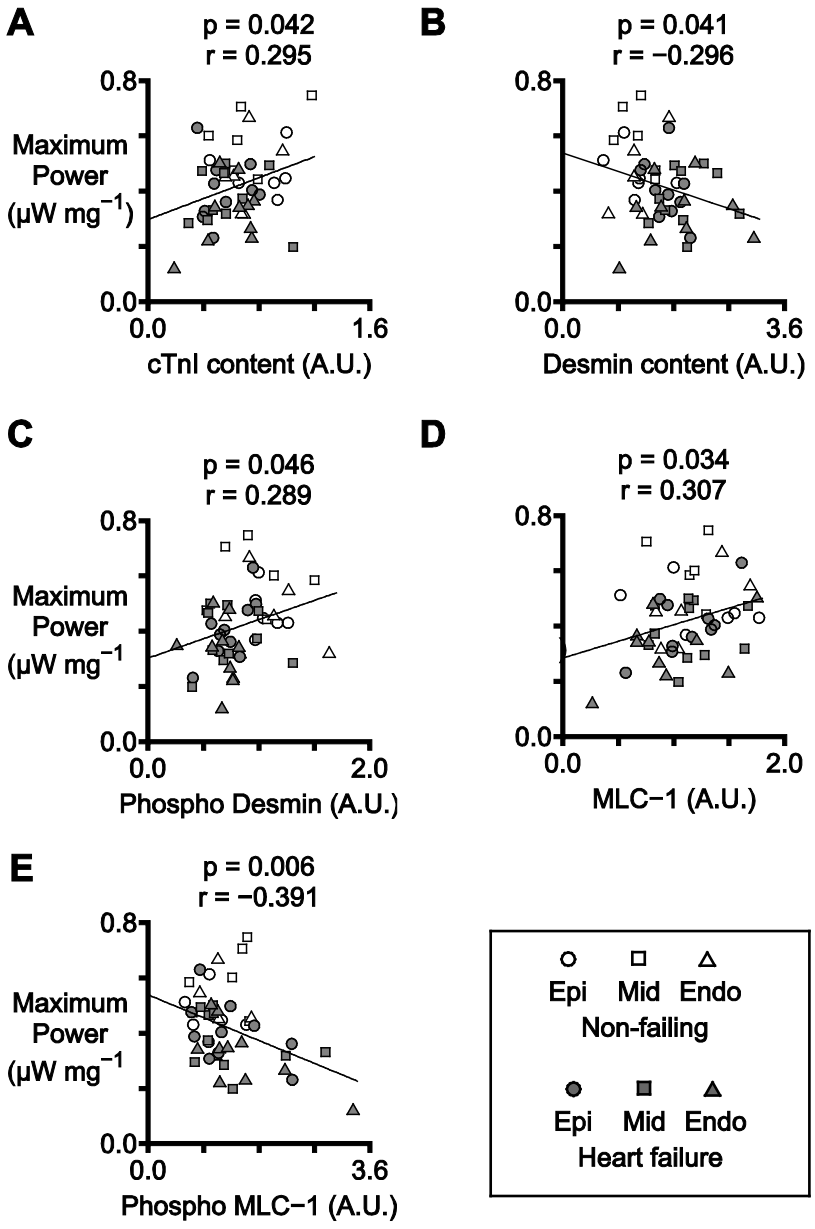

Figure 4.16. Statistically significant relationships between maximum power and biochemical data.

Each panel shows the relationship between maximum power and a selected biochemical property (for example, actin content). The y coordinate of each symbol indicates the mean value of maximum power measured from 2 or 3

preparations from each region for each heart. The x coordinate of each symbol shows the result of the biochemical assay performed using the matching sample. The plots also show the best-fit straight lines determined by linear regression and the corresponding p and r values. Table S4 provides r and p values for additional relationships that had p values less than 0.05.

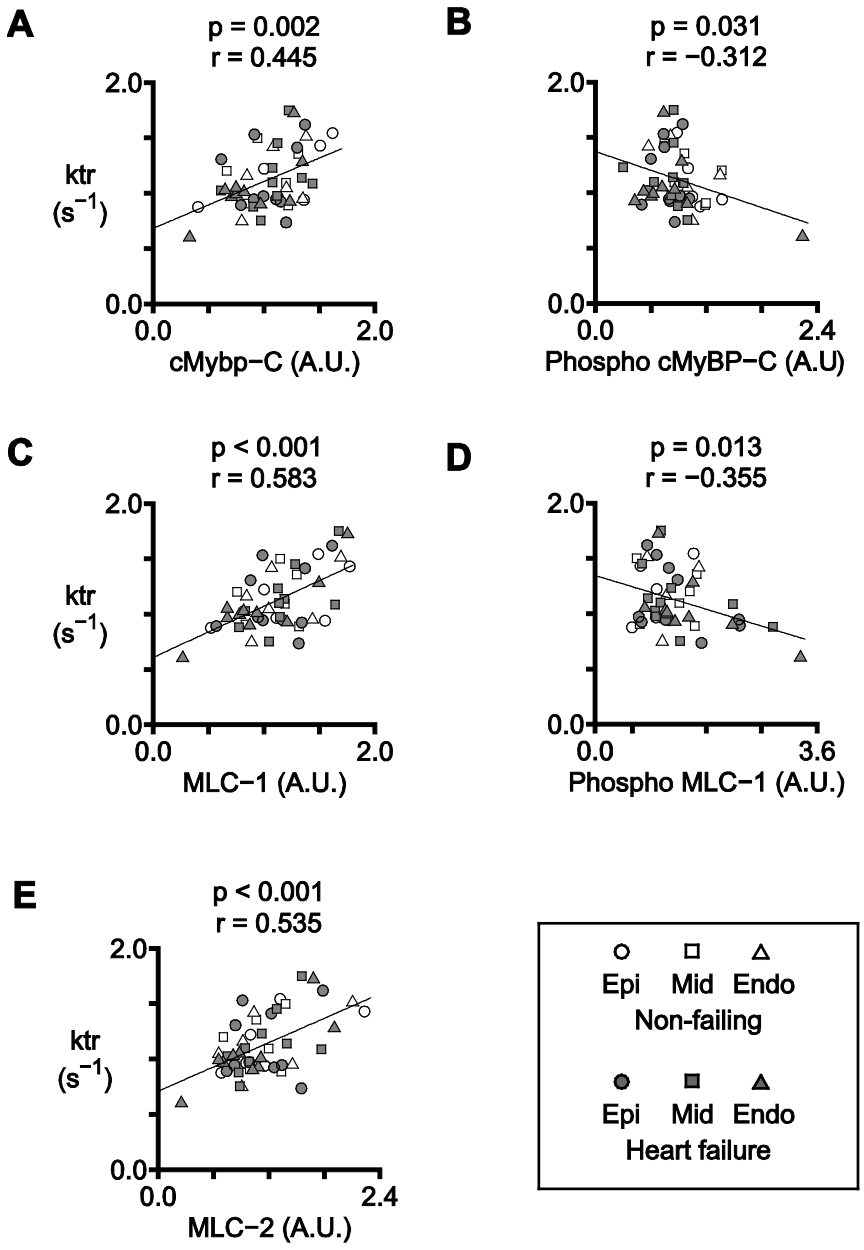

Figure 4.17. Statistically significant relationships between rate of tension redevelopment and biochemical data.

Each panel shows the relationship between ktr and a selected biochemical property (for example, actin content). The y coordinate of each symbol indicates the mean value of ktr measured from 2 or 3 preparations from each region for

each heart. The x coordinate of each symbol shows the result of the biochemical assay performed using the matching sample. The plots also show the best-fit straight lines determined by linear regression and the corresponding p and r values. Table 6 provides r and p values for additional relationships that had p values less than 0.05.

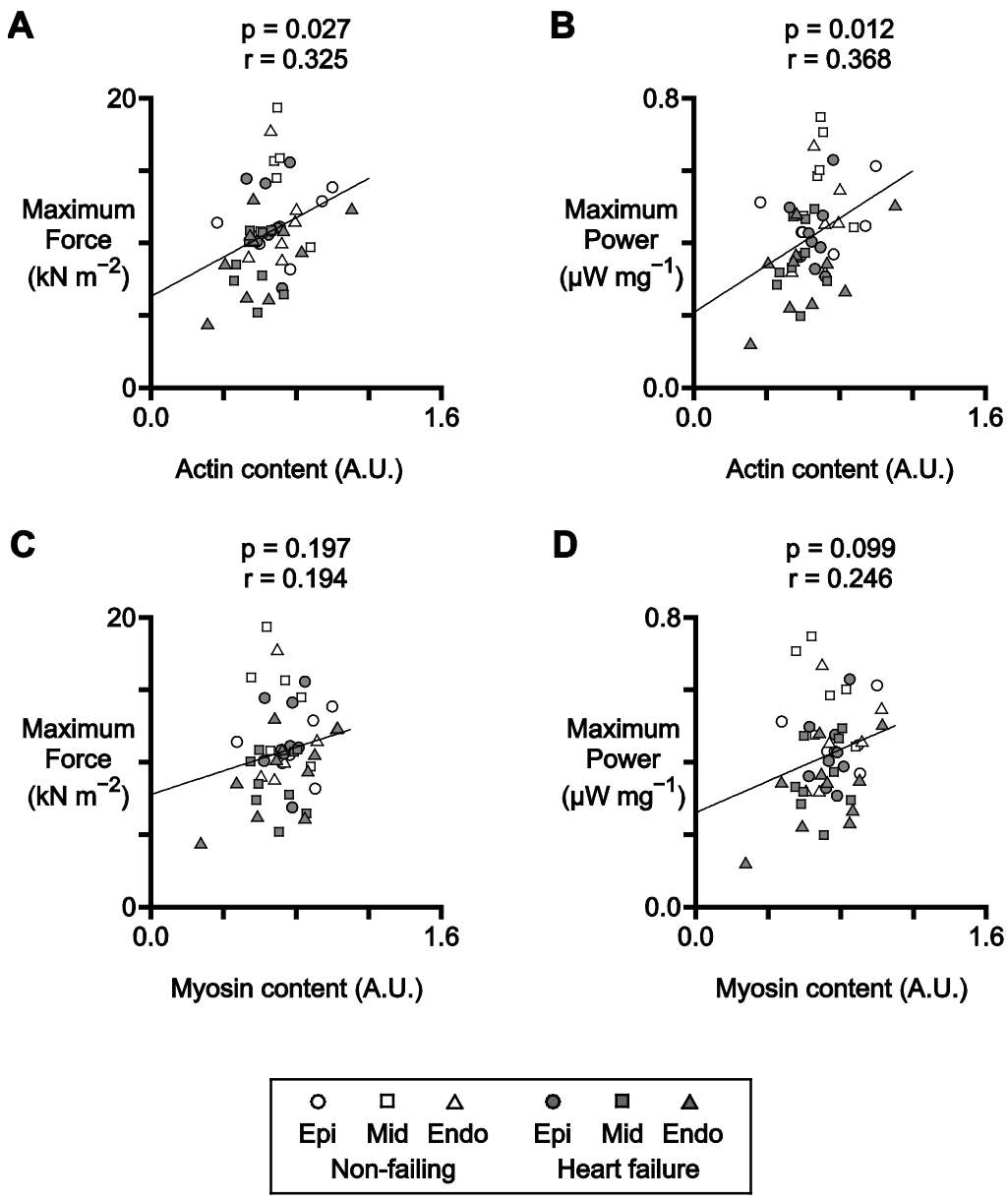

Figure 4.18. Contractile function is reduced with decrease in actin content.

A) Maximum Force and B) Maximum Power plotted against the actin content. C) Maximum Force and D) Maximum Power plotted against the myosin content. Protein content was determined by Lowry protein assays and corrected for initial weight of the tissue (Table S3 and gel electrophoresis Figure 13A). A.U. stands

for arbitrary units. The plots show the best-fit straight lines determined by linear regression and the corresponding p and r values.

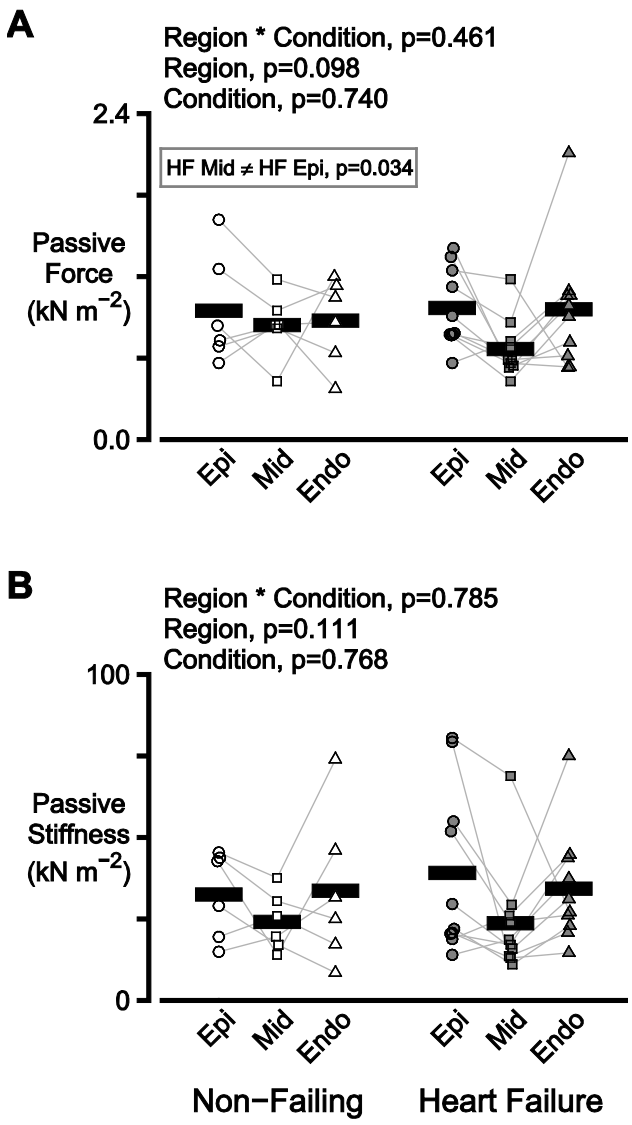

Figure 4.19. Passive force and passive stiffness do not depend on heart failure status.

A) Passive force and B) passive stiffness measured in pCa 9.0 solution. In both plots, symbols show the mean data value measured from 2 or 3 preparations from each region for each heart.

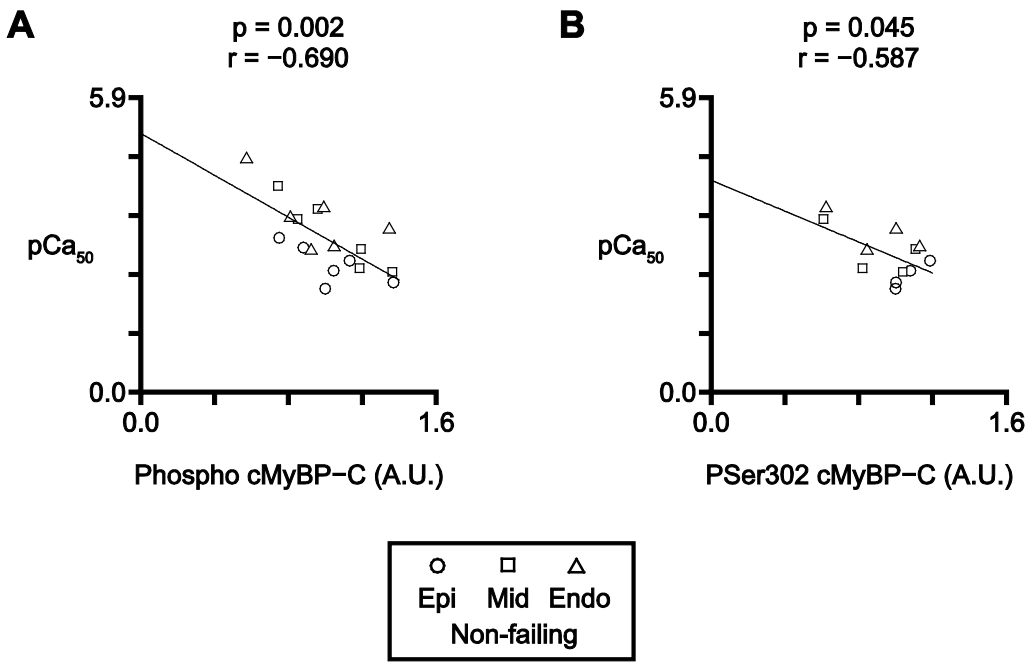

Figure 4.20. Ca^{2+} sensitivity of non-failing samples depended on the phosphorylation of cMyBP-C.

Ca^{2+} sensitivity of non-failing samples correlated significantly with A) total phosphorylation of cMyBP-C and B) site-specific phosphorylation of cMyBP-C at Ser302. A.U. stands for arbitrary units. The plots show the best-fit straight lines determined by linear regression and the corresponding p and r values.

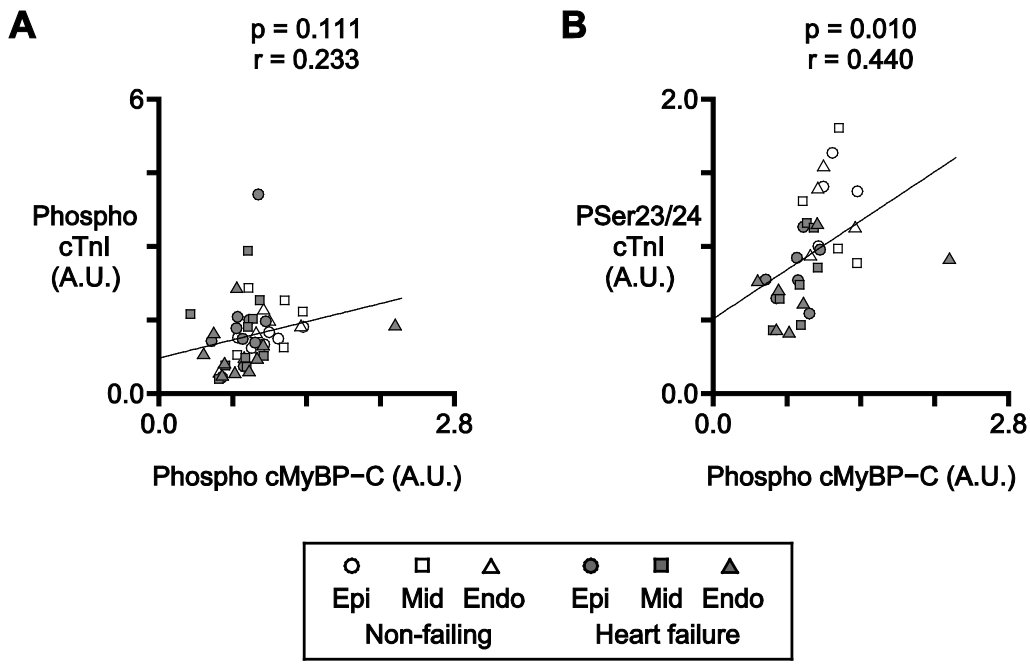

Figure 4.21. Site-specific phosphorylation of cTnI at Ser23/24 correlated with phosphorylation of cMyBP-C.

A) Total phosphorylation and B) site-specific phosphorylation of cTnI at Ser23/24 correlations with total phosphorylation of cMyBP-C. A.U. stands for arbitrary units. The plots show the best-fit straight lines determined by linear regression and the corresponding p and r values.

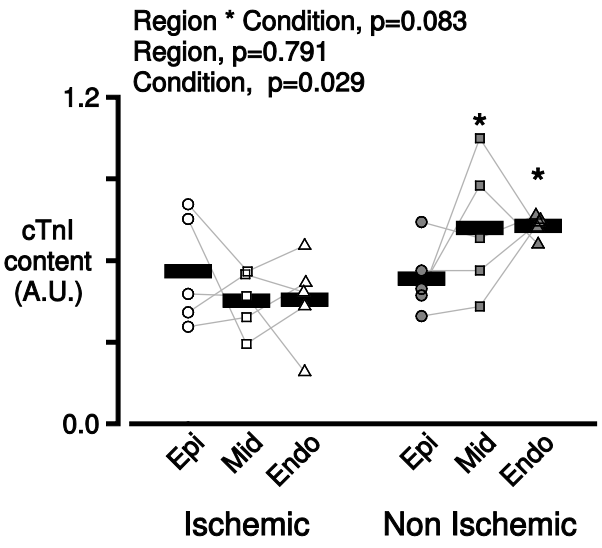

Figure 4.22. cTnI content is reduced in ischemic heart failure.

Symbols show the mean cTnI content measured for each region for failing hearts with ischemic disease (left) and non-ischemic disease (right).

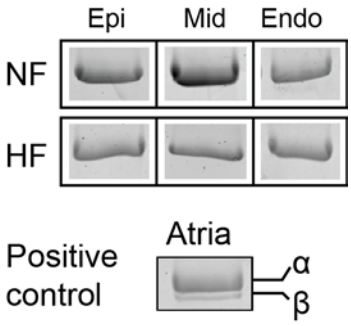

Figure 4.23. MHC isoforms.

β-MHC bands seen in the non-failing and failing samples from the transmural regions. The human atrial samples have both the α- and β-MHC resolved.

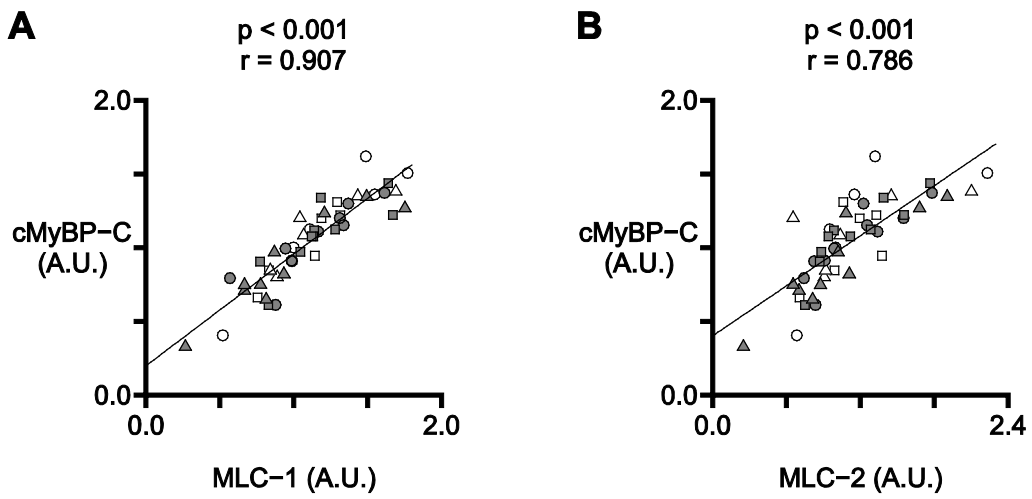

Figure 4.24. cMyBP-C strongly correlated with both MLC-1 and MLC-2.

Significant correlations between cMyBP-C and A) MLC-1 and B) MLC-2.

Chapter 5. Discussion

5.1. Overall Conclusions

The heart can fail as pump due to decreased contractility or diminished ventricular relaxation. One or both of these impairments can get progressively worse and lead to irreversible heart failure. In this dissertation, we sought to identify transmural cellular level contractile mechanisms that are modified in the left ventricle just prior to the onset of heart failure and in end-stage heart failure.

This dissertation demonstrates that normal left ventricles exhibit transmural heterogeneity in cellular level contractile properties and that with aging and heart failure there are region-specific changes in cellular level contractile mechanisms.

The aging F344 rat study detailed in Chapter 3 revealed that the 22-month old animals exhibited a region-specific decrease in phosphorylation of cTnI in the sub-epicardial samples when compared to the mid-myocardial and sub-endocardial samples of the same age. This molecular modification may contribute to the slowed relaxation of sub-epicardial myocytes in the 22-month old animals. We were thus able to identify a molecular level modification, which potentially contributes to diastolic dysfunction before the onset of aging associated heart failure.

The human heart failure study detailed in Chapter 4 revealed that the contractile properties of human hearts exhibit transmural variation in non-failing organs, and

that heart failure alters the transmural pattern as well as depressing myocardial function. These new results show that contractile properties are heterogenous in non-failing left ventricles and that there are region-specific modifications in contractile properties with heart failure. These new results help to explain why *in vivo* shortening of the middle transmural region is a better predictor of cardiovascular death than traditional global measures of ventricular function.

5.2. Limitations of the studies in this dissertation

5.2.1. Use of rodent model

Even though rodent models are very useful in understanding mechanisms of cardiac dysfunction they have some disadvantages like differential expression of ion channel, Ca^{2+} handling proteins and sarcomeric proteins compared to humans [68, 149, 150]. In Chapter 3, we discussed that 6-month old rodents express ~70 % of α-MHC (Figure 3.5). With age [65] and disease [151] the rodents switch to a greater proportion of the β-MHC isoform. Furthermore, the increase in the proportion of β-MHC isoform slows cross bridge kinetics and can affect both contraction [152] and relaxation properties [68]. Even though there is a functional effect of the β-MHC isoform shift with aging and disease in rodents, this may not be the case in humans. Non-failing human hearts already express ~ 90-100% β-MHC isoform [116, 142] (Figure 4.23) and therefore the shift in isoform if any will be very small with human heart failure [123]. This means that there are other

mechanisms that influence kinetics in humans and it would be hard to tease out these mechanisms using animal models because of the dominating effect of β-MHC isoform shift on kinetics.

5.2.1.1. Biochemical analysis

One of the limitations of the aging F344 rat study was that the n=3 animals in each age group for the biochemical analysis. This meant that the study may have been under powered. Future studies may require increase in the number of animals.

5.2.2. Use of human tissue

Humans are genetically different from each other and come from different environments. However, it is important to note that the use of human tissue provides data that is more clinically relevant than some animal studies and is thus arguably of more translational relevance.

We had logistical difficulty in obtaining the human tissue samples that were age and gender matched to the donors and patients (Table 2.2). As discussed in section 2.1.2.2, the mean age of the patients with heart failure was 49 (range 20 to 65) while that of the organ donors was 35 (range 18 to 59). Females donated 20% of the failing hearts and 50% of the non-failing organs. We performed regression analyses and showed that the key contractile properties reported in

this work did not vary with age (Figure 5.1). Furthermore, we showed that there was no significant interaction between gender and condition in our study (Figure 5.2) for the key contractile properties suggesting that heart failure was not gender dependent.

We also investigated the effect of β blocker on heart failure patients because β-adrenergic stimulation activates an important signaling pathway that can regulate various contractile proteins [63, 110, 153]. We did not find any significant difference in the key contractile properties measured and the effect of β-blocker (Figure 5.3).

It is possible that ischemic and non ischemic heart failure produce distinct changes in contractile function (Tables 5.1, 5.2, 5.3, 5.4, 5.5, 5.6, 5.7, 5.8, 5.9 and 5.10 and Figures 4.22 and 5.4). Due to the small sample size (n=5 in both heart failure groups), tests comparing ischemic and non-ischemic samples had limited statistical power. The results from Tables 5.9 and 5.10 could be interpreted as suggesting that failing non ischemic tissue has worse contractile function than failing ischemic tissue. It would be interesting to follow up on these results in future work using larger numbers of hearts.

All of the organ donors in this study had been treated in Intensive Care Units before the determination of brain death and some had comorbidities such as diabetes and/or hypertension. Therefore, it is unclear whether the non-failing hearts are truly representative of healthy organs. However, none of the donors had a prior history of ventricular dysfunction and the hearts used in this work are the best controls that are available.

5.2.2.1. Permeabilized samples

We performed functional measurements using chemically permeabilized multicellular preparations. These biospecimens were optimal for testing myofibrillar-level function and for investigating the effects of the extracellular matrix on passive mechanical properties. However, additional experiments using enzymatically isolated cells that are still electrically excitable could also have investigated potential transmural variation in calcium handling (similar to the functional experiments done in Chapter 3 [65]) [154] and mitochondrial function [155]. These measurements cannot be performed once the membranes have been permeabilized.

5.3. Linking *in vitro* mechanics to *in vivo* function

5.3.1. Pressure-volume relationship

The pressure-volume loop (PV) gives *in vivo* information about left ventricular performance during a single cardiac cycle. The PV loop can be divided into 4 phases (Figure 5.5A). In phase “a” (diastole) the mitral valve opens and ventricular filling occurs. In phase “b” (systole) the mitral valve closes and isovolumic contraction occurs where the left ventricular pressure rises and the volume remains the same. In phase “c” (systole) the aortic valve opens after the left ventricular pressure exceeds the aortic pressure, which then leads to ejection. During ejection the heart has to perform external work against an

afterload. In phase “d” (diastole), the aortic valve closes after the ventricular pressure becomes lower than the aortic pressure and isovolumic relaxation occurs. The ventricular pressure declines further and the ventricle begins to relax without a change in volume. PV loops can therefore yield information about the work done by the ventricle. Detrimental changes to any of these 4-phases can indicate cardiac dysfunction.

5.3.2. Permeabilized preparations-in vitro mechanics

The cellular level contractile properties investigated in this dissertation gives an *in vitro* index of systolic and diastolic function. In the human heart failure study detailed in Chapter 4, we measured active and passive mechanical properties of multicellular preparations, which were representative of the myocytes linked with the connective tissue in the left ventricle. Figure 5.5 summarize some of the *in vitro* parameters investigated in this study that we can compare to the different phases of the PV loop. For example, the *in vitro* measure of force and power gives us information about phase “c” (ejection) of the PV loop. In our study, there was an ~20% decrease in power in heart failure samples (Figure 4.2) and this *in vitro* measure indicates systolic dysfunction at the cellular level. Similarly, we did not see a significant difference in the rate of tension redevelopment in failing hearts (Figure 4.7) which in our study may potentially be an index of rate of pressure development (dp/dt).

It should be noted that the extrapolation of the *in vitro* mechanical properties to the PV loop is simplistic because the PV loop is indicative of global left ventricular function. However, the *in vitro* measurements are representative of the mechanical behavior of the sarcomeres and connective tissue that contribute to the various phases of the PV loop and can therefore be extremely useful to identify molecular and cellular level modifications.

5.4. Sarcomere level therapies for heart failure

Modifications to sarcomeric proteins can lead to pump dysfunction [63]. In this dissertation we reported posttranslational modifications to sarcomeric proteins, isoform switch and decrease in the relative content of sarcomeric proteins in aging (Chapter 3) and in heart failure (Chapter 4).

One of the major modifications that can regulate sarcomere function is phosphorylation of sarcomeric proteins like cTnI, cMyBP-C and titin. Studies have shown that PKA, PKC and PKG are the main kinases that phosphorylate these proteins [63, 126, 156]. Changes to the phosphorylation level of sarcomeric proteins can alter contractile function. For example, in heart failure, there is a decrease in β_2 stimulations either due to desensitization of the β_2 receptors or decrease in the content of the receptors themselves [157]. Activation of the β_2-adrenergic receptor signaling leads to an increase in cAMP, which in turn activates PKA. PKA can then phosphorylate sarcomeric proteins including cTnI, cMyBP-C and Titin [158]. In the aging F344 rat study we saw a decrease in cTnI

phosphorylation in the sub-epicardial cells of 22-month old F344 rats (Figure 3.7) and in the human heart failure study we saw a site-specific decrease in phosphorylation of cTnI at Ser 23/24 in failing hearts (Figure 4.12). In the aging F344 rat study phosphorylation of cTnI was linked to slowed relaxation and in the human heart failure study there was a significant novel correlation between site-specific phosphorylation of cTnI at Ser 23/24 and passive stiffness (Table 4.7). These results from both rodent and human studies (Chapter 3 and 4) make phosphorylated cTnI a potential contributor to relaxation and therefore a therapeutic target for diastolic dysfunction.

Sarcomere-level interventions could potentially be effective treatment for heart failure. For example, a cardiac specific myosin activator molecule [159] is in phase II clinical trials and is being evaluated for acute and chronic systolic heart failure. Its mechanism of action allows the myosin cross bridges to strongly bind to actin and stay bound for a longer duration [160]. In the human heart failure study for example, we not only saw a significant decrease in cTnI content in human heart failure (Figure 4.11) we also saw a significant correlation between power and relative cTnI content (Figure 4.16A) which is a potential sarcomeric protein that can be targeted to improve cardiac function.

5.5. Importance of transmural heterogeneity in the ventricular wall

Anatomical location is sometimes ignored when studying the left ventricle because it is assumed that it is a homogenous structure. However, in Chapter 1

(section 1.1), we discussed that the ventricular wall is made up “layers” of muscle with changing fiber angles [1-4, 6]. There are known transmural differences in action potential morphologies in human and animal hearts [42-44] and few studies in animals have shown differences in contractile properties [46, 47, 64, 101]. Our study, for the first time showed differences in contractile properties across the ventricular wall in non-failing and failing human myocardium (Chapter 4) and a region-specific molecular modification in aging F344 rats (Chapter 3).

5.5.1. The mid-myocardium in the failing human heart

Ingels, 1997 [10], laid down several working hypothesis to explain the coupling between the myocardial fiber architecture and left ventricular function. He utilized LaPlace’s law (P=Tw/r where T is wall tension; w is wall thickness and r is radius of the cavity) and proposed that the mid-myocardial circumferential fibers are optimal to develop pressure because they have a minimum radius of curvature when compared to the spiral sub-endocardial fibers which are better suited to maximize ejection fraction [10]. In the human heart failures study we saw a significant decrease in force and power and increased fibrosis in the mid-myocardial samples of the failing hearts (Figure 4.2, 4.3A, 4.8 and 4.9). These region-specific changes could contribute to the decrease in global ventricular function in patients in end-stage heart failure because the mid-myocardial circumferential fibers necessary to generate the required pressure are dysfunctional.

5.5.2. The mid-myocardial region of non-failing human hearts

The mid-myocardial samples from the non-failing human hearts exhibited increase in power and force (4.2 and 4.3A) compared to the sub-epicardial and sub-endocardial samples. There are two potential reasons as to why the myocytes from the mid-myocardial region have different contractile properties, 1) the environment that these myocytes are located in *in vivo* make them different and/or 2) myocytes from the mid-myocardial region are specialized myocytes.

5.5.2.1. Mechanosensitive pathways

The mid-myocardial fibers are arranged circumferentially in the left ventricle while the sub-epicardial and the sub-endocardial fibers are more longitudinally arranged [5]. This means that the myocytes in the mid-myocardial region potentially undergo different mechanical stress and strain stimuli than the myocytes in the sub-epicardial and sub-endocardial regions. Studies have shown that longitudinal vs. tranverse stretch can bring about different anistropic (dependent on direction) changes in myocytes and lead to differential upregulation of sarcomeric proteins [161-163]. The major signal transduction pathways that are activated by mechanical stimuli are mitogen-activated protein kinase (MAPK) pathway, the Janus-associates kinases/signal transducers and activators of transcription (JAK/STAT) [164] and/or the Ca^{2+}/calmodulin-dependent phosphatase calcineurin [165]. Particularly, z-disk proteins and titin have been

implicated in being able to sense changes in cell stress and strain, which then leads to transcriptional regulation [166, 167].

Further studies need to be done in order to understand the role of these pathways in non-failing human hearts.

5.5.2.2. M cells

There is some evidence of the existence of specialized population of myocytes in the mid-myocardium known as M cells. These cells have been extensively studied due to their distinct electrophysiological properties and are described to be a hybrid of purkinje and ventricular cells [168]. Specifically, M cells have a characteristically prolonged action potential duration when compared to the sub-epicardial and sub-endocardial myocytes [42, 168] and are present in different species including humans [169, 170 41]. A recent study demonstrated that M cells were present in island like cluster in non-failing human hearts but were not found in the failing human heart [42]. The M cells may have distinct electrophysiological properties but further studies need to be done to investigate if they also have distinct contractile properties.

5.6. Application of this work

The findings from these studies have broader implication in three major cardiovascular fields that strive for patient-specific treatments- mainly cardiac imaging, ventricular finite element modeling and stem cell research.

5.6.1. Imaging studies

Both the aging F344 rat study and the human heart failure study revealed region-specific modifications in aging and failing left ventricles. The aging F344 rat study made use of imaging tools and demonstrated that ventricular torsion changes with age [65] and previous clinical studies have shown that shortening of the mid-myocardial region in a better predictor of cardiovascular outcomes than shortening of the endocardial region and ejection fraction [26-30]. All of these studies point out that global measures of ventricular function (ejection fraction) may not be sufficient for patient prognosis. With the increased use of MRI (magnetic resonance imaging) it will become more feasible to isolate region-specific changes that occur in dysfunctional myocardium [171].

5.6.2. Ventricular modeling

Computational models of the human hearts use *in vivo* imaging data to make predictions of myocardial contractility in patients with damaged myocardium [172]. But it has become more evident that multiscale modelling maybe more accurate

in predicting ventricular function because it takes into account cellular level contractile properties [173]. Our data helps to fill this gap as we have transmural cellular level contractile data in rodents and humans.

5.6.3. Stem cell therapies

In the past several years many advances have been made to utilize stem-cell therapy for patients with heart failure. The basic idea is to replace and/or repair injured myocardium by delivering stem cells to the heart to improve its function. One of the challenges has been to find the best method of stem cell delivery that will reach the target [174]. There are three main ways to deliver stem cells, 1) systemic intravenous infusion, 2) intracoronary infusion, and 3) direct intramyocardial injection (for example-during a coronary bypass graft). Each of these delivery systems have their own advantages and disadvantages. Even though intramyocardial injections are more invasive than other delivery systems, studies have shown that the hearts are able to retain stem cells better with this approach compared to the other 2 approaches [175-178].

Our study showed that the mid-myocardial samples from the non-failing hearts generate more power and more force than sub-epicardial and sub-endocardial samples. Furthermore, the mid-myocardial samples produced the least amount of force than sub-epicardial and sub-endocardial samples of the failing hearts (Figure 4.2 and 4.3A). This means that delivering stem cells to the mid-myocardium could be especially beneficial to improve systolic function.

Specifically, in patients with non ischemic heart disease who donot have a targeted region unlike patients with myocardial infract whose infract region may be the target for stem cell delivery.

5.7. Overall perspective

Complementary studies in human tissue and animal models needs to be performed in order to prevent and cure human heart failure [179]. One way to approach this is to systematically investigate the molecular level modifications that occur with heart failure in human tissue. These modifications should then be correlated with functional parameters that strongly predict them. The molecular mechanism should then be tested in other systems like transgenic and knockout animal models or cell cultures. Integration of all these system is key. In this dissertation we have tried to accomplish this method.

Finally, we have shown that there are contractile transmural heterogeneities across the ventricular wall in normal myocardium and there are region-specific modifications that occur with aging and heart failure. These cellular level modifications can contribute to organ level function and should be taken into account.

Table 5.1. Functional contractile properties in non ischemic and ischemic tissue.

		Maximum Power ($\mu W\ mg^{-1}$)	Maximum Force ($kN\ m^{-2}$)	Maximum Velocity ($mL\ s^{-1}$)
Non ischemic	Epi	0.37±0.04	9.79±1.10	1.05±0.07
	Mid	0.34±0.03	7.69±0.68	1.09±0.09
	Endo	0.31±0.02	9.33±1.09	0.93±0.05
Ischemic	Epi	0.43±0.03	12.41±0.83	1.00±0.05
	Mid	0.40±0.04	9.90±0.63	1.01±0.07
	Endo	0.36±0.05	9.38±1.09 §	1.06±0.09
Main statistical effects and interaction (p values)	Condition	0.348	0.228	0.999
	Region	0.045*	0.007**	0.773
	Condition *Region	0.845	0.145	0.334

Protein contents are expressed in arbitrary units and were calculated by normalizing to data obtained for each protein from a non-failing sub-epicardial sample that was loaded onto every gel as a control. Difference between main statistical effects and interaction: $p<0.05$= * and $p<0.01$=**. Different from the sub-epicardial region of the same condition: $p<0.05$= §.

Table 5.2. Functional contractile properties in non ischemic and ischemic tissue.

		Maximum Power ($\mu W\ mg^{-1}$)	Maximum Force ($kN\ m^{-2}$)	pCa_{50}
Non ischemic	Epi	0.37±0.04	9.79±1.10	5.68±0.02
	Mid	0.34±0.03	7.69±0.68	5.70±0.02
	Endo	0.31±0.02	9.33±1.09	5.65±0.05
Ischemic	Epi	0.43±0.03	12.41±0.83	5.69±0.03
	Mid	0.40±0.04	9.90±0.63	5.76±0.05
	Endo	0.36±0.05	9.38±1.09 §	5.72±0.04
Main statistical effects and interaction (p values)	Condition	0.348	0.228	0.535
	Region	0.045*	0.007**	0.140
	Condition *Region	0.845	0.145	0.286

Protein contents are expressed in arbitrary units and were calculated by normalizing to data obtained for each protein from a non-failing sub-epicardial sample that was loaded onto every gel as a control. Difference between main statistical effects and interaction: $p<0.05$= * and $p<0.01$=**. Different from the sub-epicardial region of the same condition: $p<0.05$= §.

Table 5.3. Functional passive properties in non ischemic and ischemic tissue.

		Passive Force ($kN\ m^{-2}$)	Passive Stiffness ($kN\ m^{-2}$)
Non ischemic	Epi	0.84±0.08	25.14±4.45
	Mid	0.60±0.07	19.72±3.53
	Endo	0.84±0.11	33.26±6.57
Ischemic	Epi	1.09±0.13	53.20±12.78 †
	Mid	0.75±0.14	28.88±12.10
	Endo	1.01±0.15	32.54±5.87
Main statistical effects and interaction (p values)	Condition	0.080	0.166
	Region	0.030*	0.187
	Condition *Region	0.910	0.209

Protein contents are expressed in arbitrary units and were calculated by normalizing to data obtained for each protein from a non-failing sub-epicardial sample that was loaded onto every gel as a control. Difference between main statistical effects and interaction: $p<0.05$= *. Different between the same regions of non ischemic and ischemic group: $p<0.05$= †.

Table 5.4. Content of selected sarcomeric proteins in non ischemic and ischemic tissue.

		cMyBP-C	cTnT	Actinin
Non ischemic	Epi	0.88±0.08	1.09±0.52	0.95±0.10
	Mid	1.1±0.33	1.26±0.58	1.22±0.21
	Endo	1.00±0.13	1.22±0.57	1.08±0.12
Ischemic	Epi	1.19±0.08	1.11±0.36	1.17±0.08
	Mid	1.08±0.05	1.68±0.39	1.05±0.03
	Endo	0.76±0.15 §	1.00±0.43	0.89±0.15
Main statistical effects and interaction (p values)	Condition	0.904	0.853	0.732
	Region	0.084	0.937	0.402
	Condition *Region	0.025*	0.932	0.146

Protein contents are expressed in arbitrary units and were calculated by normalizing to data obtained for each protein from a non-failing sub-epicardial sample that was loaded onto every gel as a control. Difference between main statistical effects and interaction: $p<0.05$= *. Different from the sub-epicardial region of the same condition: $p<0.05$= §.

Table 5.5. Content of selected sarcomeric proteins in non ischemic and ischemic tissue.

		MLC-1	MLC-2
Non ischemic	Epi	0.91±0.10	0.96±0.10
	Mid	1.20±0.13	1.21±0.18
	Endo	0.98±.0.16	1.12±0.21
Ischemic	Epi	1.33±0.10	1.33±0.16
	Mid	1.17±0.14	1.10±0.12
	Endo	0.91±0.24 §	0.90±0.24
Main statistical effects and interaction (p values)	Condition	0.564	0.964
	Region	0.126	0.496
	Condition *Region	0.084	0.096

Protein contents are expressed in arbitrary units and were calculated by normalizing to data obtained for each protein from a non-failing sub-epicardial sample that was loaded onto every gel as a control. Difference between main statistical effects and interaction: $p<0.05$= *. Different from the sub-epicardial region of the same condition: $p<0.05$= §.

Table 5.6. Content of Myosin Heavy Chain (MHC) and Actin in non ischemic and ischemic tissue.

		MHC	Actin
Non ischemic	Epi	0.70±0.04	0.64±0.04
	Mid	0.75±0.05	0.61±0.04
	Endo	0.81±0.04	0.66±0.05
Ischemic	Epi	0.78±0.02	0.68±0.02
	Mid	0.63±0.05	0.54±0.03
	Endo	061±0.13 †	0.58±0.14
Main statistical effects and interaction (p values)	Condition	0.217	0.608
	Region	0.733	0.515
	Condition*Region	0.124	0.574

Protein contents are expressed in arbitrary units and were calculated by normalizing to data obtained for each protein from a non-failing sub-epicardial sample that was loaded onto every gel as a control, and corrected for the initial weight of the original tissue sample. Different between the same regions of non ischemic and ischemic group: $p<0.05$= †.

Table 5.7. Phosphorylation of selected sarcomeric proteins and residues in non ischemic and ischemic tissue.

		Phospho cMyBP-C	Phospho cTnT	Phospho MLC-1
Non ischemic	Epi	0.75±0.10	2.50±0.89	0.91±0.10
	Mid	0.84±0.07	1.93±0.64	1.20±0.13
	Endo	0.73±0.10	1.82±0.47	0.98±0.16
Ischemic	Epi	0.83±0.03	1.70±0.45	1.33±0.10
	Mid	0.70±0.11	1.43±0.50	1.17±0.14
	Endo	0.10±0.32	2.50±0.89	0.91±0.24 §
Main statistical effects and interaction (p values)	Condition	0.678	0.921	0.564
	Region	0.749	0.370	0.126
	Condition *Region	0.337	0.168	0.084

Phosphorylation levels are expressed in arbitrary units and were calculated by normalizing to data obtained for each protein from a non-failing sub-epicardial sample that was loaded onto every gel as a control. Difference between main statistical effects and interaction: $p<0.05$= *. Different from the mid-myocardial region of the same condition: $p<0.05$= ‡. Different from the sub-epicardial region of the same condition: $p<0.05$= §.

Table 5.8. Phosphorylation of selected sarcomeric proteins and residues in non ischemic and ischemic tissue.

		PSer273 cMyBP-C	PSer282 cMyBP-C
Non ischemic	Epi	0.94±0.28	0.88±0.10
	Mid	1.25±0.44	0.91±0.11
	Endo	0.80±0.17	0.88±0.10
Ischemic	Epi	1.80±0.49	1.09±0.11
	Mid	1.49±0.35	0.99±0.10
	Endo	1.35±0.21	1.10±0.09 ‡
Main statistical effects and interaction (p values)	Condition	0.240	0.279
	Region	0.187	0.302
	Condition *Region	0.247	0.043*

Phosphorylation levels are expressed in arbitrary units and were calculated by normalizing to data obtained for each protein from a non-failing sub-epicardial sample that was loaded onto every gel as a control. Difference between main statistical effects and interaction: $p<0.05$= *. Different from the mid-myocardial region of the same condition: $p<0.05$= ‡. Different from the sub-epicardial region of the same condition: $p<0.05$= §.

Table 5.9. Functional contractile properties in non-failing and ischemic tissue.

		Maximum Power ($\mu W\ mg^{-1}$)	Maximum Force ($kN\ m^{-2}$)	pCa_{50}
Non-failing	Epi	0.46±0.03	10.96±0.74	5.619±0.01
	Mid	0.59±0.06§	14.30±1.33§	5.67±0.02
	Endo	0.46±0.04‡	11.47±0.86‡	5.69±0.02§
Ischemic	Epi	0.43±0.03	12.41±0.83	5.69±0.03
	Mid	0.40±0.04†	9.90±0.63†	5.76±0.05§
	Endo	0.36±0.05	9.38±1.09§	5.72±0.04
Main statistical effects and interaction (p values)	Condition	0.080	0.230	0.251
	Region	0.057	0.110	***0.001***
	Condition *Region	0.132	***0.004***	0.366

Effect of ischemic status on region: † $p<0.05$. Different from the sub-epicardial region of the same condition: § $p<0.05$. Different from the mid-myocardial region of the same condition: ‡ $p<0.05$.

Table 5.10. Functional contractile properties in non-failing and non ischemic tissue.

		Maximum Power ($\mu W\ mg^{-1}$)	Maximum Force ($kN\ m^{-2}$)	pCa_{50}
Non-failing	Epi	0.46±0.03	10.96±0.74	5.619±0.01
	Mid	0.59±0.06§	14.30±1.33§	5.67±0.02
	Endo	0.46±0.04‡	11.47±0.86‡	5.69±0.02§
Non ischemic	Epi	0.37±0.04	9.79±1.10	5.68±0.02
	Mid	0.34±0.03†	7.69±0.68†	5.70±0.02
	Endo	0.31±0.02†	9.33±1.09	5.65±0.05
Main statistical effects and interaction (p values)	Condition	***0.009***	***0.040***	0.717
	Region	0.117	0.704	0.096
	Condition *Region	0.091	***0.004***	***0.004***

Effect of non ischemic status on region: † $p<0.05$. Different from the sub-epicardial region of the same condition: § $p<0.05$. Different from the mid-myocardial region of the same condition: ‡ $p<0.05$.

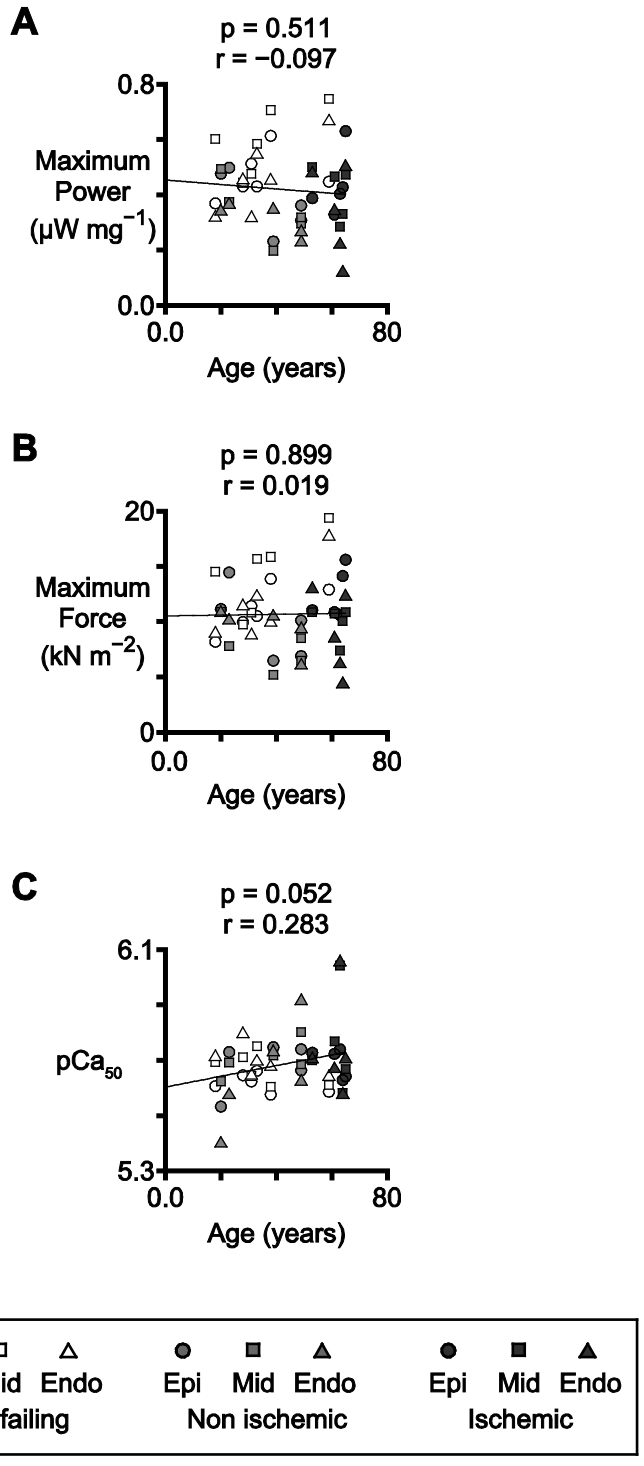
A
p = 0.511
r = −0.097
0.8
Maximum
Power
(μW mg−1)
0.0
0.0
80
Age (years)
B
p = 0.899
r = 0.019
20
Maximum
Force
(kN m−2)
0
0.0
80
Age (years)
C
p = 0.052
r = 0.283
6.1
pCa50
5.3
0.0
80
Age (years)
Epi Mid Endo
Non-failing
Epi Mid Endo
Non ischemic
Epi Mid Endo
Ischemic

Figure 5.1. No statistically significant relationships between contractile properties and age.

Each panel shows the relationship between a selected functional parameter and age. The y coordinate of each symbol indicates the mean value of a functional parameter measured from 2 or 3 preparations from each region for each heart. The x coordinate of each symbol shows the age of the individual patient/donor. The plots also show the best-fit straight lines determined by linear regression and the corresponding p and r values.

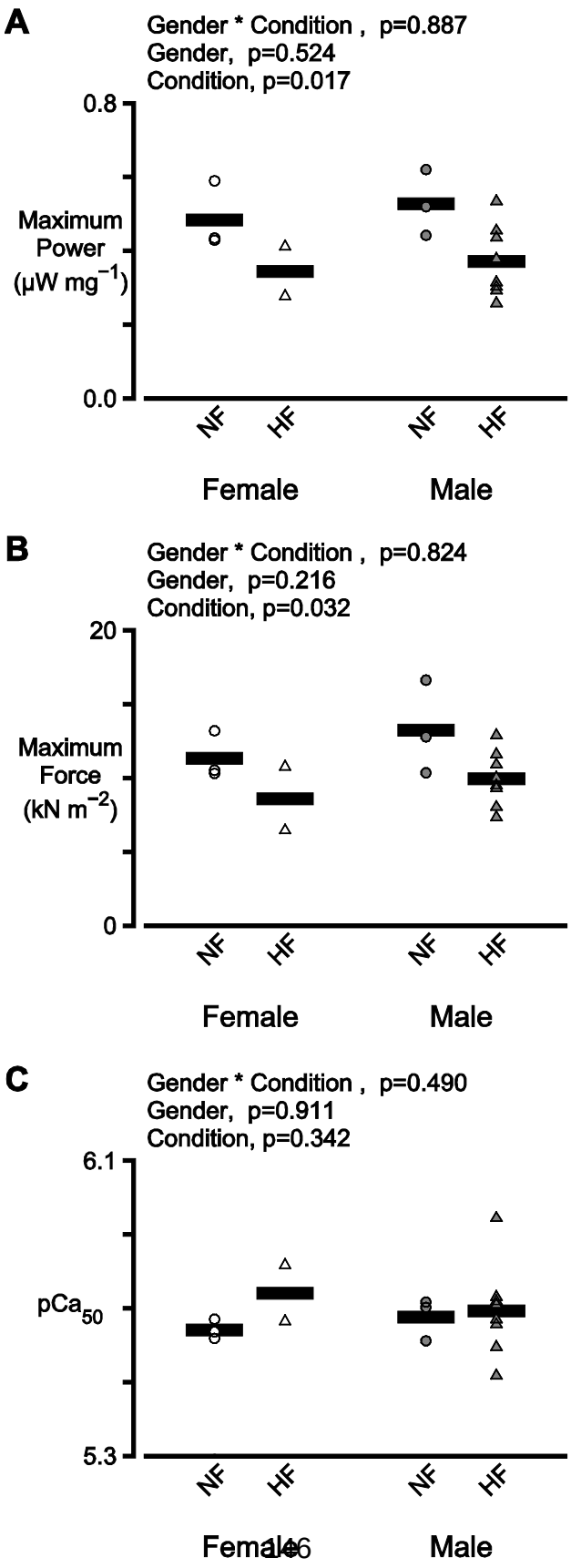
A
Gender * Condition , p=0.887
Gender, p=0.524
Condition, p=0.017
0.8
Maximum Power (μW mg−1)
0.0
NF
HF
NF
HF
Female
Male
B
Gender * Condition , p=0.824
Gender, p=0.216
Condition, p=0.032
20
Maximum Force (kN m−2)
0
NF
HF
NF
HF
Female
Male
C
Gender * Condition , p=0.490
Gender, p=0.911
Condition, p=0.342
6.1
pCa50
5.3
NF
HF
NF
HF
Female
Male

Figure 5.2. Contractile properties did not depend on gender.

Symbols show the mean of the A) Maximum Power, B) Maximum Force and C) pCa_{50} measured from 4 or 6 preparations from each condition for each heart. Thick bars show the mean data for the condition. The text above the plot shows p values for the main statistical effects.

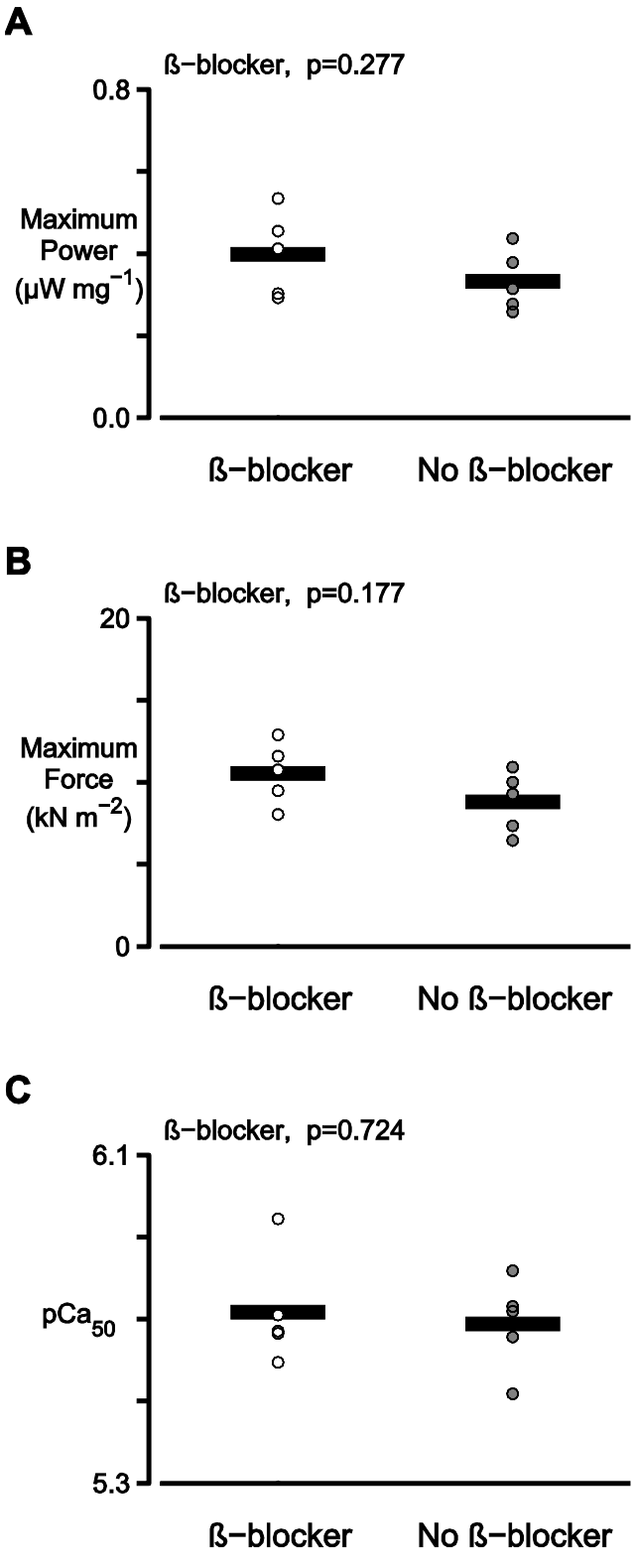
A
ß−blocker, p=0.277
0.8
Maximum
Power
(μW mg−1)
0.0
ß−blocker
No ß−blocker
B
ß−blocker, p=0.177
20
Maximum
Force
(kN m−2)
0
ß−blocker
No ß−blocker
C
ß−blocker, p=0.724
6.1
pCa50
5.3
ß−blocker
No ß−blocker

Figure 5.3. Contractile properties did not depend on β-blocker.

Symbols show the mean of the A) Maximum Power, B) Maximum Force and C) pCa_{50} measured from 4 or 6 preparations from each heart. Thick bars show the mean data with and without β-blocker. The text above the plot shows p values for the main statistical effect.

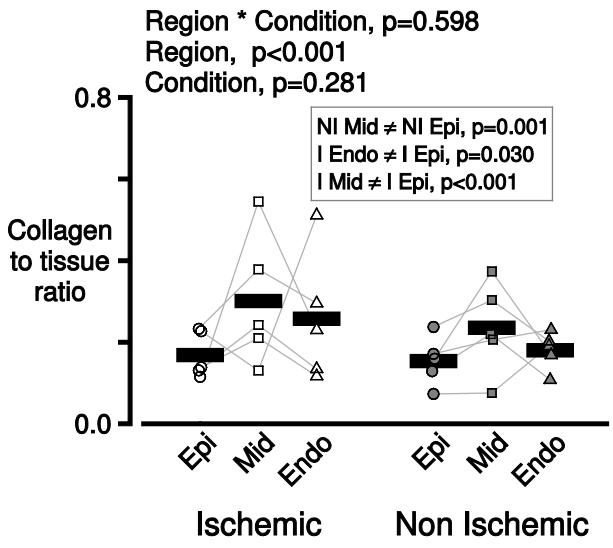

Figure 5.4. Collagen content is increased in the mid-myocardium of patients with ischemic and non-ischemic disease.

Symbols show the mean collagen to tissue ratio measured for each region for failing hearts with ischemic disease (left) and non-ischemic disease (right). A.U. stands for arbitrary units.

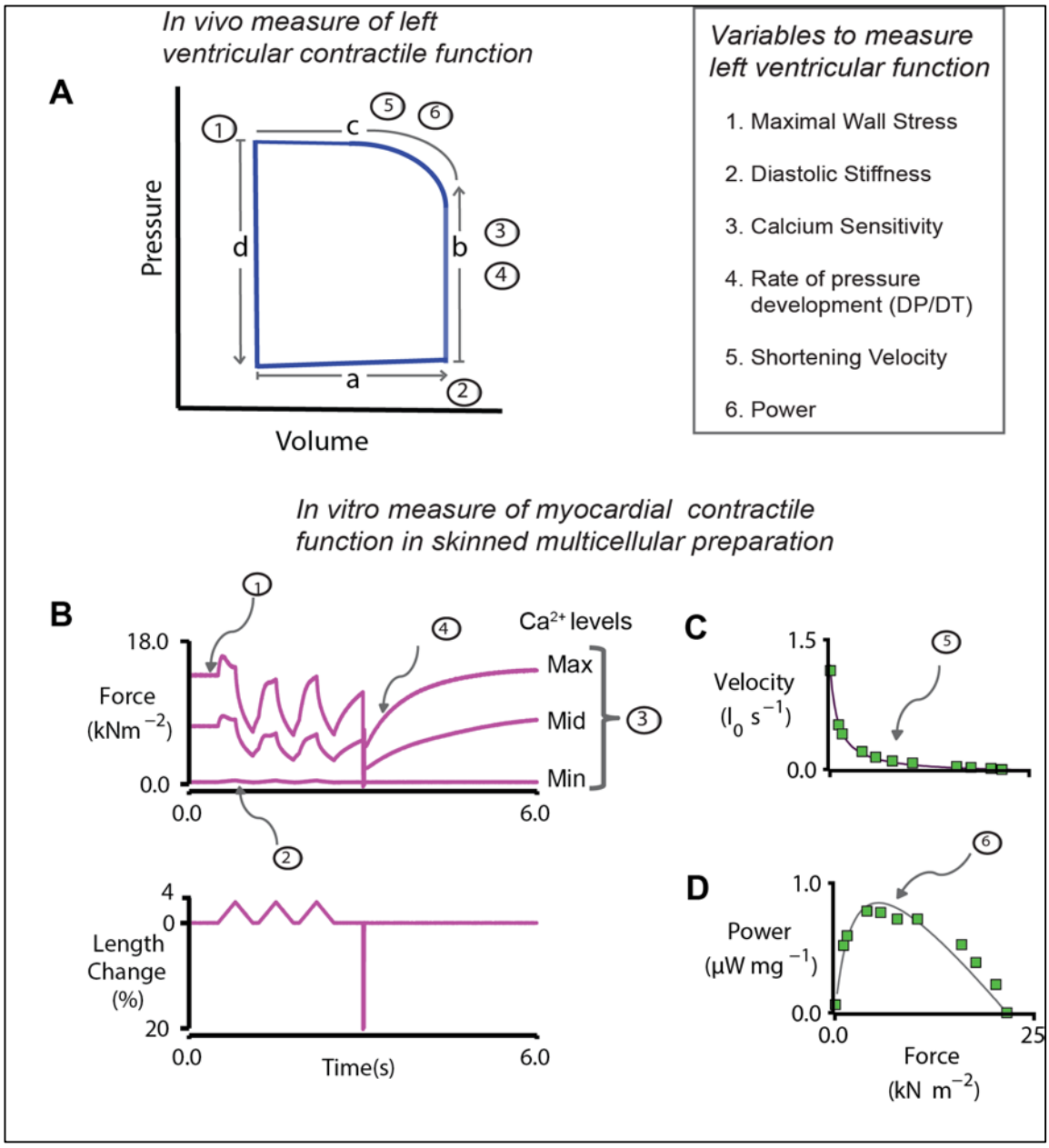

Figure 5.5. Linking *in vitro* mechanics to *in vivo* function.

A) Schematic pressure-volume loop, B) Raw traces of the 3-stretch protocol, C) Force-velocity curve and D) Force-Power curve. The top right panel shows variables measured to assess ventricle function.

Reference

1. Harvey W. On the motion of the heart and blood in animals. *London:George Bell and sons.* 1889.

2. Lower R. Tractatus de corde. *London.* 1669.

3. Pettigrew JB. On the Arrangement of the Muscular Fibres in the Ventricles of the Vertebrate Heart, with Physiological Remarks. *Phil. Trans. R. Soc. London.* 1864;154:445-500.

4. Anderson RH, Ho SY, Redmann K, Sanchez-Quintana D, Lunkenheimer PP. The anatomical arrangement of the myocardial cells making up the ventricular mass. *Eur J Cardiothorac Surg.* 2005;28:517-525.

5. Streeter DD, Jr., Spotnitz HM, Patel DP, Ross J, Jr., Sonnenblick EH. Fiber orientation in the canine left ventricle during diastole and systole. *Circ Res.* 1969;24:339-347.

6. Greenbaum RA, Ho SY, Gibson DG, Becker AE, Anderson RH. Left ventricular fibre architecture in man. *Br Heart J.* 1981;45:248-263.

7. Schmid P, Jaermann T, Boesiger P, Niederer PF, Lunkenheimer PP, Cryer CW, Anderson RH. Ventricular myocardial architecture as visualised in postmortem swine hearts using magnetic resonance diffusion tensor imaging. *Eur J Cardiothorac Surg.* 2005;27:468-472.

8. Buckberg G, Hoffman JI, Mahajan A, Saleh S, Coghlan C. Cardiac mechanics revisited: the relationship of cardiac architecture to ventricular function. *Circulation.* 2008;118:2571-2587.

9. Russel IK, Gotte MJ, Bronzwaer JG, Knaapen P, Paulus WJ, van Rossum AC. Left ventricular torsion: an expanding role in the analysis of myocardial dysfunction. *JACC Cardiovasc Imaging.* 2009;2:648-655.

10. Ingels NB, Jr. Myocardial fiber architecture and left ventricular function. *Technol Health Care.* 1997;5:45-52.

11. Yancy CW, Jessup M, Bozkurt B, Butler J, Casey DE, Jr., Drazner MH, Fonarow GC, Geraci SA, Horwich T, Januzzi JL, Johnson MR, Kasper EK, Levy WC, Masoudi FA, McBride PE, McMurray JJ, Mitchell JE, Peterson PN, Riegel B, Sam F, Stevenson LW, Tang WH, Tsai EJ, Wilkoff BL. 2013 ACCF/AHA guideline for the management of heart failure: executive summary: a report of the American College of Cardiology Foundation/American Heart Association Task Force on practice guidelines. *Circulation.* 2013;128:1810-1852.

12. Zile MR, Brutsaert DL. New concepts in diastolic dysfunction and diastolic heart failure: Part I: diagnosis, prognosis, and measurements of diastolic function. *Circulation.* 2002;105:1387-1393.

13. Go AS, Mozaffarian D, Roger VL, Benjamin EJ, Berry JD, Borden WB, Bravata DM, Dai S, Ford ES, Fox CS, Franco S, Fullerton HJ, Gillespie C, Hailpern SM, Heit JA, Howard VJ, Huffman MD, Kissela BM, Kittner SJ, Lackland DT, Lichtman JH, Lisabeth LD, Magid D, Marcus GM, Marelli A, Matchar DB, McGuire DK, Mohler ER, Moy CS, Mussolino ME, Nichol G, Paynter NP, Schreiner PJ, Sorlie PD, Stein J, Turan TN, Virani SS, Wong ND, Woo D, Turner MB. Heart disease and stroke statistics--2013 update: a report from the American Heart Association. *Circulation.* 2013;127:e6-e245.

14. Seidman CE, Seidman JG. Identifying sarcomere gene mutations in hypertrophic cardiomyopathy: a personal history. *Circ Res.* 2011;108:743-750.

15. Chang AN, Potter JD. Sarcomeric protein mutations in dilated cardiomyopathy. *Heart Fail Rev.* 2005;10:225-235.

16. Tardiff JC. Sarcomeric proteins and familial hypertrophic cardiomyopathy: linking mutations in structural proteins to complex cardiovascular phenotypes. *Heart Fail Rev.* 2005;10:237-248.

17. Cohn JN, Ferrari R, Sharpe N. Cardiac remodeling--concepts and clinical implications: a consensus paper from an international forum on cardiac remodeling. Behalf of an International Forum on Cardiac Remodeling. *J Am Coll Cardiol.* 2000;35:569-582.

18. Burchfield JS, Xie M, Hill JA. Pathological ventricular remodeling: mechanisms: part 1 of 2. *Circulation.* 2013;128:388-400.

19. Kehat I, Molkentin JD. Molecular pathways underlying cardiac remodeling during pathophysiological stimulation. *Circulation.* 2010;122:2727-2735.

20. Ho SY. Anatomy and myoarchitecture of the left ventricular wall in normal and in disease. *Eur J Echocardiogr.* 2009;10:iii3-7.

21. Levin HR, Oz MC, Chen JM, Packer M, Rose EA, Burkhoff D. Reversal of chronic ventricular dilation in patients with end-stage cardiomyopathy by prolonged mechanical unloading. *Circulation.* 1995;91:2717-2720.

22. Xie M, Burchfield JS, Hill JA. Pathological ventricular remodeling: therapies: part 2 of 2. *Circulation.* 2013;128:1021-1030.

23. Wu MT, Tseng WY, Su MY, Liu CP, Chiou KR, Wedeen VJ, Reese TG, Yang CF. Diffusion tensor magnetic resonance imaging mapping the fiber architecture remodeling in human myocardium after infarction: correlation with viability and wall motion. *Circulation.* 2006;114:1036-1045.

24. Wu Y, Zhang LJ, Zou C, Tse HF, Wu EX. Transmural heterogeneity of left ventricular myocardium remodeling in postinfarct porcine model revealed by MR diffusion tensor imaging. *J Magn Reson Imaging.* 2011;34:43-49.

25. Mekkaoui C, Huang S, Chen HH, Dai G, Reese TG, Kostis WJ, Thiagalingam A, Maurovich-Horvat P, Ruskin JN, Hoffmann U, Jackowski MP, Sosnovik DE. Fiber architecture in remodeled myocardium revealed with a quantitative diffusion CMR tractography framework and histological validation. *J Cardiovasc Magn Reson.* 2012;14:70.

26. Wachtell K, Gerdts E, Palmieri V, Olsen MH, Nieminen MS, Papademetriou V, Boman K, Dahlof B, Aurigemma GP, Rokkedal JE, Devereux RB. In-treatment midwall and endocardial fractional shortening predict cardiovascular outcome in hypertensive patients with preserved baseline systolic ventricular function: the Losartan Intervention For Endpoint reduction study. *J Hypertens.* 2010;28:1541-1546.

27. de Simone G, Devereux RB, Roman MJ, Ganau A, Saba PS, Alderman MH, Laragh JH. Assessment of left ventricular function by the midwall fractional shortening/end-systolic stress relation in human hypertension. *J Am Coll Cardiol.* 1994;23:1444-1451.

28. de Simone G, Devereux RB, Koren MJ, Mensah GA, Casale PN, Laragh JH. Midwall left ventricular mechanics. An independent predictor of cardiovascular risk in arterial hypertension. *Circulation.* 1996;93:259-265.

29. Vinch CS, Aurigemma GP, Simon HU, Hill JC, Tighe DA, Meyer TE. Analysis of left ventricular systolic function using midwall mechanics in patients >60 years of age with hypertensive heart disease and heart failure. *Am J Cardiol.* 2005;96:1299-1303.

30. Wachtell K, Papademetriou V, Smith G, Gerdts E, Dahlof B, Engblom E, Aurigemma GP, Bella JN, Ibsen H, Rokkedal J, Devereux RB. Relation of impaired left ventricular filling to systolic midwall mechanics in hypertensive patients with normal left ventricular systolic chamber function: the Losartan Intervention for Endpoint Reduction in Hypertension (LIFE) study. *Am Heart J.* 2004;148:538-544.

31. Fan D, Takawale A, Lee J, Kassiri Z. Cardiac fibroblasts, fibrosis and extracellular matrix remodeling in heart disease. *Fibrogenesis Tissue Repair.* 2012;5:15.

32. Kapur NK. Transforming growth factor-beta: governing the transition from inflammation to fibrosis in heart failure with preserved left ventricular function. *Circ Heart Fail.* 2011;4:5-7.

33. Varnava AM, Elliott PM, Sharma S, McKenna WJ, Davies MJ. Hypertrophic cardiomyopathy: the interrelation of disarray, fibrosis, and small vessel disease. *Heart.* 2000;84:476-482.

34. de Bakker JM, van Rijen HM. Continuous and discontinuous propagation in heart muscle. *J Cardiovasc Electrophysiol.* 2006;17:567-573.

35. Wiegerinck RF, de Bakker JM, Opthof T, de Jonge N, Kirkels H, Wilms-Schopman FJ, Coronel R. The effect of enhanced gap junctional conductance on ventricular conduction in explanted hearts from patients with heart failure. *Basic Res Cardiol.* 2009;104:321-332.

36. Glukhov AV, Fedorov VV, Kalish PW, Ravikumar VK, Lou Q, Janks D, Schuessler RB, Moazami N, Efimov IR. Conduction remodeling in human end-stage nonischemic left ventricular cardiomyopathy. *Circulation.* 2012;125:1835-1847.

37. Knaapen P, Gotte MJ, Paulus WJ, Zwanenburg JJ, Dijkmans PA, Boellaard R, Marcus JT, Twisk JW, Visser CA, van Rossum AC, Lammertsma AA, Visser FC. Does myocardial fibrosis hinder contractile function and perfusion in idiopathic dilated cardiomyopathy? PET and MR imaging study. *Radiology.* 2006;240:380-388.

38. Assomull RG, Prasad SK, Lyne J, Smith G, Burman ED, Khan M, Sheppard MN, Poole-Wilson PA, Pennell DJ. Cardiovascular magnetic resonance, fibrosis, and prognosis in dilated cardiomyopathy. *J Am Coll Cardiol.* 2006;48:1977-1985.

39. Gulati A, Jabbour A, Ismail TF, Guha K, Khwaja J, Raza S, Morarji K, Brown TD, Ismail NA, Dweck MR, Di Pietro E, Roughton M, Wage R, Daryani Y, O'Hanlon R, Sheppard MN, Alpendurada F, Lyon AR, Cook SA, Cowie MR, Assomull RG, Pennell DJ, Prasad SK. Association of fibrosis with mortality and sudden cardiac death in patients with nonischemic dilated cardiomyopathy. *JAMA.* 2013;309:896-908.

40. Dweck MR, Joshi S, Murigu T, Alpendurada F, Jabbour A, Melina G, Banya W, Gulati A, Roussin I, Raza S, Prasad NA, Wage R, Quarto C, Angeloni E, Refice S, Sheppard M, Cook SA, Kilner PJ, Pennell DJ, Newby DE, Mohiaddin RH, Pepper J, Prasad SK. Midwall fibrosis is an independent predictor of mortality in patients with aortic stenosis. *J Am Coll Cardiol.* 2011;58:1271-1279.

41. Drouin E, Charpentier F, Gauthier C, Laurent K, Le Marec H. Electrophysiologic characteristics of cells spanning the left ventricular wall of human heart: evidence for presence of M cells. *J Am Coll Cardiol.* 1995;26:185-192.

42. Glukhov AV, Fedorov VV, Lou Q, Ravikumar VK, Kalish PW, Schuessler RB, Moazami N, Efimov IR. Transmural dispersion of repolarization in failing and nonfailing human ventricle. *Circ Res.* 2010;106:981-991.

43. Lou Q, Fedorov VV, Glukhov AV, Moazami N, Fast VG, Efimov IR. Transmural heterogeneity and remodeling of ventricular excitation-contraction coupling in human heart failure. *Circulation.* 2011;123:1881-1890.

44. Soltysinska E, Olesen SP, Christ T, Wettwer E, Varro A, Grunnet M, Jespersen T. Transmural expression of ion channels and transporters in human nondiseased and end-stage failing hearts. *Pflugers Arch.* 2009;459:11-23.

45. Cazorla O, Le Guennec JY, White E. Length-tension relationships of sub-epicardial and sub-endocardial single ventricular myocytes from rat and ferret hearts. *J Mol Cell Cardiol.* 2000;32:735-744.

46. Cazorla O, Szilagyi S, Le Guennec JY, Vassort G, Lacampagne A. Transmural stretch-dependent regulation of contractile properties in rat heart and its alteration after myocardial infarction. *FASEB J.* 2005;19:88-90.

47. van der Velden J, Merkus D, de Beer V, Hamdani N, Linke WA, Boontje NM, Stienen GJ, Duncker DJ. Transmural heterogeneity of myofilament function and sarcomeric protein phosphorylation in remodeled myocardium of pigs with a recent myocardial infarction. *Front Physiol.* 2011;2:83.

48. Huxley AF, Niedergerke R. Structural changes in muscle during contraction; interference microscopy of living muscle fibres. *Nature.* 1954;173:971-973.

49. Huxley H, Hanson J. Changes in the cross-striations of muscle during contraction and stretch and their structural interpretation. *Nature.* 1954;173:973-976.

50. Lazarides E, Hubbard BD. Immunological characterization of the subunit of the 100 A filaments from muscle cells. *Proc Natl Acad Sci U S A.* 1976;73:4344-4348.

51. Labeit S, Kolmerer B. Titins: giant proteins in charge of muscle ultrastructure and elasticity. *Science.* 1995;270:293-296.

52. Tyska MJ, Warshaw DM. The myosin power stroke. *Cell Motil Cytoskeleton.* 2002;51:1-15.

53. Rayment I. The structural basis of the myosin ATPase activity. *J Biol Chem.* 1996;271:15850-15853.

54. Paul DM, Morris EP, Kensler RW, Squire JM. Structure and orientation of troponin in the thin filament. *J Biol Chem.* 2009;284:15007-15015.

55. Kobayashi T, Jin L, de Tombe PP. Cardiac thin filament regulation. *Pflugers Arch.* 2008;457:37-46.

56. Fabiato A. Calcium-induced release of calcium from the cardiac sarcoplasmic reticulum. *Am J Physiol.* 1983;245:C1-14.

57. Campbell KS. Impact of myocyte strain on cardiac myofilament activation. *Pflugers Arch.* 2011;462:3-14.

58. Marks AR. Calcium and the heart: a question of life and death. *J Clin Invest.* 2003;111:597-600.

59. Hanft LM, Korte FS, McDonald KS. Cardiac function and modulation of sarcomeric function by length. *Cardiovasc Res.* 2008;77:627-636.

60. Hill AV. The heat of shortening and the dynamic constants of muscle. *Proceedings of the Royal Society Series B-Biological Sciences.* 1938;126:136-195.

61. Gordon AM, Huxley AF, Julian FJ. The variation in isometric tension with sarcomere length in vertebrate muscle fibres. *J Physiol.* 1966;184:170-192.

62. Granzier HL, Irving TC. Passive tension in cardiac muscle: contribution of collagen, titin, microtubules, and intermediate filaments. *Biophys J.* 1995;68:1027-1044.

63. Hamdani N, Kooij V, van Dijk S, Merkus D, Paulus WJ, Remedios CD, Duncker DJ, Stienen GJ, van der Velden J. Sarcomeric dysfunction in heart failure. *Cardiovasc Res.* 2008;77:649-658.

64. Chung CS, Campbell KS. Temperature and transmural region influence functional measurements in unloaded left ventricular cardiomyocytes. *Physiol Rep.* 2013;1:e00158.

65. Campbell SG, Haynes P, Snapp WK, Nava KE, Campbell KS. Altered ventricular torsion and transmural patterns of myocyte relaxation precede heart failure in aging F344 rats. *Am J Physiol Heart Circ Physiol.* 2013.

66. Jweied EE, McKinney RD, Walker LA, Brodsky I, Geha AS, Massad MG, Buttrick PM, de Tombe PP. Depressed cardiac myofilament function in human diabetes mellitus. *Am J Physiol Heart Circ Physiol.* 2005;289:H2478-2483.

67. Patton C, Thompson S., Epel D. Some precautions in using chelators to buffer metals in biological solutions. *Cell Calcium.* 2004;35:427-431.

68. Mitov MI, Holbrook AM, Campbell KS. Myocardial short-range force responses increase with age in F344 rats. *J Mol Cell Cardiol.* 2009;46:39-46.

69. Campbell KS, Moss RL. History-dependent mechanical properties of permeabilized rat soleus muscle fibers. *Biophys J.* 2002;82:929-943.

70. Zafeiridis A, Jeevanandam V, Houser SR, Margulies KB. Regression of cellular hypertrophy after left ventricular assist device support. *Circulation.* 1998;98:656-662.

71. Moss RL. Sarcomere length-tension relations of frog skinned muscle fibres during calcium activation at short lengths. *J Physiol.* 1979;292:177-192.

72. Campbell KS. Tension recovery in permeabilized rat soleus muscle fibers after rapid shortening and restretch. *Biophys J.* 2006;90:1288-1294.

73. Ford LE, Nakagawa K, Desper J, Seow CY. Effect of osmotic compression on the force-velocity properties of glycerinated rabbit skeletal muscle cells. *J Gen Physiol.* 1991;97:73-88.

74. Brenner B. The necessity of using two parameters to describe isotonic shortening velocity of muscle tissues: the effect of various interventions upon initial shortening velocity (vi) and curvature (b). *Basic Res Cardiol.* 1986;81:54-69.

75. Brenner B, Jacob R. Calcium activation and maximum unloaded shortening velocity. Investigation on glycerinated skeletal and heart muscle preparations. *Basic Res Cardiol.* 1980;75:40-46.

76. Hill AV. The heat of shortening and dynamics constants of muscles. *Proc. R. Soc. Lond.* 1938.

77. Campbell KS, Moss RL. SLControl: PC-based data acquisition and analysis for muscle mechanics. *Am J Physiol Heart Circ Physiol.* 2003;285:H2857-2864.

78. Bruckner BA, Razeghi P, Stetson S, Thompson L, Lafuente J, Entman M, Loebe M, Noon G, Taegtmeyer H, Frazier OH, Youker K. Degree of cardiac fibrosis and hypertrophy at time of implantation predicts myocardial improvement during left ventricular assist device support. *J Heart Lung Transplant.* 2004;23:36-42.

79. Hanley PJ, Young AA, LeGrice IJ, Edgar SG, Loiselle DS. 3-Dimensional configuration of perimysial collagen fibres in rat cardiac muscle at resting and extended sarcomere lengths. *J Physiol.* 1999;517 (Pt 3):831-837.

80. Blough ER, Rennie ER, Zhang F, Reiser PJ. Enhanced electrophoretic separation and resolution of myosin heavy chains in mammalian and avian skeletal muscles. *Anal Biochem.* 1996;233:31-35.

81. Stride N, Larsen S, Hey-Mogensen M, Hansen CN, Prats C, Steinbruchel D, Kober L, Dela F. Impaired mitochondrial function in chronically ischemic human heart. *Am J Physiol Heart Circ Physiol.* 2013;304:H1407-1414.

82. Tikunov BA, Sweeney HL, Rome LC. Quantitative electrophoretic analysis of myosin heavy chains in single muscle fibers. *J Appl Physiol (1985).* 2001;90:1927-1935.

83. Mitov MI, Greaser ML, Campbell KS. GelBandFitter--a computer program for analysis of closely spaced electrophoretic and immunoblotted bands. *Electrophoresis.* 2009;30:848-851.

84. Terentyev D, Viatchenko-Karpinski S, Gyorke I, Volpe P, Williams SC, Gyorke S. Calsequestrin determines the functional size and stability of cardiac intracellular calcium stores: Mechanism for hereditary arrhythmia. *Proc Natl Acad Sci U S A.* 2003;100:11759-11764.

85. Monasky MM, Biesiadecki BJ, Janssen PM. Increased phosphorylation of tropomyosin, troponin I, and myosin light chain-2 after stretch in rabbit ventricular myocardium under physiological conditions. *J Mol Cell Cardiol.* 2010;48:1023-1028.

86. Warren CM, Krzesinski PR, Greaser ML. Vertical agarose gel electrophoresis and electroblotting of high-molecular-weight proteins. *Electrophoresis.* 2003;24:1695-1702.

87. Dong WJ, Jayasundar JJ, An J, Xing J, Cheung HC. Effects of PKA phosphorylation of cardiac troponin I and strong crossbridge on

conformational transitions of the N-domain of cardiac troponin C in regulated thin filaments. *Biochemistry.* 2007;46:9752-9761.

88. Govindan S, McElligott A, Muthusamy S, Nair N, Barefield D, Martin JL, Gongora E, Greis KD, Luther PK, Winegrad S, Henderson KK, Sadayappan S. Cardiac myosin binding protein-C is a potential diagnostic biomarker for myocardial infarction. *J Mol Cell Cardiol.* 2012;52:154-164.

89. Djousse L, Driver JA, Gaziano JM. Relation between modifiable lifestyle factors and lifetime risk of heart failure. *JAMA.* 2009;302:394-400.

90. DeFrances CJ, Cullen KA, Kozak LJ. National Hospital Discharge Survey: 2005 annual summary with detailed diagnosis and procedure data. *Vital Health Stat 13.* 2007:1-209.

91. Kitzman DW, Daniel KR. Diastolic heart failure in the elderly. *Clin Geriatr Med.* 2007;23:83-106.

92. Thomas DP, McCormick RJ, Zimmerman SD, Vadlamudi RK, Gosselin LE. Aging- and training-induced alterations in collagen characteristics of rat left ventricle and papillary muscle. *Am J Physiol.* 1992;263:H778-783.

93. Lakatta EG, Levy D. Arterial and cardiac aging: major shareholders in cardiovascular disease enterprises: Part II: the aging heart in health: links to heart disease. *Circulation.* 2003;107:346-354.

94. Kass DA, Bronzwaer JG, Paulus WJ. What mechanisms underlie diastolic dysfunction in heart failure? *Circ Res.* 2004;94:1533-1542.

95. Pacher P, Mabley JG, Liaudet L, Evgenov OV, Marton A, Hasko G, Kollai M, Szabo C. Left ventricular pressure-volume relationship in a rat model of advanced aging-associated heart failure. *Am J Physiol Heart Circ Physiol.* 2004;287:H2132-2137.

96. Boluyt MO, Converso K, Hwang HS, Mikkor A, Russell MW. Echocardiographic assessment of age-associated changes in systolic and diastolic function of the female F344 rat heart. *J Appl Physiol.* 2004;96:822-828.

97. Carnes CA, Geisbuhler TP, Reiser PJ. Age-dependent changes in contraction and regional myocardial myosin heavy chain isoform expression in rats. *J Appl Physiol.* 2004;97:446-453.

98. Orchard CH, Lakatta EG. Intracellular calcium transients and developed tension in rat heart muscle. A mechanism for the negative interval-strength relationship. *J Gen Physiol.* 1985;86:637-651.

99. Turturro A, Witt WW, Lewis S, Hass BS, Lipman RD, Hart RW. Growth curves and survival characteristics of the animals used in the Biomarkers of Aging Program. *J Gerontol A Biol Sci Med Sci.* 1999;54:B492-501.

100. Davis JS, Hassanzadeh S, Winitsky S, Lin H, Satorius C, Vemuri R, Aletras AH, Wen H, Epstein ND. The overall pattern of cardiac contraction depends on a spatial gradient of myosin regulatory light chain phosphorylation. *Cell.* 2001;107:631-641.

101. Stelzer JE, Norman HS, Chen PP, Patel JR, Moss RL. Transmural variation in myosin heavy chain isoform expression modulates the timing of myocardial force generation in porcine left ventricle. *J Physiol.* 2008;586:5203-5214.

102. Capasso JM, Fitzpatrick D, Anversa P. Cellular mechanisms of ventricular failure: myocyte kinetics and geometry with age. *Am J Physiol.* 1992;262:H1770-1781.

103. Taffet GE, Tate CA. CaATPase content is lower in cardiac sarcoplasmic reticulum isolated from old rats. *Am J Physiol.* 1993;264:H1609-1614.

104. Tate CA, Helgason T, Hyek MF, McBride RP, Chen M, Richardson MA, Taffet GE. SERCA2a and mitochondrial cytochrome oxidase expression are increased in hearts of exercise-trained old rats. *Am J Physiol.* 1996;271:H68-72.

105. Xu A, Narayanan N. Effects of aging on sarcoplasmic reticulum Ca2+-cycling proteins and their phosphorylation in rat myocardium. *Am J Physiol.* 1998;275:H2087-2094.

106. Rundell VL, Manaves V, Martin AF, de Tombe PP. Impact of beta-myosin heavy chain isoform expression on cross-bridge cycling kinetics. *Am J Physiol Heart Circ Physiol.* 2005;288:H896-903.

107. Zhang R, Zhao J, Mandveno A, Potter JD. Cardiac troponin I phosphorylation increases the rate of cardiac muscle relaxation. *Circ Res.* 1995;76:1028-1035.

108. van der Velden J, de Jong JW, Owen VJ, Burton PB, Stienen GJ. Effect of protein kinase A on calcium sensitivity of force and its sarcomere length dependence in human cardiomyocytes. *Cardiovasc Res.* 2000;46:487-495.

109. van der Velden J, Papp Z, Zaremba R, Boontje NM, de Jong JW, Owen VJ, Burton PB, Goldmann P, Jaquet K, Stienen GJ. Increased Ca2+-sensitivity of the contractile apparatus in end-stage human heart failure

results from altered phosphorylation of contractile proteins. *Cardiovasc Res.* 2003;57:37-47.

110. Robertson SP, Johnson JD, Holroyde MJ, Kranias EG, Potter JD, Solaro RJ. The effect of troponin I phosphorylation on the Ca2+-binding properties of the Ca2+-regulatory site of bovine cardiac troponin. *J Biol Chem.* 1982;257:260-263.

111. Andre L, Fauconnier J, Reboul C, Feillet-Coudray C, Meschin P, Farah C, Fouret G, Richard S, Lacampagne A, Cazorla O. Subendocardial increase in reactive oxygen species production affects regional contractile function in ischemic heart failure. *Antioxid Redox Signal.* 2013;18:1009-1020.

112. Sadayappan S, Gulick J, Osinska H, Barefield D, Cuello F, Avkiran M, Lasko VM, Lorenz JN, Maillet M, Martin JL, Brown JH, Bers DM, Molkentin JD, James J, Robbins J. A critical function for Ser-282 in cardiac Myosin binding protein-C phosphorylation and cardiac function. *Circ Res.* 2011;109:141-150.

113. Hanft LM, McDonald KS. Sarcomere length dependence of power output is increased after PKA treatment in rat cardiac myocytes. *Am J Physiol Heart Circ Physiol.* 2009;296:H1524-1531.

114. Lang RM, Bierig M, Devereux RB, Flachskampf FA, Foster E, Pellikka PA, Picard MH, Roman MJ, Seward J, Shanewise JS, Solomon SD, Spencer KT, Sutton MS, Stewart WJ, Chamber Quantification Writing G, American Society of Echocardiography's G, Standards C, European Association of E. Recommendations for chamber quantification: a report from the American Society of Echocardiography's Guidelines and Standards Committee and the Chamber Quantification Writing Group, developed in conjunction with the European Association of Echocardiography, a branch of the European Society of Cardiology. *J Am Soc Echocardiogr.* 2005;18:1440-1463.

115. McDonald KS, Wolff MR, Moss RL. Force-velocity and power-load curves in rat skinned cardiac myocytes. *J Physiol.* 1998;511 (Pt 2):519-531.

116. van der Velden J, Klein LJ, van der Bijl M, Huybregts MA, Stooker W, Witkop J, Eijsman L, Visser CA, Visser FC, Stienen GJ. Isometric tension development and its calcium sensitivity in skinned myocyte-sized preparations from different regions of the human heart. *Cardiovasc Res.* 1999;42:706-719.

117. Ambardekar AV, Walker JS, Walker LA, Cleveland JC, Jr., Lowes BD, Buttrick PM. Incomplete recovery of myocyte contractile function despite

improvement of myocardial architecture with left ventricular assist device support. *Circ Heart Fail.* 2011;4:425-432.

118. Wijnker PJ, Boknik P, Gergs U, Muller FU, Neumann J, dos Remedios C, Schmitz W, Sindermann JR, Stienen GJ, van der Velden J, Kirchhefer U. Protein phosphatase 2A affects myofilament contractility in non-failing but not in failing human myocardium. *J Muscle Res Cell Motil.* 2011;32:221-233.

119. van Der Velden J, Klein LJ, Zaremba R, Boontje NM, Huybregts MA, Stooker W, Eijsman L, de Jong JW, Visser CA, Visser FC, Stienen GJ. Effects of calcium, inorganic phosphate, and pH on isometric force in single skinned cardiomyocytes from donor and failing human hearts. *Circulation.* 2001;104:1140-1146.

120. Hamdani N, Borbely A, Veenstra SP, Kooij V, Vrydag W, Zaremba R, Dos Remedios C, Niessen HW, Michel MC, Paulus WJ, Stienen GJ, van der Velden J. More severe cellular phenotype in human idiopathic dilated cardiomyopathy compared to ischemic heart disease. *J Muscle Res Cell Motil.* 2010;31:289-301.

121. Makarenko I, Opitz CA, Leake MC, Neagoe C, Kulke M, Gwathmey JK, del Monte F, Hajjar RJ, Linke WA. Passive stiffness changes caused by upregulation of compliant titin isoforms in human dilated cardiomyopathy hearts. *Circ Res.* 2004;95:708-716.

122. Nagueh SF, Shah G, Wu Y, Torre-Amione G, King NM, Lahmers S, Witt CC, Becker K, Labeit S, Granzier HL. Altered titin expression, myocardial stiffness, and left ventricular function in patients with dilated cardiomyopathy. *Circulation.* 2004;110:155-162.

123. Granzier HL, Labeit S. The giant protein titin: a major player in myocardial mechanics, signaling, and disease. *Circ Res.* 2004;94:284-295.

124. Brower GL, Janicki JS. Contribution of ventricular remodeling to pathogenesis of heart failure in rats. *Am J Physiol Heart Circ Physiol.* 2001;280:H674-683.

125. van der Velden J, Narolska NA, Lamberts RR, Boontje NM, Borbely A, Zaremba R, Bronzwaer JG, Papp Z, Jaquet K, Paulus WJ, Stienen GJ. Functional effects of protein kinase C-mediated myofilament phosphorylation in human myocardium. *Cardiovasc Res.* 2006;69:876-887.

126. Layland J, Solaro RJ, Shah AM. Regulation of cardiac contractile function by troponin I phosphorylation. *Cardiovasc Res.* 2005;66:12-21.

127. Zhang P, Kirk JA, Ji W, dos Remedios CG, Kass DA, Van Eyk JE, Murphy AM. Multiple reaction monitoring to identify site-specific troponin I phosphorylated residues in the failing human heart. *Circulation.* 2012;126:1828-1837.

128. Buscemi N, Foster DB, Neverova I, Van Eyk JE. p21-activated kinase increases the calcium sensitivity of rat triton-skinned cardiac muscle fiber bundles via a mechanism potentially involving novel phosphorylation of troponin I. *Circ Res.* 2002;91:509-516.

129. Olsson MC, Patel JR, Fitzsimons DP, Walker JW, Moss RL. Basal myosin light chain phosphorylation is a determinant of Ca2+ sensitivity of force and activation dependence of the kinetics of myocardial force development. *Am J Physiol Heart Circ Physiol.* 2004;287:H2712-2718.

130. McDonough JL, Labugger R, Pickett W, Tse MY, MacKenzie S, Pang SC, Atar D, Ropchan G, Van Eyk JE. Cardiac troponin I is modified in the myocardium of bypass patients. *Circulation.* 2001;103:58-64.

131. Murphy AM, Kogler H, Georgakopoulos D, McDonough JL, Kass DA, Van Eyk JE, Marban E. Transgenic mouse model of stunned myocardium. *Science.* 2000;287:488-491.

132. Monreal G, Nicholson LM, Han B, Joshi MS, Phillips AB, Wold LE, Bauer JA, Gerhardt MA. Cytoskeletal remodeling of desmin is a more accurate measure of cardiac dysfunction than fibrosis or myocyte hypertrophy. *Life Sci.* 2008;83:786-794.

133. Chugh S, Ouzounian M, Lu Z, Mohamed S, Li W, Bousette N, Liu PP, Gramolini AO. Pilot study identifying myosin heavy chain 7, desmin, insulin-like growth factor 7, and annexin A2 as circulating biomarkers of human heart failure. *Proteomics.* 2013;13:2324-2334.

134. Pawlak A, Gil RJ, Kulawik T, Pronicki M, Karkucinska-Wieckowska A, Szymanska-Debinska T, Gil K, Lagwinski N, Czarnowska E. Type of desmin expression in cardiomyocytes - a good marker of heart failure development in idiopathic dilated cardiomyopathy. *J Intern Med.* 2012;272:287-297.

135. Hamdani N, Paulus WJ, van Heerebeek L, Borbely A, Boontje NM, Zuidwijk MJ, Bronzwaer JG, Simonides WS, Niessen HW, Stienen GJ, van der Velden J. Distinct myocardial effects of beta-blocker therapy in heart failure with normal and reduced left ventricular ejection fraction. *Eur Heart J.* 2009;30:1863-1872.

136. Morano I, Rosch J, Arner A, Ruegg JC. Phosphorylation and thiophosphorylation by myosin light chain kinase: different effects on mechanical properties of chemically skinned ventricular fibers from the pig. *J Mol Cell Cardiol.* 1990;22:805-813.

137. Arrell DK, Neverova I, Fraser H, Marban E, Van Eyk JE. Proteomic analysis of pharmacologically preconditioned cardiomyocytes reveals novel phosphorylation of myosin light chain 1. *Circ Res.* 2001;89:480-487.

138. Sawicki G, Leon H, Sawicka J, Sariahmetoglu M, Schulze CJ, Scott PG, Szczesna-Cordary D, Schulz R. Degradation of myosin light chain in isolated rat hearts subjected to ischemia-reperfusion injury: a new intracellular target for matrix metalloproteinase-2. *Circulation.* 2005;112:544-552.

139. Doroszko A, Polewicz D, Sawicka J, Richardson JS, Cheung PY, Sawicki G. Cardiac dysfunction in an animal model of neonatal asphyxia is associated with increased degradation of MLC1 by MMP-2. *Basic Res Cardiol.* 2009;104:669-679.

140. Cadete VJ, Sawicka J, Bekar LK, Sawicki G. Combined subthreshold dose inhibition of myosin light chain phosphorylation and MMP-2 activity provides cardioprotection from ischaemic/reperfusion injury in isolated rat heart. *Br J Pharmacol.* 2013;170:380-390.

141. Fitzsimons DP, Patel JR, Moss RL. Role of myosin heavy chain composition in kinetics of force development and relaxation in rat myocardium. *J Physiol.* 1998;513 (Pt 1):171-183.

142. Reiser PJ, Portman MA, Ning XH, Schomisch Moravec C. Human cardiac myosin heavy chain isoforms in fetal and failing adult atria and ventricles. *Am J Physiol Heart Circ Physiol.* 2001;280:H1814-1820.

143. Stelzer JE, Fitzsimons DP, Moss RL. Ablation of myosin-binding protein-C accelerates force development in mouse myocardium. *Biophys J.* 2006;90:4119-4127.

144. Korte FS, McDonald KS, Harris SP, Moss RL. Loaded shortening, power output, and rate of force redevelopment are increased with knockout of cardiac myosin binding protein-C. *Circ Res.* 2003;93:752-758.

145. Colson BA, Bekyarova T, Locher MR, Fitzsimons DP, Irving TC, Moss RL. Protein kinase A-mediated phosphorylation of cMyBP-C increases proximity of myosin heads to actin in resting myocardium. *Circ Res.* 2008;103:244-251.

146. Sanbe A, Gulick J, Hayes E, Warshaw D, Osinska H, Chan CB, Klevitsky R, Robbins J. Myosin light chain replacement in the heart. *Am J Physiol Heart Circ Physiol.* 2000;279:H1355-1364.

147. Colson BA, Locher MR, Bekyarova T, Patel JR, Fitzsimons DP, Irving TC, Moss RL. Differential roles of regulatory light chain and myosin binding protein-C phosphorylations in the modulation of cardiac force development. *J Physiol.* 2010;588:981-993.

148. Morano M, Zacharzowski U, Maier M, Lange PE, Alexi-Meskishvili V, Haase H, Morano I. Regulation of human heart contractility by essential myosin light chain isoforms. *J Clin Invest.* 1996;98:467-473.

149. Sanguinetti MC. Reduced transient outward K+ current and cardiac hypertrophy: causal relationship or epiphenomenon? *Circ Res.* 2002;90:497-499.

150. Hasenfuss G. Animal models of human cardiovascular disease, heart failure and hypertrophy. *Cardiovasc Res.* 1998;39:60-76.

151. Chung CS, Mitov MI, Callahan LA, Campbell KS. Increased myocardial short-range forces in a rodent model of diabetes reflect elevated content of beta myosin heavy chain. *Arch Biochem Biophys.* 2013.

152. Korte FS, Herron TJ, Rovetto MJ, McDonald KS. Power output is linearly related to MyHC content in rat skinned myocytes and isolated working hearts. *Am J Physiol Heart Circ Physiol.* 2005;289:H801-812.

153. Barefield D, Sadayappan S. Phosphorylation and function of cardiac myosin binding protein-C in health and disease. *J Mol Cell Cardiol.* 2010;48:866-875.

154. Frank KF, Bolck B, Brixius K, Kranias EG, Schwinger RH. Modulation of SERCA: implications for the failing human heart. *Basic Res Cardiol.* 2002;97 Suppl 1:I72-78.

155. Huss JM, Kelly DP. Mitochondrial energy metabolism in heart failure: a question of balance. *Journal of Clinical Investigation.* 2005;115:547-555.

156. LeWinter MM, Granzier HL. Titin is a major human disease gene. *Circulation.* 2013;127:938-944.

157. Lohse MJ, Engelhardt S, Eschenhagen T. What is the role of beta-adrenergic signaling in heart failure? *Circ Res.* 2003;93:896-906.

158. Brodde OE, Michel MC. Adrenergic and muscarinic receptors in the human heart. *Pharmacol Rev.* 1999;51:651-690.

159. Malik FI, Hartman JJ, Elias KA, Morgan BP, Rodriguez H, Brejc K, Anderson RL, Sueoka SH, Lee KH, Finer JT, Sakowicz R, Baliga R, Cox DR, Garard M, Godinez G, Kawas R, Kraynack E, Lenzi D, Lu PP, Muci A, Niu C, Qian X, Pierce DW, Pokrovskii M, Suehiro I, Sylvester S, Tochimoto T, Valdez C, Wang W, Katori T, Kass DA, Shen YT, Vatner SF, Morgans DJ. Cardiac myosin activation: a potential therapeutic approach for systolic heart failure. *Science.* 2011;331:1439-1443.

160. Cleland JG, Teerlink JR, Senior R, Nifontov EM, Mc Murray JJ, Lang CC, Tsyrlin VA, Greenberg BH, Mayet J, Francis DP, Shaburishvili T, Monaghan M, Saltzberg M, Neyses L, Wasserman SM, Lee JH, Saikali KG, Clarke CP, Goldman JH, Wolff AA, Malik FI. The effects of the cardiac myosin activator, omecamtiv mecarbil, on cardiac function in systolic heart failure: a double-blind, placebo-controlled, crossover, dose-ranging phase 2 trial. *Lancet.* 2011;378:676-683.

161. Gopalan SM, Flaim C, Bhatia SN, Hoshijima M, Knoell R, Chien KR, Omens JH, McCulloch AD. Anisotropic stretch-induced hypertrophy in neonatal ventricular myocytes micropatterned on deformable elastomers. *Biotechnol Bioeng.* 2003;81:578-587.

162. McCulloch AD, Omens JH. Myocyte shearing, myocardial sheets, and microtubules. *Circ Res.* 2006;98:1-3.

163. Stones R, Calaghan SC, Billeter R, Harrison SM, White E. Transmural variations in gene expression of stretch-modulated proteins in the rat left ventricle. *Pflugers Arch.* 2007;454:545-549.

164. Ruwhof C, van der Laarse A. Mechanical stress-induced cardiac hypertrophy: mechanisms and signal transduction pathways. *Cardiovasc Res.* 2000;47:23-37.

165. Molkentin JD, Lu JR, Antos CL, Markham B, Richardson J, Robbins J, Grant SR, Olson EN. A calcineurin-dependent transcriptional pathway for cardiac hypertrophy. *Cell.* 1998;93:215-228.

166. Pyle WG, Solaro RJ. At the crossroads of myocardial signaling: the role of Z-discs in intracellular signaling and cardiac function. *Circ Res.* 2004;94:296-305.

167. Hoshijima M. Mechanical stress-strain sensors embedded in cardiac cytoskeleton: Z disk, titin, and associated structures. *Am J Physiol Heart Circ Physiol.* 2006;290:H1313-1325.

168. Antzelevitch C. M cells in the human heart. *Circ Res.* 2010;106:815-817.

169. Yan GX, Shimizu W, Antzelevitch C. Characteristics and distribution of M cells in arterially perfused canine left ventricular wedge preparations. *Circulation.* 1998;98:1921-1927.

170. Stankovicova T, Szilard M, De Scheerder I, Sipido KR. M cells and transmural heterogeneity of action potential configuration in myocytes from the left ventricular wall of the pig heart. *Cardiovasc Res.* 2000;45:952-960.

171. Kramer SP, Powell DK, Haggerty CM, Binkley CM, Mattingly AC, Cassis LA, Epstein FH, Fornwalt BK. Obesity reduces left ventricular strains, torsion, and synchrony in mouse models: a cine displacement encoding with stimulated echoes (DENSE) cardiovascular magnetic resonance study. *J Cardiovasc Magn Reson.* 2013;15:109.

172. Wenk JF, Sun K, Zhang Z, Soleimani M, Ge L, Saloner D, Wallace AW, Ratcliffe MB, Guccione JM. Regional left ventricular myocardial contractility and stress in a finite element model of posterobasal myocardial infarction. *J Biomech Eng.* 2011;133:044501.

173. McCulloch AD, Paternostro G. Cardiac systems biology. *Ann N Y Acad Sci.* 2005;1047:283-295.

174. Sasano T, Kikuchi K, McDonald AD, Lai S, Donahue JK. Targeted high-efficiency, homogeneous myocardial gene transfer. *J Mol Cell Cardiol.* 2007;42:954-961.

175. Malliaras K, Marban E. Cardiac cell therapy: where we've been, where we are, and where we should be headed. *Br Med Bull.* 2011;98:161-185.

176. Oettgen P, Boyle AJ, Schulman SP, Hare JM. Cardiac Stem Cell Therapy. Need for Optimization of Efficacy and Safety Monitoring. *Circulation.* 2006;114:353-358.

177. Sheng CC, Zhou L, Hao J. Current stem cell delivery methods for myocardial repair. *Biomed Res Int.* 2013;2013:547902.

178. Elhami E, Dietz B, Xiang B, Deng J, Wang F, Chi C, Goertzen AL, Mzengeza S, Freed D, Arora RC, Tian G. Assessment of three techniques for delivering stem cells to the heart using PET and MR imaging. *EJNMMI Res.* 2013;3:72.

179. Rudy Y, Ackerman MJ, Bers DM, Clancy CE, Houser SR, London B, McCulloch AD, Przywara DA, Rasmusson RL, Solaro RJ, Trayanova NA, Van Wagoner DR, Varro A, Weiss JN, Lathrop DA. Systems approach to understanding electromechanical activity in the human heart: a national

heart, lung, and blood institute workshop summary. *Circulation.* 2008;118:1202-1211.

Vita

Premi Haynes

Education

2002-2006	University of the Cumberlands, Williamsburg, KY, B.S. in Biology with a minor in Chemistry
2006-2008	Morehead State University, Morehead, KY, M.S. in Biology-Microbiology
2008-present	PhD. candidate, University of Kentucky, Lexington, KY (Defense date: 19 March 2014)

Professional positions held

Fall 2006-Spring 2008	Graduate Assistant, Microbiology, Morehead State University (Mentor-Geoff Gearner PhD.)
Oct 2008-Dec 2008	Integrated Biomedical Science rotation, Microbiology (Mentor- Glenn Telling PhD.)
Jan 2009-Mar 2009	Integrated Biomedical Science rotation, Anatomy and Neurobiology (Mentor-Jonathan Lifshitz)
Mar 2009-present	Graduate Assistant, Physiology, (Mentor-Kenneth S. Campbell PhD.)

Scholastic and Professional Honors

Fall 2003	Certificate of academic achievement, University of Cumberland, Williamsburg, KY
Fall 2003	Certificate of National Academic Honor Society of freshmen, Alpha Lambda Delta
Spring 2006	“Hutton Scholar” certificate for more than 600 hours of community service
Fall 2006-Spring 2008	H.N. and Frances Berger Scholarship (Awarded $10,000)
Spring 2008	Robert Coleman foundation (Awarded $500)

Spring 2011	University of Kentucky graduate school travel fund (Awarded $400)
Fall 2011-Spring 2012	Nominated and voted as the Graduate Student Representative for the department of Physiology by the graduate students (organized student chalk talks and attended faculty meetings)
Spring 2012	University of Kentucky graduate school travel fund (Awarded $800)
10 June, 2012	Discussion leader at Gordon Research Seminar-Cardiac Regulatory Mechanism
26 July, 2012	1st prize for poster presentation at University of Kentucky-Physiology Research Retreat
8 Dec, 2012	Recipient of the Brian J. Hardin Award for hard work, compassion and making the department of Physiology fun
Fall 2013-present	Member of the Physiology Chair Search Committee (This is a National search for a Chair for the Department of Physiology at the University of Kentucky. The committee consists of 6 full professors and 1 graduate student)
6 Nov, 2013	2nd prize for poster presentation at University of Kentucky-5th Annual Center for Muscle Biology Retreat.

Professional Society Affiliations

Fall 2007-Spring 2008	American Society of Microbiology
Fall 2009-Present	Biophysical Society
Spring 2012	American Heart Association

Teaching/Mentoring

Fall 2006-May 2008	Taught 5 Principles of Microbiology Lab 317 and 5 Introduction to Elementary Medical Microbiology Lab 217 (Morehead State University)

Spring 2011-Fall 2011	Supervised Alexandria Jarrells (Undergraduate Biology Major, University of Kentucky) with human biospecimen inventory
Fall 2011	Supervised Robert N. Hesley (Rotating 1st year Graduate Student, University of Kentucky) with specialized gel electrophoresis techniques
Spring 2012	Teaching PGY 207 (Physiology Undergraduate discussion course)
Spring 2012- 2013	Supervised Kristofer E. Nava (Undergraduate Biology Major, University of Kentucky) with specialized gel electrophoresis techniques
Fall 2012	Supervised Cheavar A. Blair (Rotating 1st year Graduate Student, University of Kentucky) with establishing histology protocols for human cardiac tissue
Spring 2013	Supervised Nicholas A. Brown (Rotating 1st year Graduate Student, University of Kentucky) with RNA extraction and Microarray techniques

Publications

1. **Shekar P**, Campbell K: "This article is interesting because it suggests that, in cardiac muscle, cooperativity can be reduced..." Evaluation of: [Kreutziger KL et al. Calcium binding kinetics of troponin C strongly modulate cooperative activation and tension kinetics in cardiac muscle. J Mol Cell Cardiol. 2010 Oct 28; doi: 10.1016/j.yjmcc.2010.10.025]. Faculty of 1000, 16 Dec 2010. F1000.com/7041956

2. Campbell SG, **Haynes P**, Kelsey Snapp W, Nava KE, Campbell KS. Altered ventricular torsion and transmural patterns of myocyte relaxation precede heart failure in aging f344 rats. *American journal of physiology. Heart and circulatory physiology*. 2013;305:H676-686

3. **Haynes P**, Nava KE, Lawson BA, Chung CS, Mitov MI, Campbell SG, Stromberg AJ, Sadayappan S, Bonnell MR, Hoopes CW, Campbell KS. Transmural heterogeneity of cellular level power output is reduced in human heart failure. *Journal of Molecular and Cellular Cardiology.* 2014 Feb 20. pii: S0022-2828(14)00058-3. doi: 10.1016/j.yjmcc.2014.02.008.

4. **Haynes P** and Campbell KS. Myocardial hypertrophy reduces transmural variation in mitochondrial function. Invited Editorial. ***Submitted*** *to Frontiers in Physiology: Striated Muscle, 12th March 2014.*

5. Zhang X**, Haynes P**, Campbell KS and Wenk JF. Numerical evaluation of myofiber orientation and transmural contractile strength on left ventricular function. ***Submitted*** *to Medical Engineering & Physics, 23rd March 2014.*

Platform talks and seminars

1. Myosin ATPase activity in Heart Failure. *Muscle Forum*, University of Kentucky, Lexington, KY: 16th Dec, 2010

2. Decreased power output in failing human myocardium may reflect posttranslational modifications to sarcomeric proteins. *Physiology Seminar Series*, University of Kentucky, Lexington, KY: 11th May 2011

3. Transmural variations in cellular level contractile function in the left ventricle of patients with end-stage heart failure. *8th Annual Spring Conference for UK Center for Clinical and Translational Science*, Lexington, KY*:* 8th April 2013

4. Cellular level contractile dysfunction and proteomic modifications in patients with end-stage heart failure. *1st Annual Utah Cardiac Recovery Symposium,* Salt Lake City, Utah: 18th Jan 2013.

5. Transmural heterogeneity of cellular level power output is reduced in human heart failure. Muscle Forum, University of Kentucky, Lexington, KY: *17th October 2013.*

Published Abstracts

1. **Shekar P**, Mitov MI, Ferreira LF, Bonnell MR, Campbell KS. Measurements of power output in human myocardium. *Biophysical journal*. 2011;100:297a

2. **Shekar P**, Mitov MI, Ferreira LF, Campbell SG, Stasko SA, Jarrells AM, Lawson BA, Reid MB, Hoopes CW, Bonnell MR, Campbell KS. Transmural heterogeneity and depressed function in the mechanical properties of ventricular tissue from patients with end-stage heart failure. *Biophysical journal*. 2012;102:352a

3. **Shekar P**, Mitov MI, Ferreira LF, Campbell SG, Stasko SA, Jarrells AM, Lawson BA, Reid MB, Hoopes CW, Bonnell MR, Campbell KS. 432 transmural heterogeneity and depressed function in the mechanical properties of ventricular tissue from patients with end-stage heart failure. *The Journal of Heart and Lung Transplantation*. 2012;31:S153

4. **Shekar P**, Mitov MI, Ferreira LF, Campbell SG, Stasko SA, Jarrells AM, Lawson BA, Reid MB, Hoopes CW, Bonnell MR, Campbell KS. 1243 Alterations in phosphorylation of sarcomeric proteins contribute to the transmural differences and decrease in contractile function in patients with end-stage heart failure. American transplant congress 2012 abstracts. *American Journal of Transplantation*. 2012;12:27-542

5. **Haynes P**, Mitov MI, Campbell SG, Lawson BA, Nava KE, Sadayappan S, Bonnell MR, Hoopes CW, Campbell KS. Alterations in proteins involved in cellular level contractile dysfunction in the left ventricles of patients with end stage heart failure. *Biophysical journal*. 2013;104:152a

6. **Haynes P**, Mitov MI, Campbell SG, Lawson BA, Nava KE, Bonnell MR, Hoopes CW, Campbell KS. Myocyte power output in humans with end-stage heart failure: Effects of lvad treatment. *Biophysical journal*. 2013;104:152a-153a

7. **Haynes P**, Nava KE, Lawson BA, Chung CS, Mitov MI, Campbell SG, Stromberg AJ, Sadayappan S, Bonnell MR, Hoopes CW, Campbell KS. Transmural heterogeneity of cellular level power output is reduced in human heart failure. *Circulation. 2013,* 128:A13813

Other Abstracts and Poster Presentations

1. **Shekar P**, Osasona A, Peterson J, Reid E, Campbell KS. Direct measurements of ventricular stiffness in isolated rat hearts at 37°C. *12th Annual Gill Heart Institute Cardiovascular Research Day,* Lexington, KY: 23rd October 2009

2. **Shekar P**, Osasona A, Peterson J, Reid E, Campbell KS. Direct measurements of ventricular stiffness in isolated rat hearts at 37°C.1st *Annual Center for Muscle Biology Retreat,* Lexington, KY: 28th October 2009

3. **Shekar P**, Gairola G, Campbell KS. Exposure to cigarette smoke impairs cardiac contractile function in mice. *Physiology Research Retreat,* Jabez, KY: 18th Aug 2010

4. **Shekar P**, Mitov MI, Ferreira LF, Bonnell MR, Campbell KS. Measurements of power output in human myocardium. *13th Annual Gill Heart Institute Cardiovascular Research Day,* Lexington, KY: 22nd October 2010.

5. **Shekar P**, Mitov MI, Ferreira LF, Bonnell MR, Campbell KS. Measurements of power output in human myocardium. *2nd Annual Center for Muscle Biology Retreat,* Lexington, KY: 28th October 2010

6. **Shekar P**, Mitov MI, Ferreira LF, Campbell SG, Stasko SA, Jarrells AM, Lawson BA, Reid MB, Hoopes CW, Bonnell MR, Campbell KS. Decrease in transmural heterogeneity of the left ventricle may lead to alteration of dynamic properties in heart failure. *Modeling workshop for Trainees in Muscle Biology,* Lexington, KY: 28th July 2011

7. **Shekar P**, Mitov MI, Ferreira LF, Campbell SG, Stasko SA, Jarrells AM, Lawson BA, Reid MB, Hoopes CW, Bonnell MR, Campbell KS. Transmural heterogeneity and depressed function in the mechanical properties of ventricular tissue from patients with end-stage heart failure.*14th Annual Saha Heart Institute Cardiovascular Research Day,* Lexington, KY: 21st October 2011

8. **Shekar P**, Mitov MI, Ferreira LF, Campbell SG, Stasko SA, Jarrells AM, Lawson BA, Reid MB, Hoopes CW, Bonnell MR, Campbell KS. Transmural heterogeneity and depressed function in the mechanical properties of ventricular tissue from patients with end-stage heart failure. *3rd Annual Center for Muscle Biology Retreat,* Lexington, KY: 27th October 2011

9. **Shekar P**, Mitov MI, Ferreira LF, Campbell SG, Stasko SA, Jarrells AM, Lawson BA, Reid MB, Hoopes CW, Bonnell MR, Campbell KS. Transmural heterogeneity and depressed function in the mechanical properties of ventricular tissue from patients with end-stage heart failure.*7th Annual Spring Conference for UK Center for Clinical and Translational Science,* Lexington, KY: 29th March, 2012

10. **Shekar P**, Mitov MI, Ferreira LF, Campbell SG, Stasko SA, Jarrells AM, Lawson BA, Reid MB, Hoopes CW, Bonnell MR, Campbell KS. Transmural heterogeneity and depressed function in the mechanical properties of ventricular tissue from patients with end-stage heart failure. *Bluegrass Molecular Biophysics Symposium,* Lexington, KY: 11th May 2012

11. **Shekar P**, Mitov MI, Ferreira LF, Campbell SG, Stasko SA, Jarrells AM, Lawson BA, Reid MB, Hoopes CW, Bonnell MR, Campbell KS. Transmural heterogeneity and depressed function in the mechanical properties of ventricular tissue from patients with end-stage heart failure. *Gordon Research Seminar and Conference: Cardiac Regulatory Mechanisms, New London, NH:* 9th June 2012

12. **Shekar P**, Mitov MI, Ferreira LF, Campbell SG, Stasko SA, Jarrells AM, Lawson BA, Reid MB, Hoopes CW, Bonnell MR, Campbell KS. Transmural heterogeneity and depressed function in the mechanical properties of ventricular tissue from patients with end-stage heart failure. *Physiology Research Retreat,* Jabez, KY: 26th July 2012

13. **Shekar P**, Mitov MI, Ferreira LF, Campbell SG, Stasko SA, Jarrells AM, Lawson BA, Reid MB, Hoopes CW, Bonnell MR, Campbell KS. Alterations in

proteins involved in cellular level contractile dysfunction in the left ventricles of patients with end-stage heart failure. *15th Annual Saha Heart Institute Cardiovascular Research Day,* Lexington, KY: 5th October 2012

14. **Shekar P**, Mitov MI, Ferreira LF, Campbell SG, Stasko SA, Jarrells AM, Lawson BA, Reid MB, Hoopes CW, Bonnell MR, Campbell KS. Alterations in proteins involved in cellular level contractile dysfunction in the left ventricles of patients with end-stage heart failure. 3rd Annual Center for Muscle Biology Retreat, Lexington, KY: 25th October 2012

15. **Haynes P**, Mitov MI, Campbell SG, Lawson BA, Nava KE, Sadayappan S, Bonnell MR, Hoopes CW, Campbell KS. Cellular level contractile dysfunction and proteomic modifications in patients with end-stage heart failure. *1st Annual Utah Cardiac Recovery Symposium, Salt Lake City, Utah:* 18th Jan 2013

16. **Haynes P**, Nava KE, Lawson BA, Chung CS, Mitov MI, Campbell SG, Stromberg AJ, Sadayappan S, Bonnell MR, Hoopes CW, Campbell KS. Transmural variations in cellular level contractile function in the left ventricle of patients with end-stage heart failure. *1st Annual Kentucky Physiological Society, American Physiological Society Chapter,* Lexington, Kentucky: 25th March 2013

17. **Haynes P**, Mitov MI, Campbell SG, Lawson BA, Nava KE, Sadayappan S, Bonnell MR, Hoopes CW, Campbell KS. Myocyte power output in humans with end-stage heart failure: effects of LVAD treatment. *Bluegrass Molecular Biophysics Symposium,* Lexington, KY: 20th May 2013

18. **Haynes P**, Mitov MI, Campbell SG, Lawson BA, Nava KE, Sadayappan S, Bonnell MR, Hoopes CW, Campbell KS. Alterations in proteins involved in cellular level contractile dysfunction in the left ventricles of patients with end stage heart failure. *Bluegrass Molecular Biophysics Symposium,* Lexington, KY: 20th May 2013

19. **Haynes P**, Nava KE, Lawson BA, Chung CS, Mitov MI, Campbell SG, Stromberg AJ, Sadayappan S, Bonnell MR, Hoopes CW, Campbell KS. Transmural heterogeneity of cellular level power output is reduced in human heart failure. *16th Annual Gill Heart Institute Cardiovascular Research Day,* Lexington, KY: 11th October 2013

20. **Haynes P**, Nava KE, Lawson BA, Chung CS, Mitov MI, Campbell SG, Stromberg AJ, Sadayappan S, Bonnell MR, Hoopes CW, Campbell KS. Transmural heterogeneity of cellular level power output is reduced in human heart failure. 5rth Annual Center for Muscle Biology Retreat, Lexington, KY: 7th Nov, 2013